Angiogenic Potential of Mesenchymal Cells and T Lymphocytes Induced by Mechanical Stimuli that Improve Bone Healing –

An *In Vitro* 2D and 3D Bioreactor Study

vorgelegt von
Diplom-Ingenieurin (FH), Master of Science
Friederike H. Bieler, geb. Bleckwehl
aus Bremen

Von der Fakultät III - Prozesswissenschaften
der Technischen Universität Berlin
zur Erlangung des wissenschaftlichen Grades
Doktorin der Ingenieurwissenschaften
Dr.-Ing.

genehmigte Dissertation

Promotionsausschuss:

Vorsitzender: Prof. Dr.-Ing. Frank-Jürgen Methner
Berichter: Prof. Dr. rer. nat. Roland Lauster
Berichter: Prof. Dr.-Ing. Georg N. Duda
Berichter: Prof. Dr. rer. nat. Leif-Alexander Garbe

Tag der wissenschaftlichen Aussprache: 14. Dezember 2010

Berlin 2011

D83

Acknowledgements

First of all, I would like to thank Prof. Dr. Georg N. Duda. He was not only a great supervisor supporting and guiding the work my thesis is based on, but he also enabled my research at the Julius Wolff Institute (JWI), Charité – Universitätsmedizin Berlin. I am glad that I got the opportunity to hand in my thesis at the TU Berlin. This would not have been possible without Prof. Dr. Roland Lauster and the other appointed referees.

Especially Dr. Mark S. Thompson deserves my gratitude. He initiated my PhD project at the JWI. Although Mark moved on to Oxford University, already at the beginning of my PhD project, he was always present with great advice, support and ideas that helped a lot to proceed. Some of my gratitude is related to the great time at the JWI, which I do not want to miss, and some to the honest support I experienced in the Mechanobiology and the Cell Therapy team. Here I would also like to thank their team leaders, especially Dr. Grit Kasper, who initiated my bioreactor study. I highly appreciate the advice I received, especially regarding newly learned lab-techniques, from Sven Geissler and the experi-mental work performed together with Aline Groothuis, Florian Witt, and Annett Kurtz.

I would further like to thank my intern Lauren Ehardt and all technical assistants at the JWI. They were a great help in the laboratory. Additionally, the clinicians and veterinaries who prepared the bone material for mesenchymal cell isolations deserve a big thank you, as well as the MTL at our institute for building the microscope *x-y* table adaptor. Also, all collaborators, especially from the Institute of Medical Genetics (Charité) and the MPI for Molecular Genetics, should be mentioned. Dr. J. Adjaye and Dr. A. Prigione from the latter enabled and greatly supported my gene expression analysis. In general, I would like to tell the people who reviewed the thesis at hand how much I appreciate their advice and opinion. Their thoughts helped to make this thesis what it is.

The encouragement I received from my family and friends helped me a lot in finalizing this work. Without my parents I would not have been able to achieve this. They always supported my goals and enabled my good education. But my deepest gratitude goes to my patient husband Sven Bieler. He had to suffer a lot during the past few years from my moods and from my ambition and still, he always supported me, not only personally but also scientifically.

Finally, this study was financially supported by a grant partially from the German Research Foundation (DFG SFB 760, Berlin), partially from the Berlin-Brandenburg Center for Regenerative Therapies (BCRT), and, to a large extent, from the AO Foundation.

Content

Abstract

Delayed healing and non-unions of bone fractures can result among others from impaired revascularisation. Mechanical stimulation is able to improve bone healing by enhancing revascularisation and bone formation but if exceeding a limit or being too low the opposite can occur. Different cell types and molecular processes are involved in the course of bone healing. Mesenchymal stem cells (MSCs) and their differentiated successors are known to play a role in angiogenesis and tissue regeneration enhanced by mechanical stimulation. They are detectable a few days after fracture in the haematoma that has formed in the fracture gap. Lymphocytes are mainly present in the very beginning after fracture and their depletion seems to accelerate healing. However, detailed knowledge of the mechano-response of cells, especially T lymphocytes, during fracture healing on the molecular level is missing. The present *in vitro* study aimed to examine effects of mechanical stimuli, as occurring during the onset of bone healing, to identify relevant molecular events improving bone healing.

To study mechano-responses of mesenchymal cells a thorough mechanical characterisation of the strain and fluid shear stress environment of a 2D cell stimulation device was performed using digital image correlation and computational fluid dynamics. The strain environment was found to be consistent only within a short time frame and about half of the strain applied was transferred to cells. The strains and fluid shear stresses acting in concert were found to be in a range relevant for mesenchymal cell responses. A short-term stimulation of mesenchymal cells under now well defined boundary conditions resulted in the clustering of the angiogenesis related protein αVβ3 integrin. To study the interaction of MSCs and T lymphocytes, a fracture haematoma-like 3D environment was chosen to test the effect of a cyclic compression known to be favourable for bone healing. MSCs and their co-cultures with T lymphocytes showed after stimulation an increased angiogenic potential, concluded from their protein expression and a tube formation assay. T lymphocytes alone showed no angiogenic potential but were mechano-responsive on mRNA level. However, the angiogenic potential in co-cultures was lower than that of MSCs, possibly due to an ongoing immune response, as an allogenic setting was used. On mRNA level, the immune response was reduced after mechanical stimulation.

In conclusion, mechanical stimulation in sizes relevant for an improvement of bone healing, stimulates angiogenesis promoted by mesenchymal cells and seems to reduce present immune reactions in the haematoma. Especially the latter is a new finding of great interest for the clinic as it further elucidates how mechanical stimulation improves the healing outcome.

Zusammenfassung

Eine Ursache für die verzögerte oder ausbleibende Heilung von Knochenbrüchen kann die fehlende Revaskularisierung sein. Auch ist bekannt, dass mechanische Stimulation die Knochenheilung durch die Verbesserung der Revaskularisierung und Knochenbildung fördern kann, allerdings darf sie dabei ein gewisses Maß nicht über- bzw. unterschreiten, da sonst die Heilung beeinträchtigt würde. Verschiedene Zelltypen und molekulare Prozesse sind im Verlauf der Knochenheilung involviert. Mesenchymale Stammzellen (MSCs) und ihre differenzierten Nachfolgezellen sind dafür bekannt, eine Rolle in der Angiogenese und Geweberegeneration einzunehmen, die durch mechanische Stimulation verstärkt werden kann. Sie sind wenige Tage nach der Fraktur im entstandenen Hämatom und im Frakturspalt nachweisbar. Auch Lymphozyten sind in dieser frühen Phase im Frakturspalt zu finden und ihre Entfernung scheint die Heilung zu beschleunigen. Aber genaue Kenntnisse über die mechanisch induzierte Antwort von Zellen, insbesondere von T-Lymphozyten, auf molekularer Ebene während der Knochenheilung fehlen bisher. Die gegenwärtige *in vitro* Studie hat das Ziel, den Einfluss mechanischer Stimuli, wie sie während der frühen Knochenheilung auftreten, zu untersuchen und relevante, die Knochenheilung fördernde molekulare Prozesse zu identifizieren.

Um die mechanisch induzierte Antwort zu untersuchen, wurde eine umfassende Charakterisierung der Dehnungs- und Flüssigkeitsscherung in der 2D Zellkultur mittels „digital image correlation“ und „computational fluid dynamics“ durchgeführt. Dabei zeigte sich, dass die Dehnungsumgebung nur in einem kleinen Zeitfenster reproduzierbar ist und nur etwa die Hälfte der applizierten Dehnung auch auf einzelne Zellen übertragen wird. Dehnung und Flüssigkeitsscherung agieren beide in einer Größenordnung, die für mechanische Stimulation von mesenchymalen Zellen relevant sind. Eine Kurzzeitstimulation mesenchymaler Zellen, unter den ermittelten Rahmenbedingungen, führte zur Clusterbildung von αVβ3 Integrin, welches auch an der Angiogenese beteiligt ist. Um die Interaktion zwischen MSCs und T-Lymphozyten zu untersuchen, wurde eine an das Frakturhämatom angepasste 3D Umgebung gewählt Damit wurde die Auswirkung von zyklischen Kompressionen, die bekanntermaßen vorteilhaft für die Knochenheilung sein sollen, getestet. MSCs und ihre Ko-Kultur mit T-Lymphozyten zeigten nach der Stimulation ein erhöhtes angiogenes Potential, welches mittels Proteinexpression und einem Gefäßbildungsassay ermittelt wurde. T-Lymphozyten allein zeigten dies nicht, nur ein differentiell verändertes mRNA Expressionsprofil nach mechanischer Stimulation. Insgesamt war das angiogene Potential der Ko-Kulturen niedriger als das der MSCs, vermutlich durch eine Immunantwort

auf die allogenen Kulturbedingungen. Auf mRNA-Ebene zeigte sich nach mechanischer Stimulation eine verminderte Expression immunrelevanter Gene.

Zusammenfassend ist zu sagen, dass die heilungsfördernde mechanische Stimulation die Angiogenese, vermittelt durch mesenchymal Zellen, verbessert. Außerdem scheint mechanische Belastung die vorhandene Immunantwort im Frakturhämatom zu verringern. Letzteres ist neu und daher von großem Interesse für die klinische Forschung, da ein weiterer Ansatz gefunden wurde, wie mechanische Stimulation zur Verbesserung des Heilungsergebnisses beiträgt.

1 Introduction

In this chapter the background and the motivation driving the thesis at hand are highlighted, followed by a description of the aims and hypothesis. Further, the current knowledge about bone healing and angiogenesis is presented.

1.1 Background

Delayed healing or non-union of fractures is a clinical problem still not solved though research has been addressing this issue for many years. Delayed healing of tibial fractures that were caused by low energy trauma occurs in 4.4% of those fractures. Non-union in the same type of fractures occurs in 2.5% of the cases. The prevalence of both impaired healing situations increases to >13% in open fractures [1]. Causes for non-unions and delayed healing are among others infections and high energy impact destroying the fracture surrounding soft and hard tissue, but also impaired blood supply from the periosteal vascular system. The local vascularity and its regeneration (angiogenesis) may be impaired due to debridement and also smoking. In addition, malnutrition can also cause delays [1]. The immune system also influences fracture healing and vice versa [2]. Treatment for non-unions in long bones is available but was reported to involve costs greater than GBP 15,000 per patient in a best-case scenario [3]. But it is not only a financially costly scenario but also regarding the patients' well-being, mobility and quality of life. Therefore, research on possibilities for avoiding impaired healing and improving the healing outcome is urgently required.

It has long been known that optimising the mechanical environment, resulting from the kind of fracture fixation and its stability and the time point after fracture weight bearing is started and the amount of weight bearing allowed [4], may improve the course of healing. However, not only the mechanical environment is important but also the biological/biochemical environment. The latter may be improved by the local administration of antibiotics, bisphosphonates or bone morphogenetic proteins using for instance an intramedullary nail as a delivery system [5-7]. But also application of mesenchymal stem cells (MSCs) or their pre-differentiated successors may positively affect the healing outcome [8]. They are known to act pro-angiogenic which is further enhanced by mechanical stimulation [9]. Furthermore, depletion of the adaptive immune response, lymphocytes, was observed to accelerate bone healing in mice [10]. These observations support the development of the primary hypothesis tested in this project that mechano-regulated angiogenesis is driven by mesenchymal cells and reduced in the presence of immune cells.

To elucidate the interplay between the mechanical, cellular, and biochemical environment, understanding of the effects of mechanics on the cells present during fracture healing is needed. This will help to improve treatment and therapies for tissue regeneration and also to avoid occurrence of impaired healing.

1.2 Motivation

The interplay between mechanical, cellular, and biochemical environment is still not fully understood, which is vital to be able to improve the healing outcome of fractures. There are many different cell types present during bone healing, including endothelial cells, mesenchymal cells, and immune cells such as T lymphocytes. However, it is unclear which cells participate in mechano-regulated processes that result in an improved angiogenesis leading to improved bone regeneration.

Different approaches are applicable to study mechano-regulated processes. *In vitro* studies are more affordable compared to *in vivo* ones and their results are easier to obtain in larger numbers and to link directly to the mechanical environment. Still, they are not able to fully resemble the *in vivo* situation. Monolayer cell culture approaches lack the transferability to *in vivo* due to the two-dimensional environment but offer a well defined environment regarding mechanics and biochemistry, whereas three-dimensional ones usually have a poorly defined mechanical environment but more closely resemble the *in vivo* situation.

1.3 Goals and outline of thesis

The goal of the present *in vitro* study, while approximating the mechanical environment present during the onset of bone healing in 2D and 3D experiments, is to study cellular and molecular processes related to mechanically inducible angiogenesis. The findings will help to understand the process of healing in regard to the mechanical environment and will offer signposts and pointers for potential therapies to improve the healing outcome.

The current chapter addresses the background, motivation and goals as well as the hypothesis driving this thesis. Further, it will review the current knowledge of bone healing, some of the related cell types and molecular factors that are involved, mechanical stimuli occurring during bone healing and their effects. In addition, mechanical stimulation of cells and resulting mechanotransduction will be addressed.

Chapter 2 describes the methods used to fulfil the individual aims of this thesis. The first one is the characterisation of the mechanical environment in regard to strain and fluid shear in a device that applies tensile strains, and to test the determined settings on mesenchymal cells by studying their response in 2D. The second individual aim is to determine the importance of

mesenchymal stem cells, T lymphocytes, and their co-culture for mechano-regulated angiogenesis and possibly involved immunomodulatory effetcs achieved by a comparison of their cellular response to cyclic compression in a haematoma-like environment.

The third chapter elaborates the results obtained by the methods described in chapter 2.

Finally, in chapter 4, the results presented in chapter 3 are summarised and discussed in relation to both, future scientific investigations and their meaning for clinical practice.

1.4 Hypothesis

Mechano-regulated angiogenesis is driven by mesenchymal cells and reduced in the presence of immune cells.

1.5 Current knowledge: Bone healing and angiogenesis – cells, proteins, and mechanics

This section gives an overview of angiogenesis, and of the overall process of bone healing, including which cells and proteins are involved. In addition, the mechanical conditions occurring during bone healing and the influence of different loading environments on bone healing are described. Finally, devices that aim to reproduce such loading environments and the effect of the latter on the cellular level are addressed.

1.5.1 Angiogenesis – involvement of plasminogen activation system and matrix metalloproteases and other proteins

Angiogenesis is a process essential for tissue regeneration, commencing in the early phase of bone healing. It improves the nutrition and oxygen supply of the tissue and thereby promotes healing [11]. The process of angiogenesis may be shortly described as the sprouting of new vessels from pre-existing ones [12]. This begins with an increase of permeability of an existing vessel which is induced by vascular endothelial growth factor (VEGF). Thereby plasma proteins leak into the surrounding tissue, extravasation, forming a provisional scaffold for emigrating endothelial cells (ECs). To allow emigration, the detachment of endothelial cells from the endothelium needs to be mediated. This likely involves angiopoietin-2 and proteinases such as matrix metalloproteases (MMPs) and plasminogen activators clearing space for migration of proliferating ECs. VEGF isoforms and their receptors support and promote angiogenesis, but angiopoietin-1 is needed for maturation of the newly formed vessels. After cords of ECs have formed, lumen formation is initiated involving again VEGF and also $\alpha V\beta 3$ and $\alpha 5$ integrin. As soon as a vessel is assembled the ECs become quiescent [13].

As just mentioned, one set of proteins involved in angiogenesis is part of the plasminogen activation system (PAS). The first member is the inactive proenzyme plasminogen which is activated by tissue-type (tPA) and urokinase (uPA) plasminogen activator. Both are serine proteases that convert plasminogen into active plasmin being a serine protease itself [14]. Plasmin degrades fibrin and some ECM components and releases and activates growth factors and MMPs [15, 16]. One inhibitor of serine proteases is the serpin family member plasminogen activator inhibitor 1 (PAI-1) [15]. tPA is mainly responsible for fibrin degradation (fibrinolysis) [14, 17], whereas uPA is usually bound to its receptor uPAR enhancing plasmin activity [14]. If PAI-1 inhibits uPA by binding, this protein complex of uPAR-uPA-PAI-1 is endocytosed and recycled. PAI-1 regulates further αVβ3 integrin, which is endocytosed if PAI-1 was bound [18]. The endocytosis of uPA and integrins is believed to result in a directional migration of cells [14]. Further, as PAI-1 binds to the ECM protein vitronectin, it is thought to stabilise cell adhesions, which is as well essential for cell migration. PAI-1's RNA transcription is for instance mediated by transforming growth factor-β (TGF-β) and hypoxia [14, 15]. TGF-β-1 further down-regulates uPA [16] whereas VEGF and basic fibroblast growth factor (bFGF) are known to induce both activators and the inhibitor [19]. Both, cell migration and ECM/fibrin degradation, are essential processes for angiogenesis [13-15, 20].

Another set of proteins important for angiogenesis are the MMPs, a group of endopeptidases, which are dependent on zinc ions to be catalytically active [20-22]. 23 MMPs have been described in humans and most of them are secreted proteins. Their proteolytic activity is able to create space for cell migration and to produce by cleavage biologically active substrate fragments. In addition, MMPs can regulate tissue architecture and activate, deactivate or modify the activity of signalling molecules. The (de)activation may be induced both directly and indirectly [20].

MMP-2 is assumed to be vital for neovascularisation as a MMP-2-null mutant showed reduced neovascularisation [23]. MMP-2 is activated via MMP-14, a membrane bound MMP, also called MT1-MMP, and TIMP-2. MMP-14 binds to TIMP-2 which binds to pro-MMP-2 positioning it for activation by another MMP-14 molecule [24].

In the review of Page-McCaw et al., it is described that MMPs may contribute to vascular remodelling by proteolysis of collagen type I, modification of PDGF signalling, regulation of perivascular cells and processing of VEGF. VEGF binds to the ECM upon secretion to be stored extracellularly [25] and is released by MMPs to initiate angiogenesis. Further, MMPs

may act pro- and anti-inflammatory, are involved in inflammatory cell recruitment and regulation of the inflammatory response by cleaving inflammatory mediators [20].

Other proteins involved in angiogenesis are VEGF, TGF-β, bFGF, interleukins-1 and -6 (IL-1 and -6), and tumour necrosis factor-α (TNF-α). VEGF is an essential mediator of neoangiogenesis and EC specific mitogens regulating recruitment, survival, and activity of ECs. Additionally, it is thought to couple angiogenesis and osteogenesis [26, 27]. The VEGF described is the isoform VEGF-A, which has four different cleavage products, the most active one of which is VEGF-165 [27].

TGF-β is produced by platelets and later on during bone healing by chondrocytes and osteoblasts [28] acting mitogenically and in this early stage as chemotactic stimulator of MSCs. Generally, it is known to enhance proliferation of cells of mesenchymal origin as well as proliferation and migration that is associated with vessel formation. Further, it induces extracellular matrix (ECM) production (for vessel maturation, differentiation, and cartilage and bone formation), angiogenesis, and VEGF [26, 27].

bFGF action is exerted by binding to tyrosine kinases and is expressed by MSCs, osteoblasts, chondrocytes, macrophages, and monocytes promoting growth and differentiation [26]. It is supposed to play a critical role in angiogenesis [26] and MSC mitogenesis. In addition, it is mediated by TGF-β and induces VEGF [26, 28].

IL-1, -6 and TNF-α are proinflammatory cytokines that act chemotactically on inflammatory cells, enhance ECM synthesis, stimulate angiogenesis, and promote recruitment of mesenchymal stem cells (MSCs) [29].

1.5.2 The course of bone healing and the proteins involved

Schindeler et al. and Carano divided bone healing into four different interlinked stages (see Fig. 1.1) [26, 30].

As well as the failure of hard mineralised tissue, bone fracture usually involves a disruption of the local soft tissue integrity, interruption of the vascular network, and distortion of the marrow architecture. The interruption of the vascular network results in a hypoxic environment deprived of nutrients, growth factors (GFs), calcium and many other materials needed for bone regeneration [11, 27]. Non-specific wound-healing pathways involving the immune system are activated by the tissue damage and, due to bleeding into the fracture gap, a haematoma forms. Inflammatory cells (platelets, macrophages, granulocytes, lymphocytes, and monocytes) then infiltrate the latter while they fight the inflammation, secrete cytokines

and growth factors (GFs), and are also involved in clotting of the haematoma into a fibrinous thrombus (Fig. 1.1a) [26, 30].

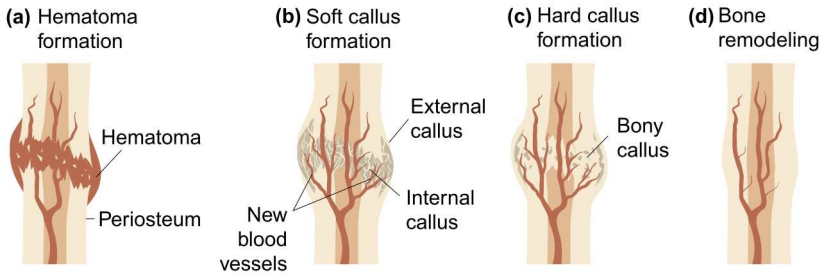

***Fig. 1.1*: The stages of fracture repair.**

(a) Hematoma formation: following injury, disruption of blood vessels leads to formation of a hematoma; (b) Soft callus formation: this stage involves the formation of new blood vessels from pre-existing ones (angiogenesis), the external callus (intramembranous ossification) and the internal callus (fibrocartilage); (c) Hard callus formation: the callus becomes mineralised, forming a hard callus of woven bone; (d) Bone remodeling: the large fracture callus is replaced with secondary lamellar bone, and the vascular supply returns to normal; adopted from [26].

During the onset of the haematoma phase T lymphocytes made up about a fourth of the total amount of cells and were present in the haematoma in sheep in a ratio of 2:1 of $CD4^+$/helper/effector to $CD8^+$/cytotoxic/suppressor T lymphocytes [31]. Whereas fracture haematomata of healthy adults contained about 2.5-times more $CD4^+$ than $CD8^+$ T lymphocytes and lymphocytes made up 16% of the immune cell population found [32].

Capillaries then start growing into the haematoma and reorganisation into granulation tissue proceeds. The cytokines and GFs secreted are TGF-β, platelet derived growth factor (PDGF), bFGF, VEGF, macrophage colony stimulating growth factor (M-CSF), IL-1 and -6, bone morphogenetic proteins (BMPs), and TNF-α [30]. Due to the cytokines and GFs, additional inflammatory cells are recruited into the fracture gap and migration and invasion of multipotent MSCs is induced within the first days of healing. MSCs present in the fracture gap may originate from several sources including the periosteum, endosteum, blood, and bone marrow [33-35]. They are important during fracture healing as they are able to differentiate among others into chondrocytes and osteoblasts. In *in vitro* experiments, a possible signalling effect on osteoclasts has been demonstrated. However, this is not known for *in vivo* [33, 34].

Fibroblasts and chondrocytes start in the second stage to lay down the soft or internal callus in the fracture gap consisting of fibrous and cartilaginous tissue which gives the fracture mechanical stability and serves as a template for the following bony callus (Fig. 1.1b). Due to the expression of factors, like acidic fibroblast growth factor (aFGF), PDGF, insulin-like growth factor (IGF), TGF-β2+3, and BMPs, the proliferation of both fibroblasts and

chondrocytes is promoted, resulting in progression of chondrogenesis. This initiates endochondral or indirect bone formation. Some of the factors (aFGF, TGF-β, BMPs) and VEGF act as pro-angiogenic factors, attracting vascular endothelial cells and stimulating angiogenesis [26, 29, 30]) and capillary ingrowth. Meanwhile, the external callus is created by intramembranous ossification (direct bone formation) at the periosteum [26].

In the third stage, osteoblasts form a mineralised bone matrix (osteogenesis) that replaces the fibrocartilaginous matrix of the soft callus (Fig. 1.1c). This phase is also referred to as primary bone formation. Matrix metalloproteases (MMPs) are needed for the soft callus remodelling. During the endochondral bone formation, MMP-13 (collagenase-3), MMP-2 (gelatinase A) and MMP-9 (gelatinase B) are needed to degrade the cartilaginous matrix to clear space for the bony matrix and vascular ingrowth [20, 22]. The latter improves the oxygen supply at the fracture site, which had a low oxygen tension till now. This is supposed to facilitate the differentiation of MSCs to osteoblasts and promotes fracture healing [29, 30].

Finally, the hard callus is remodelled into the cortical bone's original shape (Fig. 1.1d). This phase is also referred to as secondary bone formation. Here osteoclasts play a major role. They resorb the woven bone supported by osteoblasts, which lay down new bone at the resorption sites to regain a trabecular bone structure. Osteoblasts secrete RANKL and M-CSF. Further, factors like ILs, TNF, TGF, and BMPs are present in the healing fracture and all those factors are known to stimulate osteoclasts. ILs and TNF are known to induce chondrocyte apoptosis. If those factors are absent, a delayed resorption occurs and new bone formation is prohibited [29].

1.5.3 Loading environment occurring during fracture healing

In order to study the effects of an *in vivo*-like mechanical stimulation, the loading parameters need to be assessed in humans or in animal models. The degree of loading depends on the fracture fixation, its type and stability, and the use of the affected limb. During fracture healing different loading situations may occur: axial compression, torsion, and shear.

External fixators are common in studies of fracture healing in large animal models allowing for varying degrees of axial, torsional, and shear movement. Those studies usually describe bone healing, regarding the amount of bone formed and vascularisation induced, in relation to the loading situation. Further, finite element models (FEM) are used to investigate the effect of different loading situations contributing to tissue differentiation and healing outcome.

Normally induced interfragmentary movement was measured in patients wearing external fixators to stabilise tibial fractures. The gap size was 1.0 ± 0.5mm and appeared to be

compressed by up to 100%. Most likely, the largest compressions determined had an inhibitory effect on healing in the early phase as suggested by previous animal studies. However, the patient cohort was too small to give detailed information about the healing outcome [36]. With an external fixator used to stabilise ovine and human fractures, a displacement of up to 30% resulted, if applied for a short period each day, in enhanced healing observed as an increased rate of mineralisation and fracture stiffness [4]. Further, compression of an osteotomy gap in sheep, reaching up to 19%, resulted in a 25-times larger callus and therefore increased bone formation compared to distraction. However, bony bridging of the gap did not occur [37]. Interfragmentary movements should not exceed a level where mainly fibrocartilaginous matrix is formed. Small interfragmentary movements were found to have a higher vessel formation, especially close to the periosteum correlating positively with the amount of bone formation. This led the authors to the conclusion that fracture stability in the late phase is important for tissue differentiation and revascularisation [38]. Although larger interfragmentary movements in the initial phase induced a higher torsional stiffness of the bone at the study's endpoint [39], larger shear movements reduced the initial blood supply resulting in a less optimal healing path [40]. Therefore, an initial stability is important, too. Further, mechanical instability resulted in delayed healing with reduced angiogenesis correlated with a differential change in angiogenic factor expression compared to standard healing under stable conditions [41].

There are different theories out there how mechanical loads affect tissue formation/differentiation. An early one is from Pauwels, hypothesizing that deviatoric stresses accompanied by some kind of strain result in either fibrous or bony tissue and hydrostatic stresses result in cartilaginous tissue [42]. To reach an effective intramembranous bone formation, the strain situation needs to be favourable for osteoblasts' proliferation and activity [43]. The newer quantitative tissue differentiation theory by Claes and Heigele (1999) proposes that new tissue formation correlates with the local mechanical stimuli resulting in new bone formation primarily along fronts of existing bone or calcified tissue. They used this theory in a FEM based on a 3mm osteotomy gap with 1mm interfragmentary movement. Over the modelled course of healing (eight weeks), the interfragmentary movement decreased from 1.2mm to 0.1mm [44]. The model predicted intramembranous bone formation periosteally for strains of ±5% and endochondral ossification first endosteally than periosteally at strains of ±15%. Another FEM predicted that axial strain has the strongest effect on tissue differentiation during the onset of healing [45]. Experimental assessment of the strain

distribution in a freshly harvested section of an ovine osteotomy callus supported the findings of both models [46].

1.5.4 Mechanical stimulation of cells

Different devices and kinds of stimuli can be employed to assess the effect of mechanical stimulation on the cellular response.

1.5.4.1 Devices and different kinds of stimuli

As reviewed by Brown in 2000, there are many different kinds of *in vitro* devices and techniques to apply different kinds of mechanical stimuli to cells in 2D cultures [47]. Some of those devices are commercial ones but plenty of custom-made devices also exist. The devices can be distinguished by their primary loading modalities. They may apply either compression (hydrostatic or platen abutment, confined or unconfined), tension (uni- or biaxial, where in uniaxial tension the Poisson effect is experienced), bending (combination of compression and tension), fluid shear stress, or a combination of mechanical stimuli.

However, the combinational application of different stimuli is usually a side effect and not wanted as this does not allow distinguishing from which mechanical stimulus the biochemical effects on cellular level result. If, for instance, an out of plane distension of the cell culture substrate is used to apply tension, additionally fluid shear forces will act on the cells.

To apply tension to cells often silicon substrates are used, mostly coated with ECM proteins (here collagen) adjusted to the cell type to be seeded on them [43, 48-51]. One widespread commercial system using such substrates is the Flexercell (Flexcell International Corporation, Hillsborough, NC, USA). In 1987 Banes and colleagues commercialised the parent model of the Flexercell, then still using plastic Petri dishes allowing only the application of very small strains by application of a vacuum deforming the bottom of the dish [52]. The design was constantly analysed and improved in the 1990's [53, 54]. A recent Flexercell model, the FX-4000T is designed to apply biaxial strains between 0.7% and 20% if used with 25mm loading posts. A vacuum is used to strain the silicone substrate over the loading post (Fig. 1.2).

Not only 2D cell cultures are mechanically stimulated but also cells cultured in 3D matrices often referred to as scaffolds. There are many custom-made 3D bioreactor systems applying different kinds of stimuli like perfusion or compression (for general review see [55, 56]). Those bioreactors were developed to resemble the *in vivo* situation *in vitro* as close as possible. Therefore, those results gained have a higher clinical relevance than the ones from 2D experiments.

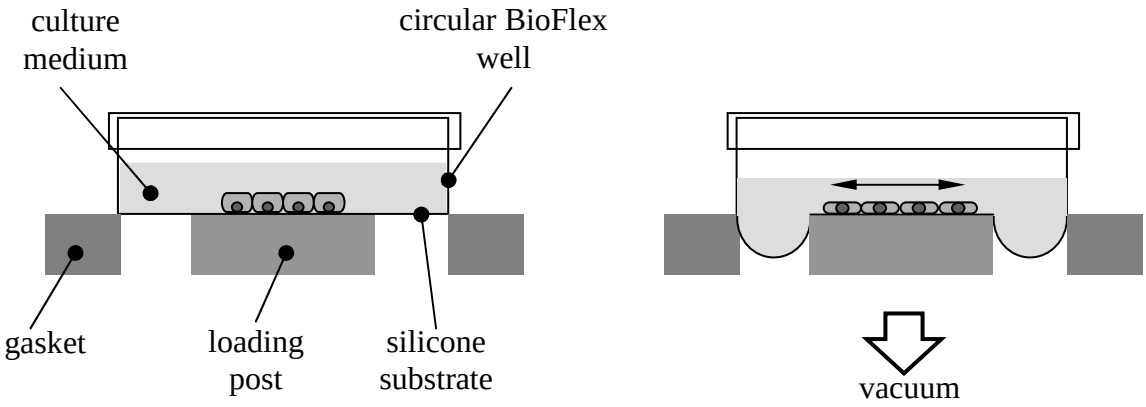

Fig. 1.2: Functional principle of the Flexercell.

Reproduced from Flexcell International Corporation, Hillsborough, NC, USA.

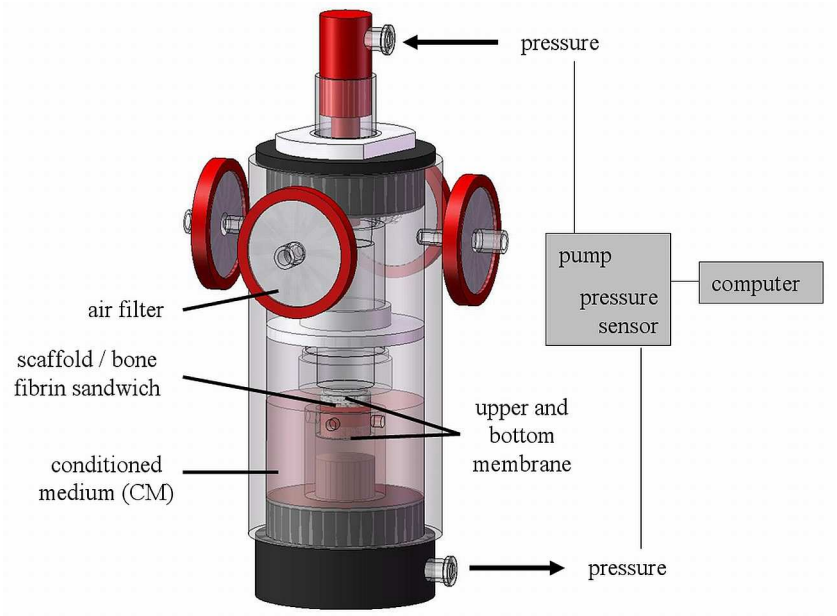

Fig. 1.3: Bioreactor setup.

Included with kind permission from J.-E. Hoffmann, Julius Wolff Institute, Charité – Universitätsmedizin Berlin, Germany.

A bioreactor described by Matziolis and colleagues applies compression to scaffolds [57]. The up-to-date setup is shown in Figure 1.3. Briefly, the scaffold is placed between two silicone membranes of which the upper membrane is displaced pneumatically to deform the scaffold. The bottom membrane is via a tube connected to a pressure transducer. The mechanical stimulation of the scaffold is controlled using a closed loop controller, implemented on a PC. It allows for compression in the range of axial interfragmentary movement, described earlier, during fracture healing.

1.5.4.2 Mechanotransduction

The process by which a mechanical stimulus results in a biochemical effect is called mechanotransduction and must be understood in multilevel terms, from the macroscopic level (body/organ/tissue) down to the microscopic (cellular, ECM) and nanoscopic (molecular) level [58, 59].

There are several cellular components known to take part in mechanotransduction: integrins, stretch activated ion channels (SACs), receptor tyrosine kinases (RTKs), the cytoskeleton, mitogen-activated protein kinases (MAPK, including extracellular signal-regulated kinase (ERK1/2), p38-mitogen-activated protein kinase, and JNK), and G-proteins [60]. Rubin et al. (2006) described candidate/putative mechanoreceptors more generally as channels, membrane structures, cytoskeleton and integrins. These structures require a direct or indirect connection with the outside by attachment to a substrate or an intermediary as the apical membrane [61]. Further, cell-cell contact via, for instance, gap junctions are thought to be important, too [62]. An illustration of the mechanotransduction process is shown in Figure 1.4.

Integrins are transmembrane heterodimers that consist of one covalently bound α and β subunit each. Many different integrins can be combined from 24 different α and 9 β subunits. Each α-β combination is specific for certain ligands [63]. They connect the ECM with the intracellular cytoskeleton. To the latter they are bound via a protein complex containing among others paxillin, caveolin and focal adhesion kinase (FAK). Upon binding to ECM ligands a signal is transferred over the membrane whereby several cellular functions as cellular attachment, proliferation, migration and differentiation are regulated. During those processes several kinases are activated leading to an induction of signalling cascades involving for instance the phosphorylation of ERK1/2 and JNK [60, 62]. According to Wang and Thampatty (2006) the ECM – integrin – cytoskeleton pathway is one of the most studied signalling pathways in mechanotransduction.

The cytoskeleton itself withstands deformation to allow the cell to maintain its shape. It is a filamentous network of microfilaments (composed of actin), microtubules and intermediate filaments of which each filament type has a different strength and elasticity. Therefore, if an integrin receives a mechanical stimulus the structure of the cytoskeleton can change and results in an activation of a signalling cascade [60].

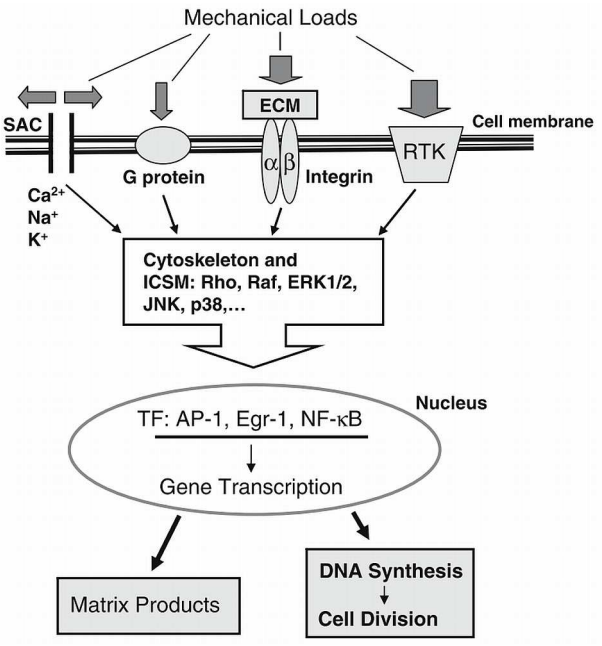

Fig. 1.4: Conceptual illustration of the mechanotransduction process.

TF: transcriptional factors, ICSM: intracellular signalling molecules, adopted from [60].

SACs are either activated/opened due to a stretch applied to the cell membrane or as a result of their cytosolic phosphorylation. They are linked to the cytoskeleton and enable the movement of ions like Na^+, K^+, and Ca^{2+} into and out of the cell. Changes in the Ca^{2+} level regulate cellular processes as cell growth, movement, contraction, apoptosis, and differentiation [60, 62].

RTKs are a group of transmembrane proteins which are involved in signal transduction. They appear to be important in integrin mediated signalling. Upon binding of a ligand as, for instance, a growth factor a receptor dimerisation occurs and results in a cascade of complex signalling events. Further, they are involved in the activation of MAPK [60].

G-Proteins initiate a signalling cascade due to a conformational change resulting from mechanical forces acting on them [60].

Many different cell types – among those different mesenchymal cells: chondrocytes, fibroblasts, osteoblasts, MSCs – have been subjected to a mechanical stimulus followed most often by an analysis of the biochemical/molecular effects, gene and protein expression, but also changes in cellular shape, orientation, and strain, cytoskeleton or position of mechanotransducers were investigated [9, 43, 49, 50, 64-67].

Proliferation, ECM gene and protein expression is affected by mechanical stimulation of cells [60]. Bone marrow-derived progenitor cells appeared to proliferate less upon cyclic uniaxial mechanical stimulation with 10% strain at 1Hz for 7 days. Further, the cells showed

alignment perpendicular to the direction of stretch with formation of aligned actin stress fibres [68]. Both application of 1% biaxial strain and microgravity for ten minutes induced in osteoblastic cells activation of all members of the immediate early response transcription factor activating protein-1 (AP-1) complex [69]. This protein complex is mainly composed of Jun, Fos and ATF protein dimers [70]. Results suggested the translocation of AP-1 is mediated by extracellular signal-regulated kinases (ERK1/2) [69]. Cyclic biaxial straining of MSCs with 3% strain at a low frequency for up to 12 days in the presence of osteogenic medium reduced the proliferation. Further, it was shown that mineralisation by MSCs is mediated through ERK1/2 signalling but p38 MAPK pathway appears to have an inhibitory role in osteogenic differentiation [71]. Intermittent stimulation of osteoblasts with 1.3% strain at 0.25Hz over 4 days resulted in an accumulation of vinculin and fibronectin, both ECM proteins, and changes in the cytoskeletal arrangement likely facilitating tighter adhesion of the cells to the ECM [67].

It was proposed that αVβ3 integrin plays a key role in mechanotransduction in osteocytes and that αVβ3's signalling interacts with SAC function [72]. Further, hydrostatic pressure was shown to increase proliferation of ECs which could be blocked by an αV antagonist [73]. Integrin αVβ3 is important for angiogenesis [74, 75] and therefore possibly plays a role in bone healing. Human bone marrow stromal cells, shown to be part of the osteoblast lineage, were subjected to an average strain of 7% for two days. This induced formation of αVβ3 integrin plaques that co-localised with osteopontin and focal adhesion kinase (FAK) but no other classically to focal adhesion associated proteins as vinculin and talin. It was concluded that αVβ3 may participate in ECM organisation [76]. A similar observation regarding a position change of integrins was made for β1 integrin under fluid shear in osteoblastic cells [66]. Still, in this case the integrins were recruited to focal adhesions. Fluid flow was as well shown to induce clustering of αVβ3 integrin and phosphorylation of ERK. However, those processes seem not to be coupled as shown by blocking of that integrin [77]. Tang and colleagues describe six hours after a 20min ultrasonic stimulation of osteoblastic cells clustering of β1 and β3 integrin. Further, phosphorylation of FAK at tyrosine 397 – a marker for FAK activation – ERK, p85, and serine 473 of Akt increased in a time dependent manner with a maximum around 15 minutes after stimulation which was diminished upon blocking of αVβ3 integrin. This is supposed, together with the other findings they made, to support their hypothesis that US stimulation promotes bone formation via the integrin/FAK/OI3K/Akt and ERK signalling pathway [78]. Further, cyclic application of 1% strain to osteoblasts induced a significant enhancement of TGF-β and cell proliferation [79].

In 3D *in vitro* studies, flow induced shear stress applied to agarose constructs containing chondrocytes induced an increase in the glycosaminoglycan content after 21 days of intermittent perfusion [80]. Further, compression of fibrin constructs containing MSCs resulted in an up-regulated protein expression of MMP-2 and its antagonist TIMP-2. However, the mRNA levels of MMP-2 were not affected, pointing to involvement of a post-transcriptional regulatory process in response to mechanical stimulation. Further, furin activity might be involved in elevation of extracellular levels of MMP-2 [65]. A similar study revealed that mechanical stimulation of MSCs induces signalling acting in a paracrine manner on ECs. This was concluded from increased tube formation induced by media, conditioned by mechanical stimulation of MSCs, that were applied to ECs. Further, pro-angiogenic protein levels, namely of TGF-β and MMP-2 were elevated. However, VEGF remained unaffected. [9].

2 Materials and Methods

This chapter describes the materials and methods used in the 2D and 3D bioreactor study to prove the hypothesis of this thesis with a brief introduction into the scientific context of each approach.

2.1 2D bioreactor study

Mechano-responsive mesenchymal stem cells and their osteoblastic descendants are key players in bone regeneration [81, 82]. They have shown, dependent on the magnitude of stimuli, a differential response in synthesis of several factors important for bone healing [83-86]. One of those factors, αVβ3 integrin, shows cluster formation and co-localised with phosphorylated focal adhesion kinase (FAK) due to mechanical stimulation of osteoblastic cells [76-78]. It is involved in angiogenesis [74, 75], which is a vital process for successful tissue regeneration.

Two-dimensional stimulation of cells is a common and straight forward method to study mechano-responsiveness and resulting effects. For this purpose several *in vitro* devices applying tensile strains have been employed over the last two decades [43, 48, 62, 87]. However, in order to examine mechanotransduction detailed knowledge of the stimulation environment as the effector is needed. Several attempts have been made to characterise strains in such custom-made and commercially available devices [49, 50, 87-89]. One contact-free technique that has been used to quantify the strains applied to substrates and adhering cells is the digital image correlation (DIC) [49, 50]. Two-dimensional DIC is based upon matching a surface pattern with varying grey value intensities on an unloaded surface (reference) to the same, but deformed pattern on a loaded surface, to allow the measurement of the resulting displacement. From the displacement measured, the Lagrangian strain tensor is calculated for every point on the surface with an accuracy of 0.02% strain [90].

The FX-4000T (Flexcell International Corp., Hillsborough, NC, USA) is a well-established device for mechanical stimulation of cells. Combined with BioFlex six-well plates (Flexcell International Corp., Hillsborough, NC, USA), this device is designed to apply biaxial, homogeneous tensile strains to cells cultured on flexible silicone rubber membranes, which are deformed by a vacuum pulling them over circular loading posts (see also Fig. 1.2). However, during the operation of the device fluid shear stresses occur additionally due to the movement of cell culture fluid [47].

Two studies from 1997 that varied fluid flow and substrate stretch independently [91, 92] suggested that osteoblast response was governed by fluid flow and not affected by substrate

strain and strain rate magnitude, while simulations pointed to differing influences on cell deformation for substrate stretch and fluid flow [93].

To date, neither a full-field experimental mechanical characterisation of the strain to which the cells are exposed within the FX-4000T nor the fluid shear stimuli is available. In order to resolve these issues and provide a framework for interpreting the results of stimulation experiments, the present study aimed to provide a comprehensive, validated characterisation of mechanical conditions in this cell stimulation device. First the strain distribution on the membrane was to be examined, in particular its consistency with rising numbers of cycles, as well as the amount of strain transferred to cells adhering to the surface. Furthermore, the time varying fluid shear stress field experienced by cells cultured in BioFlex wells in the FX-4000T device was to be assessed, including its spatial homogeneity and the effects of stimulation frequency and magnitude and of culture medium viscosity. With this new information on the mechanical boundary conditions in the device, the study aimed additionally to investigate the effects of this mechanical environment on mesenchymal (osteoblastic) cells.

Digital image correlation was chosen to study the strain fields. Computational Fluid Dynamics (CFD) and particle tracking for experimental validation of the former were used to study the fluid shear stress field, and immunocytochemistry was used to assess the molecular cell response.

2.1.1 Materials

Tab. 2.1: Materials used for 2D bioreactor study.

Product	Company	Product No	Comment
2-Propanol	Roth	9866,1	
Alexa Fluor 546	invitrogen	A11030	
α-MEM	Lonza	BE-12-196F	
αVβ3 antibody	abcam	ab7166	
Ampuwa	Fresenius Kabi France Louviers	7151-3	
BSA	Sigma	A7906	
DAPI	invitrogen	D1306	
EDTA	Sigma	E6511	

Continued on following page.

Tab. 2.1: continued.

Product	Company	Product No	Comment
Ethanol	Roth	5054,1	
FAK Tyr397 ELISA	Merck UK, Calbiochem	CBA062	
FCS	Lonza	DE14-802F	Lot 5SB0018
Fluoromount-G	SouthernBiotech	0100-01	
iScript^{TM} cDNA synthesis kit	BioRad	170-8891	
L-Glutamine 200mM	Gibco	250-30-024	
Paraformaldehyde	Merck	1.040.051.000	
PBS	PAA	H15-002	
PBS (10x)	Chroma	3L-175	immunohistology
Penicillin 10,000 U/ml / Streptomycin 10,000 µg/ml	Biochrom	A 2212	rat cells
Penicillin 5,000 U/ml / Streptomycin 5,000 U/ml	Lonza	DE17-603E	chicken cells
Phalloidin Alexa 488	Invitrogen	A12379	
Polystyrene microparticles, 10µm, green fluorescing	Duke Scientific (Thermo Scientific)	G1000	
Sodium pyruvate 100mM	Lonza	13-115E	
Triton X 100	Sigma	T8787	
Trizol	invitrogen	15596-018	
Trypsin	Serva	37290	
Ultraglutamine I 200mM	Lonza	BE17-605E/U1	

2.1.2 Flexercell characterisation

This characterisation includes the determination of the strain distribution, its consistency, and its transfer to cells as well as the assessment of the fluid shear stress environment within the Flexercell.

2.1.2.1 Characterisation of applied strains using DIC

The strain field characterisation was performed as published [51]. Briefly, collagen type I coated BioFlex plates of the same batch received an airbrush speckle pattern as landmarks for quantification of membrane surface strains ($\boldsymbol{\varepsilon_{mem}}$). Thirteen wells were photographed at different programmed static strains ($\boldsymbol{\varepsilon_{prog}}$) between 2.5% and 10% (in steps of 2.5%) stretched over 25mm loading posts using the FX-4000T. For brevity, only strain abbreviations as given in Tab. 2.2 were used after first appearance.

The images of the strained membrane (silicon substrate) were compared with the reference image using DIC taken at $\boldsymbol{\varepsilon_{mem}}$ = 0% (Vic2D, Correlated Solutions, Columbia, SC, USA). A preliminary test using DIC on the whole membrane across the loading post in four wells

identified a circular area with a radius, R ≈ 9mm showing homogeneous strain with a mean of the standard deviations equal to 0.09% strain at $\boldsymbol{\varepsilon_{prog}}$ = 2.5% and 0.23% strain at $\boldsymbol{\varepsilon_{prog}}$ = 10%. Subsequent principal strains (mean $\boldsymbol{\varepsilon_{mem}}$ ± SD) measurements were only performed within this homogenous area (region of interest = ROI) at each analysed cycle number. The mean εmem of approx. 4000 data points per ROI was compared to the mean strains reported by the controller ($\boldsymbol{\varepsilon_{rep}}$) during image acquisition. To test the strain consistency with rising number of cycles, applied at 2.0Hz with 5% sinusoidal strain between image acquisitions, εmem was determined after 0, 2700, 5400, and 10800 load cycles.

Tab. 2.2: Abbreviations used for strains studied, adapted from [51].

abbreviation	name	explanation
$\boldsymbol{\varepsilon_{prog}}$	programmed strain	user programmed strain entered in device software
$\boldsymbol{\varepsilon_{rep}}$	reported strain	strain reported by transducers in the FX-4000T controller device
$\boldsymbol{\varepsilon_{mem}}$	membrane strain	strain determined on surface of BioFlex membrane by DIC
$\boldsymbol{\varepsilon_{cell}}$	cellular strain	strain determined on cell processes, bodies, and carpets

To check for a change in material properties after 10800 cycles, the effective Young's modulus of six membrane specimens cut from the six wells of an unused BioFlex well plate was calculated and compared to that of six previously stretched membranes. This was, as part of a collaboration, performed at the Institute of Biomedical Engineering, Department of Engineering Science, University of Oxford, UK with British Standard type 1B specimens (BS 2782-2, 1996) cut with a scalpel from each well containing a speckle pattern as previously described. They used a similar procedure including DIC to determine average strains within the gauge section of each specimen, which delivered the input data for subsequent calculation of the Young's modulus. For details on the procedure see [51].

Data analysis was performed by linear regression and tests of significance, using mean values calculated from DIC data. The Wilcoxon test for two non-parametric, associated samples with $p < 0.05$ (SPSS 14.0.1, USA) was used to test for significant differences.

2.1.2.2 Determination of strain transferred to mesenchymal cells

To determine the extent of strain transfer to cells in the FX-4000T, chicken bone marrow-derived stromal cells (BMSCs) were strained using collagen type I coated BioFlex six-well plates. During this process they were imaged using fluorescence microscopy. For this procedure BMSCs were isolated from embryonic stage E18 chicken tibiae and infected with Replication-Competent ASLV long terminal repeat with a Splice acceptor (RCAS) vector system [94] carrying the coding sequence for eGFP. Those preparations were collaboratively

performed at Max-Planck-Institute for Molecular Genetics, Berlin, Germany. For details see [51].

With about 30% confluence fluorescent passage 6 to 7 BMSCs were seeded onto BioFlex six-well plates. For at least 24 hours before visualisation, they were cultured in α-minimum essential medium (MEM) with 10% FBS (5SB00018), 50U/ml penicillin, 50µg/ml streptomycin, and 2mM Ultraglutamine to allow for sufficient adherence.

For visualisation of the fluorescently labelled cells in culture, the FX-4000T base plate holding the BioFlex plates was placed onto a custom-made adaptor for the motorised *x-y* table of an Axiotech vario microscope (Zeiss, Germany). The microscope was equipped with an Achroplan 10x/0.30 W Ph1 water immersion objective (Zeiss, Germany). Images (2.5pixels/µm) were taken sequentially of the cells in the reference state (0%) and at programmed static strains of 2.5%, 5%, 7.5%, and 10%, using an epi-illumination technique and an AxioCam HRc (Zeiss, Germany), without reset to the reference state in between. Thereby the earliest imaging time point was 15 seconds after strain application. Cell deformation was only determined within the specified homogenously strained membrane area staying on the loading post during stimulation.

Coordinates of prominent positions, either in cell processes, on the cell body edge or on cell carpets (80–100% confluent monolayers, reference positions: nuclei, vacuoles, etc., on average 4-5 times the cell size apart) were used to determine the strain transferred to the cells employing ImageJ 1.38x (Wayne Rasband, National Institutes of Health, USA). Subsequently calculation of the distance vectors in pixels between all the prominent positions in one image of a cell at each strain and in the reference image was performed using an R-language routine [95]. This routine determined the ratio of strained to unstrained distance which yielded the strain transferred to the cell, and the median cell strain was calculated from all $\boldsymbol{\varepsilon_{cell}}$ measurements performed. Further, these cell strains were then related to $\boldsymbol{\varepsilon_{mem}}$.

2.1.2.3 Characterisation of fluid mechanics

This was mainly performed at the Institute of Biomedical Engineering, Department of Engineering Science, University of Oxford, UK with an axisymmetric fluid structure interaction CFD model. It incorporated a pre-deformed grid to accommodate large deformations and FE simulation of contact between the post and the silicone substrate membrane, to the underside of which the pump control pressure was applied. Flow verification experiments using 10µm diameter fluorescent microspheres were carried out at the Julius Wolff Institute.

Details on the CFD model and the employed load cases will soon be published together with the experimental validation [96]. For the experimental flow verification green fluorescent (508nm, nominal diameter 10µm) neutrally buoyant polystyrene microparticles from Duke Scientific (Palo Alto, CA) were dispersed in culture medium (~1 x 10^6 particles ml^{-1}) and then with 0.1mm syringe injected during continuous operation of the FX-4000T at 0.5Hz. From injection for 12 cycles the particle motion was followed using a vertically mounted digital SLR camera (D70, Nikon, Japan) with a bellows enlarging lens giving 2.3µm/pixel at a capture rate of 3Hz. The lens was adjusted to give a focal plane lying approximately 1 mm above the membrane surface. The images were analysed using ImageJ and the ParticleTracker plug-in [97] to calculate resultant velocities per cycle.

2.1.3 Influence of characterised mechanical environment on mesenchymal cells

The influence of the now characterised mechanical environment on mesenchymal cells, namely osteoprogenitors, was then assessed using an immunocytochemical approach.

2.1.3.1 Cell culture of osteoprogenitor/osteoblast like cells and mechanical stimulation

Under aseptic conditions, long bones with surrounding soft tissue were extracted from cadavers of three months old Sprague Dawley rats. All remaining soft tissue and the periosteum, as far as possible, were removed. Subsequently, the epiphysis was removed and the bones were chopped into small pieces using a bone forceps. The bone pieces were vortexed with PBS repeatedly until there was no blood visible anymore. The clean bone chips of two long bones from the same animal were transferred into T75 culture flasks and culture medium (α-minimum essential medium, 10% heat-inactivated FBS (5SB00018), 100U/ml penicillin plus 100µg/ml streptomycin, 2mM L-glutamine, 1mM sodium pyruvate was added. Cells were left to grow out of the bone until they reached 70-80% confluence and were then passaged. Medium was exchanged every three to four days.

In passages one, three and four, the osteoblast-like cells were lysed using the Trizol reagent, subsequently the RNA was extracted and cDNA was synthesised using the iScript™ cDNA synthesis kit according to the manufacturer's instructions. This was followed by a screening for osteogenic markers (Bglap2, TNSALP, Ibsp, Spp1, Col1a2, Cbfa1Runx2; Primer sequences in Tab. 2.3) where cDNA from murine MSCs, derived from bone marrow, served as negative control. The marker expression was clearly higher in the osteoblast-like cells.

To stimulate those cells mechanically, they were seeded at a density of $2x10^4$ cells/well onto the central region of BioFlex wells using custom made glass cylinders. This region is supposed to be stretched homogeneously when using the FX-4000T [51]. On day 8 after

seeding, 1200cycles of 4% sinusoidal ε_{mem} were applied at 1Hz using the FX-4000T. This resulted according to the previously mentioned CFD model in an approximate fluid shear stress of 0.09Pa. Unstimulated cells cultured under the same conditions served as control. Those strain conditions offer reproducible strains (deviation <10%) over time, as determined in the Flexercell characterisation (see also 2.1.2). The stimulus used was the smallest possible strain that could be applied reproducibly by the system. Further, this strain was found to be well tolerated by osteoblast-like cells as found in a pre-screening experiment as no detachment was observed right after application of the stimulus. Furthermore, tensile strains up to 5% were predicted to be favourable for intramembranous bone formation [44].

Tab. 2.3: Primer sequences used to test for osteoblastic phenotype.

House keeping genes			
Glyceraldehyde-3-phosphate dehydrogenase	GAPDH	Left Primer	ATGGGAAGCTGGTCATCAAC
Glyceraldehyde-3-phosphate dehydrogenase	GAPDH	Right Primer	GTGGTTCACACCCATCACAA
Actin, cytoplasmic 1 (Beta-actin)	ACTB	Left Primer	TGTCACCAACTGGGACGATA
Actin, cytoplasmic 1 (Beta-actin)	ACTB	Right Primer	GGGGTGTTGAAGGTCTCAAA
Marker genes for osteogenic lineage			
Collagen type I	Col1a2	Left Primer	GGAGAGAGTGCCAACTCCAG
Collagen type I	Col1a2	Right Primer	CCACCCCAGGGATAAAAACT
Runt-related transcription factor 2	Runx2	Left Primer	GCCGGGAATGATGAGAACTA
Runt-related transcription factor 2	Runx2	Right Primer	GGACCGTCCACTGTCACTTT
Osteocalcin	Bglap2	Left Primer	TGAGGACCCTCTCTCTGCTC
Osteocalcin	Bglap2	Right Primer	AGGTAGCGCCGGAGTCTATT
Alkaline phosphatase	TNSALP	Left Primer	CCTTGAAAAATGCCCTGAAA
Alkaline phosphatase	TNSALP	Right Primer	CTTGGAGAGAGCCACAAAGG
Osteopontin	Spp1	Left Primer	GAGGAGAAGGCGCATTACAG
Osteopontin	Spp1	Right Primer	ATGGCTTTCATTGGAGTTGC
Bone sialoprotein 2	Ibsp	Left Primer	TCTGCATTTTGGGGATGG
Bone sialoprotein 2	Ibsp	Right Primer	CCGTTTCAGAGGAGGATAAAAG

2.1.3.2 Immunohistology

BioFlex wells with cells in passage three were washed twice with PBS (1x) three days after mechanical stimulation, fixed with 4% PFA for 10', and washed three times with PBS. The cell free bottom of the BioFlex wells was marked to distinguish samples and the Bioflex membranes were cut out of the wells using a scalpel. Cells were permeabilised using 0.2% Triton (5min), washed three times with PBS, and were then blocked with 3% bovine serum albumin (BSA) in PBS for 20min. 60' incubation with the primary antibody (αVβ3, 1:100) in PBS/BSA followed, with three subsequent washing steps. The secondary antibody (Alexa Fluor 546 anti-mouse, 1:200) in PBS/BSA was applied for 45'. Further, the slides were washed once and counterstained with 1:1000 phalloidin Alexa 488 for 2' to visualise the actin filaments. After two more washing steps, the nuclei were stained with 1:1000 DAPI for 2'.

Two more washing steps with PBS and one with distilled water followed before the slides were finally covered with Fluoromount G and a cover slip.

2.1.3.3 ELISA

BioFlex wells with cells in passage four (donor A+B) and one (donor C) were washed twice with ice-cold PBS 15min and three hours after mechanical stimulation. 100µl of cell lysis buffer were added to each well and incubated for 30min. This buffer was prepared in advance following the recipe recommended by the manufacturer of the PhosphoDetect™ FAK ($pTyr^{397}$) ELISA Kit. Cells were then scraped and the suspension was transferred into tubes and spun down. The supernatant was transferred into a new tube. From here on the protocol of the ELISA manufacturer was followed. Units of phosphorylated FAK were measured in duplicates per sample.

2.2 3D bioreactor study

Mechanical stimuli are able to improve, but also to delay bone healing [4, 36, 38-40]. They result in a change of revascularisation, bone formation, and differential change in the expression of angiogenic factors [37, 38, 41] Further, in delayed healing expression of markers for cartilage formation, bone formation, ossification, and bone remodelling was found to be reduced compared to normal bone healing including TGF-β1 [98]. Mechano-responsive cells, like MSCs and their differentiated successors, are responsible for the processes occurring on the molecular level, which are important for tissue development and healing [9, 71, 78].

Furthermore, MSCs are known to have an immunomodulating character [99]. The immune reaction – proliferation, cytokine production, and cytolytic T lymphocyte activity – of $CD4^+$ and $CD8^+$, naïve and memory T cells is suppressed by MSCs in a dose dependent manner [100, 101]. In addition, MSCs promote differentiation of $CD4^+$ cells towards regulatory T lymphocytes ($CD25^+$ and/or $CTLA4^+$) [101]. Krampera et al. suggested that MSCs physically hinder contact of T lymphocytes with antigen presenting cells (APCs) [102].

If cell-cell contact is possible, activated T lymphocytes could rapidly bind to allogenic MSCs and transmigrate among them. This cell-cell contact significantly increases the inhibitory effect of soluble mediators such as interferon γ (INF-γ) generated by the lymphocytes themselves on their proliferation [103]. INF-γ activates indoleamine 2,3-dioxygenase in MSCs, which results in a depletion of tryptophan leading to a proliferation arrest in T lymphocytes [103, 104]. MSCs express only low levels of major histocompatibility complex (MHC)-I but no MHC-II. However, if a large number of MSCs is present as well as INF-γ, MSCs gain the ability to present antigens *in vitro* [104]. Furthermore, MSCs strongly inhibit proliferation of activated T lymphocytes as they arrest them in G0/G1 phase of the cell cycle [104].

T lymphocytes are mainly known to occupy a vital role in the adaptive immune response. Activators for them are antigen presenting cells (APCs) via MHC molecule I or II bound antigens and co-stimulating factors, such as B7-1 and -2 for $CD4^+$ cells. $CD4^+$ cells via stimulation of APCs are co-stimulators of $CD8^+$ cells. MHC-II bound antigens activate $CD4^+$ whereas MHC-I bound antigens activate $CD8^+$ cells. Activated $CD4^+$ cells secrete IL-2. MHC-I is expressed on every nucleated cell in the human body but MHC-II only by APCs [105].

However, T lymphocytes are regulators of wound healing, too [106]. While depletion of $CD8^+$ T lymphocytes improves wound healing, pointing to a counter-regulatory role, depletion of $CD4^+$ T lymphocytes does not have this effect [107]. Still, in MHC-II deficient mice, lacking $CD4^+$ dependent immune reactions, wound healing was compromised [108]. If the subset expression CD3, a pan T lymphocyte marker, was depleted wound healing was impaired, too [109]. Yet, the role of T lymphocytes in bone healing has not been elucidated, although early bone formation and subsequent mechanical competence of fractures is accelerated in lymphocyte deficient $RAG1^{-/-}$ mice. The latter are lacking the adaptive immune response [10] that is facilitated by cells, such as T lymphocytes. RAG1 and 2 are genes encoding for gene recombinases that are needed during the maturation of lymphocytes going through somatic recombination of antigen recognizing receptors to enable the diversity of antigen recognition [105].

To gain a better insight into the processes involved in bone healing on the molecular level, which are induced by mechanical stimulation, *in vitro* studies are extremely useful. Within a reasonable time frame and without animal studies, the molecular events may be studied. Therefore, experimental setups are necessary that resemble the *in vivo* situation as close as possible with well defined boundary conditions. For instance, a bioreactor setup that resembles the fracture haematoma may be chosen. The haematoma consists of a fibrinous clot containing immune cells and a very small portion of mesenchymal cells.

A compression of up to 30% of a 3mm gap between bone fragments was previously found to be favourable for bone healing [4, 44]. An in-house study used cyclic compression of a fibrin matrix of approx. 3mm thickness, which contained mesenchymal stem cells (MSCs), in order to study how it affects the angiogenic potential of MSCs. Pro-angiogenic factors as TGF-β1, MMP-2, and bFGF were enhanced after stimulation. It was further demonstrated that medium conditioned by stimulation of the cell-matrix constructs induced an increased tube formation of endothelial cells seeded onto Matrigel, possibly due to paracrine-acting pro-angiogenic factors [9].

However, angiogenic and other molecular processes going on during mechanically induced tissue regeneration have not fully been elucidated. Especially, the involvement of immune cells, namely T lymphocytes, and the effect of mechanical stimulation on them has not been studied so far. This will close the gap between two in-house-studies, i.e. the above described stimulation of MSCs in a fibrin matrix and the stimulation of human fracture haematomata, too, embedded in fibrin, which was examined in a parallel study performed by Aline Groothuis.

Therefore, the present study aimed at comparing the molecular response of MSCs, T lymphocytes and their co-culture to cyclic compression in a haematoma-like environment to determine their importance for mechano-regulated angiogenesis, which is essential for tissue regeneration. It was hypothesised that T lymphocytes are less mechano-responsive than MSCs and, if co-cultured, their mechano-response regarding their angiogenic potential is affected by immunomodulation.

As a proof of principle, MSCs were stimulated in a bioreactor as used by Kasper et al. A detailed description of the bioreactor may be found in chapter 2.4.1. In parallel, T lymphocytes and their co-cultures with MSCs were subjected to the same stimuli. Subsequently, the protein secretion and paracrine effect on angiogenesis in a 2D tube formation assay was assessed for both cell types and their co-culture. The latter is supposed to give hints on the interaction of MSCs and T lymphocytes in a fracture haematoma, especially under mechanical stimulation. In addition, the mRNA expression of all experimental groups was analysed using a gene expression array.

2.2.1 Materials

Tab. 2.4: Materials used for 3D bioreactor study.

Product	Company	Product No	Comment
2-mercaptoethanol	Sigma	M7522	
2-propanol	Roth	9866,1	
AB complex	Vector	AK 5000	
Alkalische Phosphatase Universal Kit	Vector	AK-5200	
Amicon Ultra-4 PL-5	Millipore	UFC8 005 24	
Ampuwa	Fresenius Kabi France Louviers	7151-3	
Aquatex	Merck	1,08562	
bFGF ELISA	R&D	DFB50	
biotinylated goat-anti-rabbit IgG	Vector	BA-1000	
BSA	Sigma	A7906	
CD105 APC labelled	eBioscience	17-1057-71	
CD14 PE labelled	BD Bioscience	555398	
CD19 APC labelled	BD Bioscience	555415	
CD34 FITC labelled	BD Bioscience	555821	
CD4 MicroBeads	Miltenyi	130-045-201	
CD4 PE labelled	Miltenyi	130-091-231	
CD45RA APC labelled	invitrogen	MHCD45RA05	

Continued on following page.

Tab. 2.4: continued 1.

Product	Company	Product No	Comment
CD73 PE labelled	BD Bioscience	550257	
CD8 FITC labelled	Miltenyi	130-080-601	
CD8 MicroBeads	Miltenyi	130-045-101	
CD90 PE labelled	BD Bioscience	555596	
CellTiter 96® AQueous Non-Radioactive Cell Proliferation Assay	Promega	G5421	
Dako (antibody) Diluent	Dako	S3022	
DMEM	Gibco	41965	
EDTA	Sigma	E6511	trypsinisation, histology
EDTA	Sigma	EDS22	MACS
Endoglin rabbit polyclonal IgG	Santa Cruz	sc-20632	
Ethanol	Herbeta	200-578-6	histology, bioreactor sterilisation
Ethanol	Roth	5054,1	RNA isolation
fat pen (Dakopen)	Dako	S2002	
FCS	Biochrom	S0115	Lot 1038K
Flebogamma (50mg/ml)	Grifols		
Harris' Haematoxylin	Merck	1,09253	
HEPES	Sigma	H4034	
Histopaque-10771	Sigma Aldrich	10771	
HLA-DR PE labelled	BD Bioscience	555812	
Hydrocortisone	Invitrogen	H0888	
IL-2 ELISA	R&D	D2050	
iScript™ cDNA synthesis kit	BioRad	170-8891	
L-Glutamine 200mM	Gibco	250-30-024	
LS columns	Miltenyi	130-042-401	
Matrigel	BD Bioscience	354234	
Mayer's Haematoxylin	Merck	1,09249	
MCDB131	Gibco	10372	
MMP-2 ELISA	R&D	DMP2F0	
MMP-9 ELISA	R&D	DMP900	
NaCl	Merck	6404	
Normal serum goat	Vector	S1000	
Pan T cell isolation kit II	Miltenyi	130-091-156	
Paraffin (Paraplast Plus Tissue Embedding Medium)	McCormick Scientific	502004	

Continued on following page.

Tab. 2.4: continued 2.

Product	Company	Product No	Comment
Paraformaldehyde	Merck	1.040.051.000	
PBS	PAA	H15-002	
PBS (10x)	Chroma	3L-175	
Penicillin 10,000 U/ml / Streptomycin 10,000 µg/ml	Biochrom	A 2212	
Propidium Iodide	Sigma	P4170	
RNase-Free DNase Set	Quiagen	79254	
RNeasy Mini kit (50)	Quiagen	74104	
RPMI1640	Gibco	31870	
Sodium azide	Merck	1.06688.0100	
Substrate Kit	Vector	SK-5100	
TGF-beta1 ELISA	R&D	DB100B	
TIMP-2 ELISA	R&D	DTM200	
Tissucol-kit 2.0 Immuno	Baxter	2546654	
Trasylol (10,000 KIU/ml)	Bayer	Zul.Nr. 34579.00.00	
Tris Base	Sigma	T1503	
Tris HCl	Sigma	T3253	
Triton X 100	Sigma	T8787	
Trizol	invitrogen	15596-018	
Trypsin	Serva	37290	
Tween 20	Sigma	P1379	
VEGF (C-1) mouse monoclonal IgG	Santa Cruz	sc-7269	
VEGF-A ELISA	R&D	DVE00	
Xylol	J.T. Baker	8080	

2.2.2 MSCs' isolation, culture, and characterisation

Human MSCs were isolated from bone marrow aspirates gained from seven patients undergoing hip replacement. Those patients gave their informed consent and were aged between 52 and 68 years. Investigations using these cells were approved by the Ethics Commission of the Charité - Universitätsmedizin Berlin (ethics application number EA2/126/07).

Briefly, bone marrow aspirates were washed with PBS within the sample tube. Via a density gradient using Histopaque-10771, mononuclear cells were separated from all other cells and debris present in the liquid sample. The mononuclear cell layer was transferred to a T75 culture flask containing fresh cell culture medium. Cell culture medium contained DMEM, 10% FBS, and 100U/ml penicillin plus 100µg/ml streptomycin. The medium was exchanged

within 48hrs of isolation to remove non-adherent cells and after that every 3-4 days. The cells were passaged at 70-80% confluence and used for experiments from passage two to four.

MSCs were characterised by cell surface markers (CD14, CD19, CD34, CD45RA, CD73, CD90, CD105, and HLA-DR), a part of the minimal criteria to define MSCs, as stated by the International Society of Cellular Therapy [110]. Further, differentiation potential of MSCs into different mesenchymal lineages is tested on a regular basis in the lab and was not in the focus of the presented work.

The staining for the MSC specific surface markers was performed as follows: Trypsinised passage 3 MSCs were pelleted at 400x*g* for 5', once washed with 1ml FACS-buffer (PBS / 0.5% BSA / 0.02% sodium azide) per $1x10^5$ cells and then incubated with 10% Flebogamma for 10'. This was followed by a 15' incubation with the cell surface marker specific antibodies at a dilution of 1:25 at 4°C. The cells were washed as described and then fixed for 20' with 2% PFA in FACS-buffer. The cells were washed once more and resuspended in 200µl FACS-buffer. Unstained cells served as negative control. CellTrics® with 30µm filter mesh width (Partec, Germany) were used to assure that there were no cell clots possibly blocking the cytometer cuvette left in the cell suspension before performing flow cytometry (FACS CantoII, BD). The data gained was analysed using FlowJo 7.5 (Tree Star, Inc., Ashland OR, USA).

2.2.3 T lymphocytes' isolation, culture, and characterisation

First of all, hPBMCs were isolated from peripheral blood by density gradient centrifugation. Blood was gained from buffy coats purchased from the German Red Cross (DRK) Berlin. In total blood of nine different donors was used in this study. Of six donors the age was known, ranging from 43 to 65 (mean = 58) years. The blood taken from the buffy coats was diluted with ice-cold PBS/EDTA (2mM) until a total volume of 140ml was reached (1:2) and 35ml of the diluted blood were carefully layered on top of 15ml Histopaque-10771 in a 50ml Falcon tube. After a 40' centrifugation (without breaking) at 400x*g* at room temperature (RT), the mononuclear cell layer was transferred into fresh 50ml tubes and washed several times with PBS/EDTA to remove remaining platelets. Everything was performed according to the protocol "Isolation of mononuclear cells from human peripheral blood by density gradient centrifugation" recommended by Miltenyi Biotec GmbH (Bergisch Gladbach, Germany).

T lymphocytes were extracted from the hPBMCs using the Pan-T kit for magnetic cell sorting (MACS) following the manufacturer's protocol. Subsequently, the mixed T lymphocyte population was separated into a $CD8^+$, $CD4^+$ and $CD8^-CD4^-$ fraction following the

manufacturer's protocol employing LS columns. Only centrifugation times for all MACS procedures were adjusted to seven minutes as cell pellets were difficult to resuspend after the recommended time of 10'. The three T lymphocyte fractions were cultured at a density of $1x10^6$ cells/ml over night in a humidified incubator at 37°C and 5% CO_2. The culture medium contained RPMI-1640, 10% FCS, 100U/ml penicillin plus 100µg/ml streptomycin, 2mM L-glutamine, 50µM 2-mercaptoethanol, and 25mM HEPES.

The purity of $CD4^+$ and $CD8^+$ cell fraction was checked with FACS CantoII (BD) using CD4 and CD8 fluorescently labelled antibodies following the manufacturer's instructions. The gained flow cytometric data was analysed using FlowJo 7.5 (Tree Star, Inc., Ashland, OR, USA).

2.2.4 Bioreactor experiment – generation of conditioned media and determination of cell viability after mechanical stimulation

The $CD4^+$ and $CD8^+$ T lymphocyte fractions isolated on the previous day were counted using a cell counter (CASY, Schärfe Systeme, Germany) and mixed at a 2.5:1 ratio. Fracture haematoma of healthy adults contain approx. this ratio [32]. The cell mixture was centrifuged at 300x*g* for 7' and $2x10^7$ cells were either resuspended in 350µl T lymphocytes culture medium for the pure T lymphocyte fibrin constructs or in 175µl for the co-cultures.

MSCs in passage 2 to 4 were trypsinised, counted and pelleted at 375x*g*. $1x10^6$ cells were resuspended in either 350µl T lymphocytes culture medium for the pure MSC fibrin constructs or in 175µl for the co-cultures. The 175µl suspension of T lymphocytes was mixed with the according 175µl MSC suspension to receive a 350µl co-culture suspension.

Either 350µl of cell suspension or for cell free controls (negative control) 350µl T lymphocytes' culture medium was laid into a 15ml tube (TPP - Techno Plastic Products AG, Switzerland). For eight fibrin constructs 1400µl of fibrinogen concentrate (Tissucol kit 2,0 Immuno) were slowly mixed with 1400µl T lymphocytes culture medium and 240µl Thrombin S (Tissucol kit 2.0 Immuno) were mixed with 240µl T lymphocytes culture medium. For each condition (Tab. 2.5) 350µl of the fibrinogen-medium-mixture were carefully mixed with the laid cell suspensions avoiding air bubble formation. 50µl of the thrombin-medium-mixture were applied to the rim of the 15ml tube while holding it horizontally, the cap was closed tightly and the tube inverted and rotated to mix cells, fibrinogen and thrombin. The inverted tubes were placed into a humidified incubator (37°C, 5% CO_2) for at least 30' and a maximum of 1 hour to allow for gelling of the fibrin construct.

Then a spatula was used to take the constructs carefully out of the tubes. Each fibrin construct, sandwiched between two steam sterilised cancellous bone chips, was placed into the sample holder of an ethanol sterilised bioreactor. The cells embedded in fibrin were to resemble the haematoma in the early phase of bone healing between the two bone fragments. The bioreactor was then filled up with 25ml freshly prepared T lymphocyte culture medium. For details on the bioreactor used see Chapter 1.5.4.1.

Tab. 2.5: Cell compositions and conditions used in bioreactor (+ = with, - = without).

Condition / Cells used	1	2	3	4	5	6	7	8
MSCs ($1x10^6$)	+	+	-	-	-	-	+	+
T lymphocytes ($2x10^7$)	-	-	+	+	-	-	+	+
Mechanical stimulation	+	-	+	-	+	-	+	-

The bioreactors were connected to a pneumatic pump and a pressure sensor and the fibrin constructs were stimulated with ~20% compression at 1Hz for three days. This compression is within the range of favourable stimuli for bone healing as described above at the frequency of a normal gait cycle. At the end of the mechanical stimulation, the now conditioned media (CMs) were collected (kindly supported by Lauren Ehardt during her internship) and kept at -80°C until further usage. The fibrin constructs were either shock frozen in liquid NO_2 and transferred to -80°C for subsequent RNA isolation (see Chapter 2.2.9), fixed, dehydrated and embedded in paraffin for histology (see Chapter 2.2.8), or digested using trypsin to check for viability of the included cells.

To digest the fibrin constructs, each was placed into a well of a 24-well multititer plate and 1ml sterile filtered trypsin , containing 225U per millilitre PBS, was applied per construct for 15’. The cell suspension was transferred to a 15ml Falcon tube containing 5ml T lymphocyte culture medium and 2ml Trasylol (10,000 KIU/ml) to stop the enzymatic digestion. Trypsinisation was continued until all fibrin was digested, which took up to 1h. The digestion was followed by a determination of the viability of the cells using the CASY cell counter and a flow cytometric analysis.

For the flow cytometric analysis of the number of dead cells to determine cell viability, the cells were pelleted and resuspended in PBS / 2mM EDTA / 0.5% BSA. Right before the flow cytometric analysis, propidium iodide (50µg/ml) was added to the cell suspension.

2.2.5 2D tube formation

Within two weeks after finishing a bioreactor experiment, an *in vitro* 2D tube formation assay was performed to test the angiogenic potential of the CMs of the bioreactor experiments. HMEC-1, an endothelial cell line, kindly provided by Prof. Schönfelder (Institut für klinische Pharmakologie und Toxikologie, Charité – Universitätsmedizin Berlin, Germany), were seeded at a density of $5.5x10^4$ cells/well resuspended in 100µl culture medium on 24-well multititer plates. The latter were coated with 50µl Matrigel (mixed 5:1 with HMEC-1 culture medium). The culture medium for HMEC-1 was composed of MCDB 131, 5% FBS, 2mM L-glutamine and 100U/ml penicillin plus 100µg/ml streptomycin, 1µg/ml hydrocortisone, the latter was omitted during assay. The Matrigel was allowed to gel for 30min at 37°C before cells were seeded. Subsequently, 500µl of the medium conditioned in the bioreactor was applied to them.

Each condition was tested in duplicates and six repetitions, including three male and three female MSC donors, were conducted. Wells without cells served as negative control. Cells cultured with standard HMEC-1 medium served as positive control for the tube formation. The assay was incubated for 17h in a humidified incubator (37°C, 5% CO_2) before results were visualised on an inverted microscope. Digital images were taken of each well centrally at a magnification of 30x. The length of tubes that formed during the assay duration was measured using NIH ImageJ (version 1.39u, 2007, W.S. Rasband, U.S. National Institutes of Health, Bethesda, Maryland, USA, http://rsbweb.nih.gov/ij/). With a threshold of 30 pixels per tube the mean cumulative tube length for each condition in each single assay was determined.

After having taken the images, an assay to detect differences in cell numbers by variations in cell activity, the CellTiter 96® AQueous Non-Radioactive Cell Proliferation Assay, was performed according to manufacturer's instructions.

Some of these angiogenesis and cell activity assays as well as the measurement of the tube lengths were kindly performed by Lauren Ehardt during her internship at the Julius Wolff Institute.

2.2.6 ELISAs

All ELISAs were obtained from R&D Systems and performed according to the manufacturer's instructions. CMs from six bioreactor experiments were analysed for pro-angiogenic factors (VEGF-A, TGF-β1, MMP-2 and -9), one antagonist (TIMP-2) and a marker for T lymphocyte activation (IL-2). VEGF-A, TGF-β1, MMP-2 and -9, TIMP-2

concentrations were determined in undiluted CMs whereas CM was 30x concentrated using Amicon Ultra-4 PL-5 filter to allow for determination of bFGF and IL-2 levels. MMP-9 and IL-2 could not be detected.

2.2.7 Lactate and Glucose level

200µl of conditioned media of each condition (Tab. 2.5) were sent to "Zentralinstitut für Laboratoriumsmedizin und Pathobiochemie" at Charité – Universitätsmedizin Berlin, Germany and analysed for glucose and lactate content. In total, media from six different bioreactor experiments were tested to elucidate if the metabolism of the cells had been affected by mechanical stimulation. Condition 5 and 6, CMs of cell free constructs, served as negative controls/blank.

2.2.8 Immunohistology

Immunohistology was performed to be able to check for cell distribution, to validate the expression of CD105 by MSCs in order to distinguish cell types, and to determine which cells produce VEGF. The latter was supposed to validate the ELISA results.

A fibrin construct of each experimental condition of one bioreactor experiment, with cells of female MSC and T lymphocyte donors, was placed into a well of a 24-well multititer plate, washed once with PBS and incubated over night in 2ml of 4% PFA. Further, each construct, placed into a plastic cassette, underwent a dehydration procedure with the following steps: 1h in 70% ethanol, 1h in 80% ethanol, over night in 96% Ethanol, 2h in 100% ethanol, 1h in xylol and 1h max in liquid paraffin (60°C). Finally, each sample was embedded in a block of paraffin and kept at RT until microtomy with a thickness of 4µm. This sample preparation was kindly performed by Lauren Ehardt and Gabriela Korus.

For immunohistochemical staining of CD105, an MSC surface marker, and VEGFA, an angiogenic factor, the paraffin sections had to be deparaffinised as follows: 2 x 10' xylol, 2 x 2' 100% ethanol, 1 x 2' 96% ethanol, 1 x 2' 80% ethanol, 1 x 2' 70% ethanol, and 1 x 2' aqua dest. This was followed by 2 washing steps in fresh PBS for 5' each. To unmask the antigens with heat, sections were placed in Tris-EDTA buffer, brought to boil in the microwave and then held boiling for 20' at 250W. The sections were then placed under running tap water to cool down, slightly dried and samples were encircled using a fat pen. After this they were washed twice for 5' in fresh PBS. A blocking step in PBS with 2% normal serum, from the species in which the secondary antibody was raised, followed for 30' at RT. Then the serum was removed by pouring it off and the primary antibody diluted in DAKO-diluent was added. The VEGF antibody (1:30) was left to incubate for 2h at RT and the CD105 antibody (1:200)

incubated over night at 4°C. The sections were again washed twice for 5’ in fresh PBS. The biotinylated secondary antibody (1:50 and 1:100, respectively) diluted in PBS with 2% normal serum was added and incubated for 50’ and 30’ at RT, respectively. Two 5’ washing steps in PBS followed. Then the sections were 50’ incubated with AB complex, prepared according to the manufacturer’s instructions, and washed twice as before. Two incubations for 5’ in a chromogen buffer followed. That buffer was poured off and an incubation with AP substrate, prepared according to the manufacturer’s instructions, followed for 5-10’ under visual control. The sections were again washed in PBS and then twice in aqua dest. A counter stain for cell nuclei was performed using Mayer’s haematoxylin for 1-2’, dipping into aqua dest. and flushing with running tap water for 5’. After dipping the sections into aqua dest. Aquatex was added and a cover slip mounted. The sections were left to dry under a fume hood until microscopic inspection. Images of representative fields of each stained section were taken, using an AxioCam MRc and AxioVision 4.7 software (both Carl Zeiss, Germany).

As negative control, sections with fibrin containing MSCs were stained with the secondary antibody only to prove that there occurs no unspecific binding of the antibody.

All incubations with serum, antibodies, chromogen and substrate were performed in a humidified and dark chamber. Detailed recipes for buffers used are listed in the appendix.

The stainings were kindly performed by the technical assistants Gabriela Korus and Gabriele Hardung.

2.2.9 Gene expression array

In total, 18 samples underwent a gene array analysis to validate the results found on the protein level, determine further effects induced by mechanical stimulation and check for immunomodulatory effects. Therefore, three bioreactor experiments with three different male donors for each cell type and the co-culture were performed as described above. The MSCs used in those experiments have been previously cryo-preserved, defrosted and expanded.

To lyse the fibrin constructs for RNA isolation, a homogeniser and Trizol were used. For this a construct was slowly defrosted at RT and the homogeniser was cleaned in 100% and then in 70% ethanol and finally in Ampuwa (sterile, non-pyrogenic aqua dest). From here on all work was performed under a fume hood. The sample was then placed into a sterile glass round bottom tube, using sterile forcipes, and 1ml of Trizol was added. The homogenisation was performed for a few minutes until the Trizol-fibrin-cell suspension could be pipetted into an RNase free 2ml Eppendorf tube and 0.2ml chloroform were added. The suspension was

vortexed and left to incubate for 15' at RT. A 45' centrifugation at 15,000x*g* and 4°C followed. The top phase, containing RNA, was then transferred into a fresh RNase-free 1.5ml tube and 0.5ml 2-propanol were added. The tube was inverted 3 times and left to incubate for 10' at RT. The sample was then centrifuged for 15' at 15,000x*g* and 4°C. Usually a pellet was now visible and the supernatant was carefully removed. Two washing steps with 70% and then 100% ethanol with a subsequent centrifugation for 15' at 15,000x*g* and 4°C followed. The gained pellet was shortly dried in a vacuum centrifuge to remove remaining ethanol. 100µl of RNase-free water were added to dissolve the pellet. Sometimes a short incubation at 50°C was needed to achieve this. From here on Quiagen's RNeasy Mini Kit was used to improve the purity of the mRNA samples. 350µl RLT buffer were added to the sample, mixed and 250µl 100% ethanol were then added. From here on the manufacturer's instructions from step 5 on, including a DNA digestion step, were followed (RNeasy Mini Handbook, 04/2006, p. 29-30 and p. 69).

RNA concentration and quality were checked using the NanoDrop 1000 device followed by electrophoresis of a 1.5% agarose gel containing ethidium bromide to visualise 28 and 18 rRNA bands to check for possible RNA degradation.

Biotin-labelled cRNA was produced using the Illumina TotalPrep RNA Amplification Kit with 400ng of quality-checked total RNA as input. Hybridisations, washing, Cy3-streptavidin staining and scanning were performed on the Illumina BeadStation 500 platform (Illumina, San Diego, CA, United States), according to manufacturer's instruction. cRNA samples were hybridised as biological triplicates onto three Illumina Human-Ref8 BeadChips version 3.

All basic expression data analysis was carried out using the manufacturer's software BeadStudio 3.0. Raw data were background-subtracted and normalised using the "rank invariant" algorithm. Normalised data were then filtered for significant expression (detection $p<0.01$) on the basis of negative control beads. Differentially (at least 1.5 fold) regulated genes with $p<0.05$ were further filtered according to Gene Ontology (GO) terms or mapped to Panther pathways using the Panther Classification system (http://www.pantherdb.org/) [111, 112]. For analysis, lists of Gene Symbols or Entrez Gene IDs were used as input. Results were further checked for their relevance in the present study using EntrezGene (http://www.ncbi.nlm.nih.gov/gene) and UniProt (http://www.uniprot.org).

2.2.10 Statistical analysis

All statistics were performed using PASW18.0 (SPSS Inc., Chicago, Illinois, USA) except for gene array data. For the latter, the software BeadStudio 3.0 performed a t-test automatically. For all assays conducted, the exact 2-sided Wilcoxon-test for non-parametric, paired samples and the exact 2-sided Mann-Whitney-U-Test for independent samples were used with $p<0.05$. The former was used for comparison between stimulated and unstimulated samples and the latter to test for differences between cell types and co-cultures.

3 Results

This chapter describes the results of the 2D and 3D bioreactor study proving the hypothesis that mechano-regulated angiogenesis is driven by mesenchymal cells and reduced in the presence of immune cells.

3.1 Mechanical stimuli in bone healing – 2D *in vitro* application

This subchapter deals with mechanical stimuli as occurring during bone healing and their influence on the cellular reaction when applied in a 2D cell stimulation device. Therefore, first of all a characterisation of a 2D stimulation device was needed. This included, on the one hand, a characterisation of the substrate strains applied and the strains transferred to cells stimulated within this device, and on the other hand, an examination of the fluid flow environment and the fluid shear stresses acting within the device. Additionally, the cellular response to a 2D mechanical stimulation was examined by looking at a possible mechanotransducer and one of its downstream targets most likely involved in mechanotransduction.

Parts of this subchapter, namely the characterisation of the 2D stimulation environment, have already been published in peer reviewed journals [51, 96].

3.1.1 Flexercell characterisation - Results

3.1.1.1 Characteristics of applied strains

The static $\boldsymbol{\varepsilon_{rep}}$ reported by the FX-4000T controller and $\boldsymbol{\varepsilon_{prog}}$ programmed with the controller software were as expected linearly related ($R^2 > 0.99$) and similar in magnitude (6.1% ± 3.6%, mean ± SD of % difference between $\boldsymbol{\varepsilon_{rep}}$ and $\boldsymbol{\varepsilon_{prog}}$); for instance, at $\boldsymbol{\varepsilon_{prog}}$ = 2.5%, $\boldsymbol{\varepsilon_{rep}}$ ranged from 2.3% to 2.7% strain. For the following results, all $\boldsymbol{\varepsilon_{mem}}$ measurements are compared to $\boldsymbol{\varepsilon_{rep}}$.

For the homogeneously strained area $\boldsymbol{\varepsilon_{mem}}$ was found to have a linear relationship ($R^2 = 0.98$) to $\boldsymbol{\varepsilon_{rep}}$ (Fig. 3.1, left) where $\boldsymbol{\varepsilon_{mem}}$ was higher by 1.47–3.17% (mean: 2.26%) strain than $\boldsymbol{\varepsilon_{rep}}$ at all numbers of cycles studied (Fig. 3.1, left). The difference (offset) between those two strains was significant ($p < 0.002$) at all cycle numbers analysed (Fig. 3.1, left). Furthermore, it was significantly ($p < 0.05$) greater at cycle numbers ≥2700 than with a fresh plate (Fig. 3.1, right). Table 3.1 shows the corresponding absolute increase in mean $\boldsymbol{\varepsilon_{mem}}$ ± SD from 0 to 2700, 0 to 5400, and 0 to 10800 load cycles, respectively.

Multiple images of a single membrane with the same static $\boldsymbol{\varepsilon_{prog}}$ were taken at random intervals during the course of 300 static load cycles to estimate the maximum random error of

measurement in using DIC to determine membrane strains. It ranged between 0.10% strain at ε_{prog} = 10% and 0.17% strain at ε_{prog} = 2.5%.

Already after 2700 load cycles, DIC revealed a significant increase of static ε_{mem}. Therefore, additional tests were performed to check for changes in material properties. Images of one six-well plate in the unstrained state after all load cycle numbers revealed a significant (p < 0.03) zero-load strain at cycle numbers ≥2700. Additionally, a tensile test was performed on British Standard type 1B specimens cut from six used BioFlex wells. A Young's modulus of 1.68MPa ± 0.086MPa (mean ± SD) was determined for previously strained plates being lower than that of specimens cut from a fresh plate (1.75MPa ± 0.145MPa), suggesting that a permanent change in the material had occurred, perhaps due to molecular alignment or cross linking.

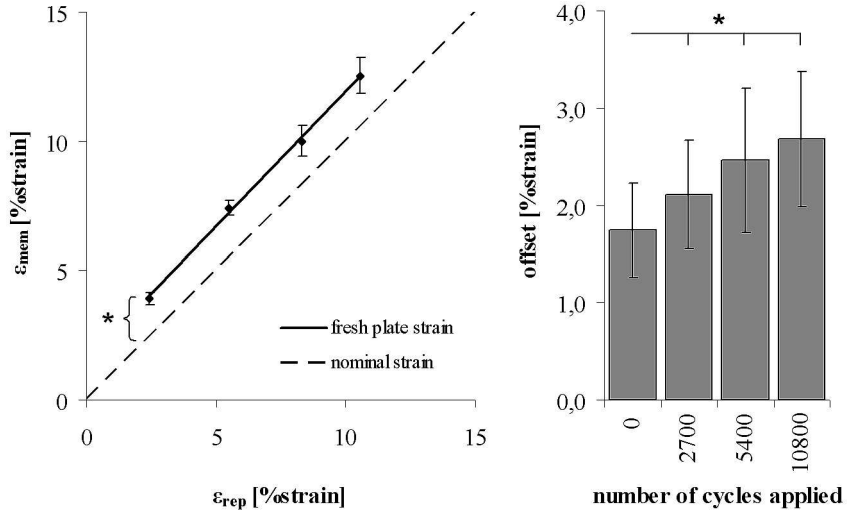

Fig. 3.1: Strains measured in Flexercell.

*(left) Linear relationship between ε_{mem} determined for 13 wells using DIC and the strains reported by the controller device of the FX-4000T (ε_{rep}). ε_{mem} (fresh plate strain) showed a significant ($p < 0.002$) offset from ε_{rep} (nominal strain). This offset ranged from 1.47–3.17% and is marked by *. Reproduced from [51].*

*(right) Comparison of the offset [$\varepsilon_{mem} - \varepsilon_{rep}$] between different numbers of load cycles is shown. The static measurement of strains revealed a significantly ($p < 0.05$) larger offset after ≥2700 load cycles compared to 0 load cycles. The significance is indicated by *. Reproduced from [51].*

Tab. 3.1: Absolute increase of ε_{mem}.

Increase shown in %strain after 2700, 5400, and 10800 load cycles, respectively, at static 2.5%, 5%, 7.5%, and 10% ε_{prog} [$\varepsilon_{mem\_2700,\ 5400,\ 10800\ cycles} - \varepsilon_{mem\_0\ cycles}$]. Adapted from [51]

	absolute increase of ε_{mem} [%strain] at							
	ε_{prog} = 2.5%		ε_{prog} = 5.0%		ε_{prog} = 7.5%		ε_{prog} = 10.0%	
No. of load cycles	**mean**	**SD**	**mean**	**SD**	**mean**	**SD**	**mean**	**SD**
2700	0.31	0.06	0.35	0.13	0.76	0.31	0.65	0.47
5400	0.43	0.12	0.42	0.21	0.86	0.52	1.70	3.58
10800	0.61	0.10	0.67	0.21	1.30	0.41	2.10	3.69

3.1.1.2 Strain transferred to cells

The strain transferred to cells varied with confluence being highest in confluent cell carpets (Tab. 3.2). In three out of 16 images, it was observed that cell processes detached at strains $\boldsymbol{\varepsilon_{mem}} \geq 10\%$. Measurements of cell process and body strain at zero loading after stretching revealed cells reduced in size (negative $\boldsymbol{\varepsilon_{cell}}$) (Fig. 3.2e, f). In general, $\boldsymbol{\varepsilon_{cell}}$ varied highly (Fig. 3.2d-f).

Tab. 3.2: Range of strain transferred to cells.

Transfer showed no dependency on amount of strain applied for cell processes and bodies.

cell carpets (n=6)	cell processes (n=10)	cell bodies (n=7)
91–109% at 2.5% ε_{prog} **81–91% at 10%** ε_{prog}	**46–60%**	**45–60%**

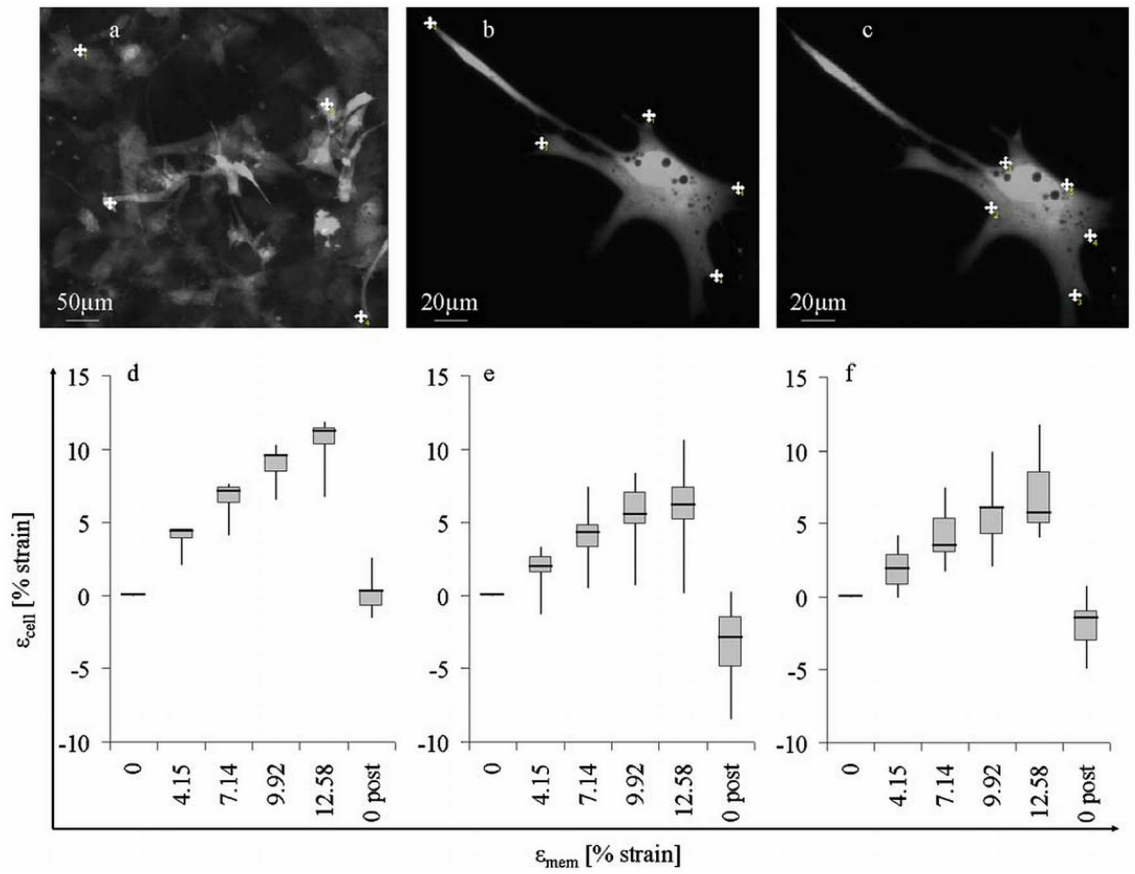

Fig. 3.2: Strain transfer to BMSCs.

Exemplary images of fluorescent bone marrow derived stromal cells and results of strain measured to be transferred to cells ($\boldsymbol{\varepsilon_{cell}}$). Prominent positions in exemplary images are indicated by white crosses for cell carpets (a), cell processes (b), and cell bodies (c) and $\boldsymbol{\varepsilon_{cell}}$ is displayed as boxplot versus the strain measured on the membrane ($\boldsymbol{\varepsilon_{mem}}$) of a fresh BioFlex well plate at 2.5% - 10% $\boldsymbol{\varepsilon_{prog}}$. "0 post" shows cells after stretching at 0% strain. Cell carpets (N = 6) show full strain transfer (d), cell processes (N = 10) (e), and cell bodies (N = 7) (f) show about 50% strain transfer. Adopted from [51].

Up to four images were taken within 55 seconds at each strain applied and the mean SD for all strain measurements (up to 21 distances per cell) was calculated to estimate the maximum random error of measurement. It was largest for cell bodies (2.4% strain) and smallest for cell carpets (1% strain).

3.1.1.3 Characteristics of fluid mechanics

Since in the Flexercell the substrate is stretched over a loading post by out of plane distension using a vacuum, clearly resulting in flow of culture medium, the desired substrate stretch is always accompanied by fluid shear stresses. The CFD model used revealed that these fluid shear stresses increased with increasing frequency of strain application and predicted that the Flexercell applies a range (0.09 – 5.2 Pa) of relevant shear stress magnitudes. Unlike the strain, the shear stress was not homogeneously distributed across the central post varying approx. linearly with radial position on the loading post. The particle tracking used for experimental validation of the model showed fair agreement with the predictions (Fig. 3.3). Further, the model's prediction for a homogeneously strained membrane area as well as the strains predicted for doubling of the applied vacuum pressure agreed with the strain characterisation experimentally performed.

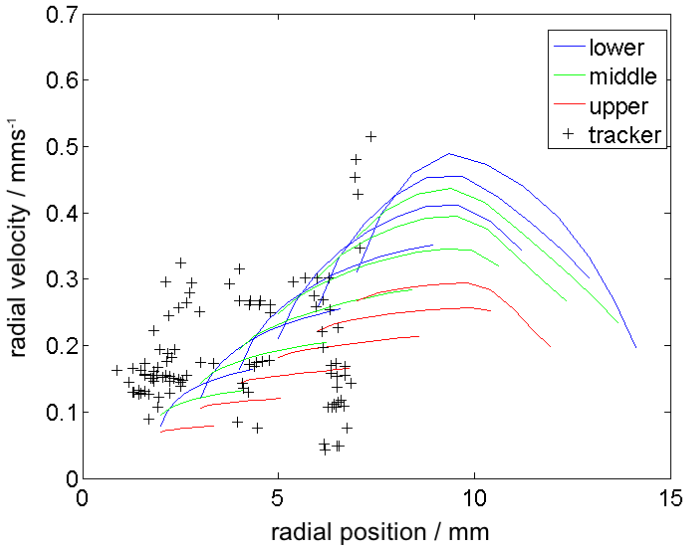

Fig. 3.3: Flow verification.

Radial velocity against current radial position: comparison of CFD predictions (solid lines: lower, middle and upper rows in particle array) and experimental measurement (image tracked fluorescent microspheres). Reproduced from [96].

3.1.2 Influence of characterised mechanical environment on mesenchymal cells - Results

3.1.2.1 Immunohistology

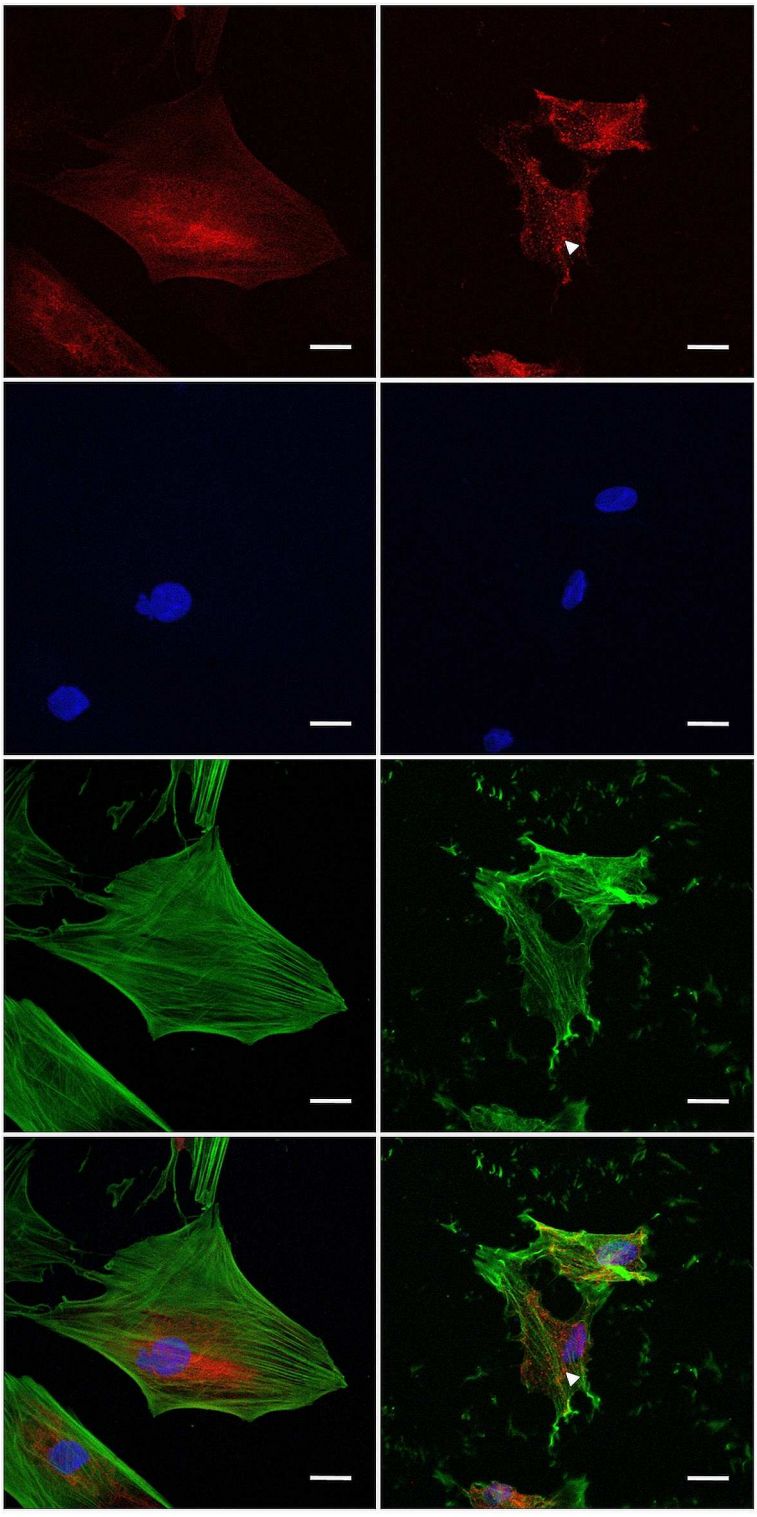

Fig. 3.4: Integrin αVβ3 distribution w/o stimulation.

Images of unstimulated (left) and stimulated (right) osteoblast-like cells. Stainings from top to bottom: αVβ3 integrin, nuclei, actin filaments, merged image. White arrows indicate integrin cluster. The scale bar represents 20µm.

Mechanical stimulation with 4% strain at 1Hz for 20min induced three days after application of the stimulus the formation of αVβ3 integrin clusters distributed all over the cell compared to unstimulated controls, which showed a diffuse distribution of this integrin with a higher concentration around the nucleus (Fig. 3.4). Further, the cells' morphology was affected. They appeared to be less spread and the cytoskeleton was less organised.

3.1.2.2 FAK ELISA

15 minutes and three hours after the strain application, no significant change in the level of phosphorylated FAK (pFAK) was detected (N=3, Fig. 3.5). However, the amount of pFAK seemed to be slightly lower after three hours.

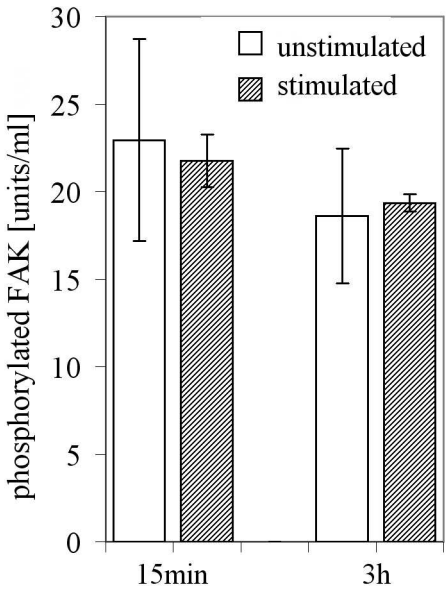

Fig. 3.5: Amount of phosphorylated FAK

This graph shows the units of phosphorylated FAK 15min and 3h after mechanical stimulation. The amount of phosphorylated FAK remained unchanged by mechanical stimulation but decreased over time.

3.2 Mechanical stimuli in bone healing – effects of 3D *in vitro* application

The effect of the application of a cyclic compression, which is known to be favourable for bone healing, to 3D cell constructs is describeded in this subchapter. The 3D constructs stimulated in a bioreactor contained MSCs and/or T lymphocytes resembling an initial fracture haematoma. This experiment offered a more realistic environment than the previously described 2D experiment giving the results a greater relevance for the clinic. Here, primarily the effect on proteins involved in angiogenesis was studied but also gene expression patterns regarding mechanotransduction and immunomodulation.

3.2.1 Results for MSCs

3.2.1.1 MSC characterisation

Cell surface markers, defined as minimal characteristic criteria for MSCs, were expressed as described in literature. The cells were negative for CD45Ra, CD34, CD19, HLA-DR, and CD14 and positive for CD105, CD73, and CD90 (Fig. 3.6).

3.2.1.2 Bioreactor experiment – determination of MSC viability after mechanical stimulation

The determination of cell viability using CASY showed a viability >80% before stimulation and >70% after stimulation. The retrieval of cells before flow cytometry included one washing step to get rid of the trypsin and achieve the right cell concentration that removed some dead cells. Hence, flow cytometry revealed >95% viability of cells taken after three days from the fibrin constructs for both stimulated and unstimulated ones.

3.2.1.3 2D tube formation induced by CMs of MSCs

MSCs showed a paracrine regulation of EC tube formation enhanced by mechanical stimulation. Five out of six CMs of stimulated MSCs induced an obvious but not significant increase in tube formation of HMEC-1 compared to unstimulated MSCs ($p=0.063$) and cell free controls (Fig. 3.9). Cell numbers were evenly distributed among wells (deviation <10%), as tested by CellTiter 96® AQueous Non-Radioactive Cell Proliferation Assay. Negative controls showed no tube formation and positive controls about 79% of the median cumulative tube length induced by CMs of stimulated MSCs.

3.2.1.4 ELISAs

TGF-β1 was expressed by MSCs (median [1st quartile – 3rd quartile]: 760 [733 – 771] pg/ml) and further was significantly ($p<0.04$) mechanically up-regulated in MSCs (898 [835 – 967] pg/ml). The basal level of TGF (~635pg/ml) determined in the negative

control originated from the serum present in the culture medium and was significantly different from the ones in CMs of MSCs (see also Fig 3.10).

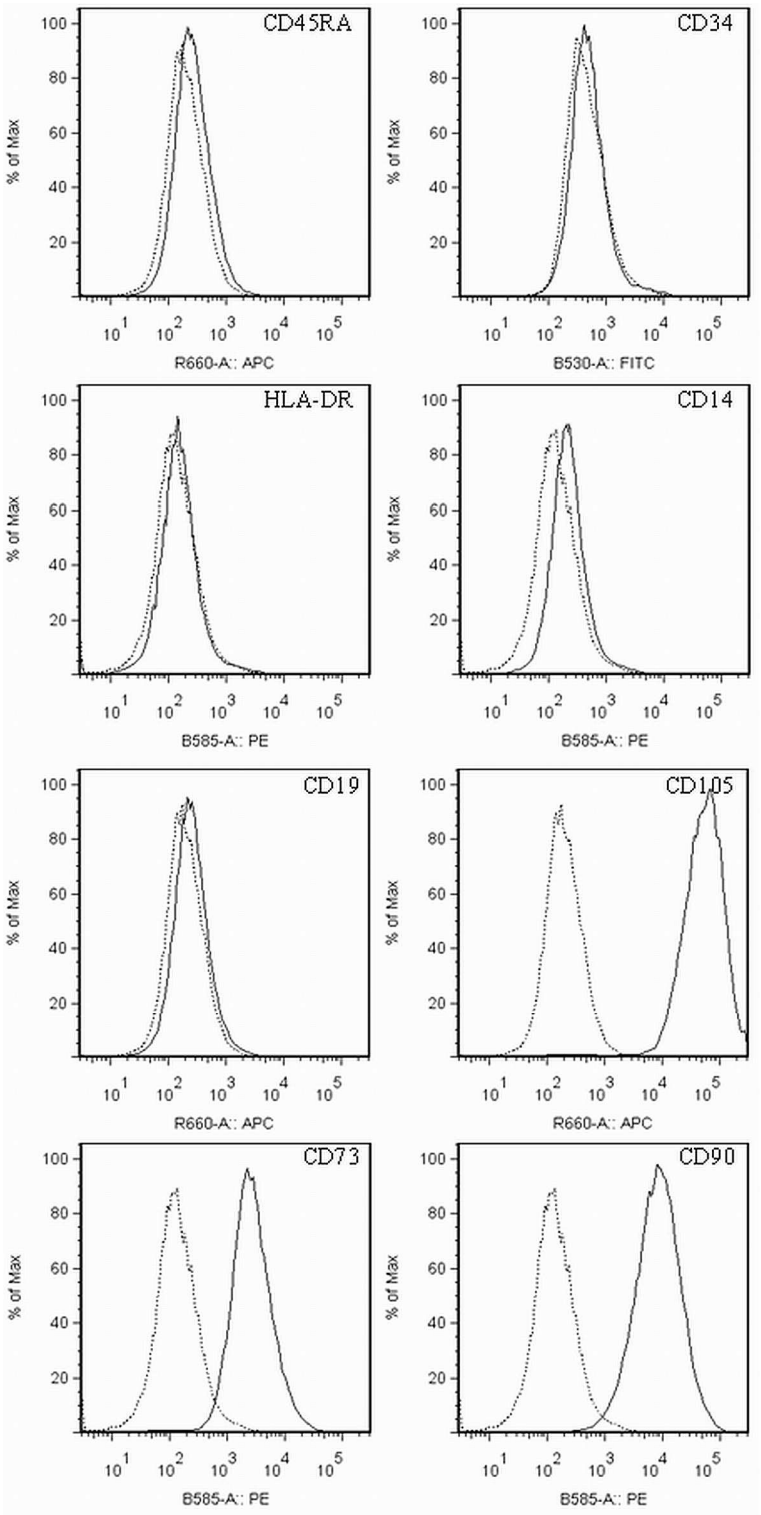

Fig. 3.6: Cell surface marker pattern for human MSCs.

As determined by flow cytometry and defined in literature, the pattern was negative for CD45RA, CD34, HLA-DR, CD14, CD19, and positive for CD105, CD73, and CD90.

VEGF level in CMs was significantly ($p<0.04$) mechanically up-regulated in MSCs (183 [156 – 193] pg/ml) compared to unstimulated controls (112 [100 – 133] pg/ml). No VEGF was detected in negative controls (see also Fig 3.11).

MMP-2 was also significantly ($p<0.04$) mechanically up-regulated in MSCs, from 19 [18 – 24] ng/ml to 25 [22 – 30] ng/ml, whereas the expression level of its antagonist TIMP-2 (6ng/ml) was not affected by mechanical stimulation. Both proteins ranged around detection limit (<0.5 ng/ml) in negative controls (see also Fig 3.12 + 3.13).

bFGF is expressed by MSCs (0.8 pg/ml) but was not affected by mechanical stimulation. The negative control ranged with large variations (0 – 0.37pg/ml) around the detection limit of the assay. This high variation observed most likely resulted from the procedure used to concentrate the CMs. Possibly a small amount of bFGF is already present in the serum used in the culture medium.

Hence, MSCs show an enhanced level of some pro-angiogenic proteins after mechanical stimulation.

3.2.1.5 Lactate and Glucose level in CMs of MSCs

The lactate concentration was significantly ($p<0.03$) higher in CM of mechanically stimulated MSCs (median [1^{st} quartile – 3^{rd} quartile]: 9.25 [8.15 – 9.38] mg/dl) compared to unstimulated (5.9 [5.05 – 6.68] mg/dl) (see also Fig. 3.14) and significantly ($p<0.04$) different from that in negative controls, which were subtracted as blank. The metabolism of MSCs seemed to be affected by mechanical stimulation.

However, the glucose concentration was not significantly different (stimulated and unstimulated median: 176 and 174 mg/dl) but significantly lower ($p<0.05$) than in cell free controls. The median glucose level determined in the negative control was similar to the one present in original medium: ~1.8g/L. It remained unchanged by mechanical stimulation but showed a high variation of >8 mg/dl representing the measurement error.

3.2.1.6 Immunohistology

The staining for CD105 proved expression of the MSC specific cell surface marker (Fig. 3.7A) without unspecific binding (Fig. 3.7C). Additionally, the counter stain with haematoxylin revealed a fairly even cell distribution over the fibrin construct (Fig. 3.7C). With lower magnifications, visualizing a larger portion of the constructs, qualitatively the cell distribution was even in all sections stained.

With the staining for VEGF-A, it was difficult to distinguish between positively stained cells and the fibrin matrix containing VEGF-A itself [113] (Fig. 3.8A+B). However, the MSCs did not appear to be negative, validating the ELISA data for VEGF-A.

Furthermore, stimulated constructs with MSCs showed obvious fibrin degradation around the cells resulting in holes within the sections (Fig. 3.7A + 3.8A, left).

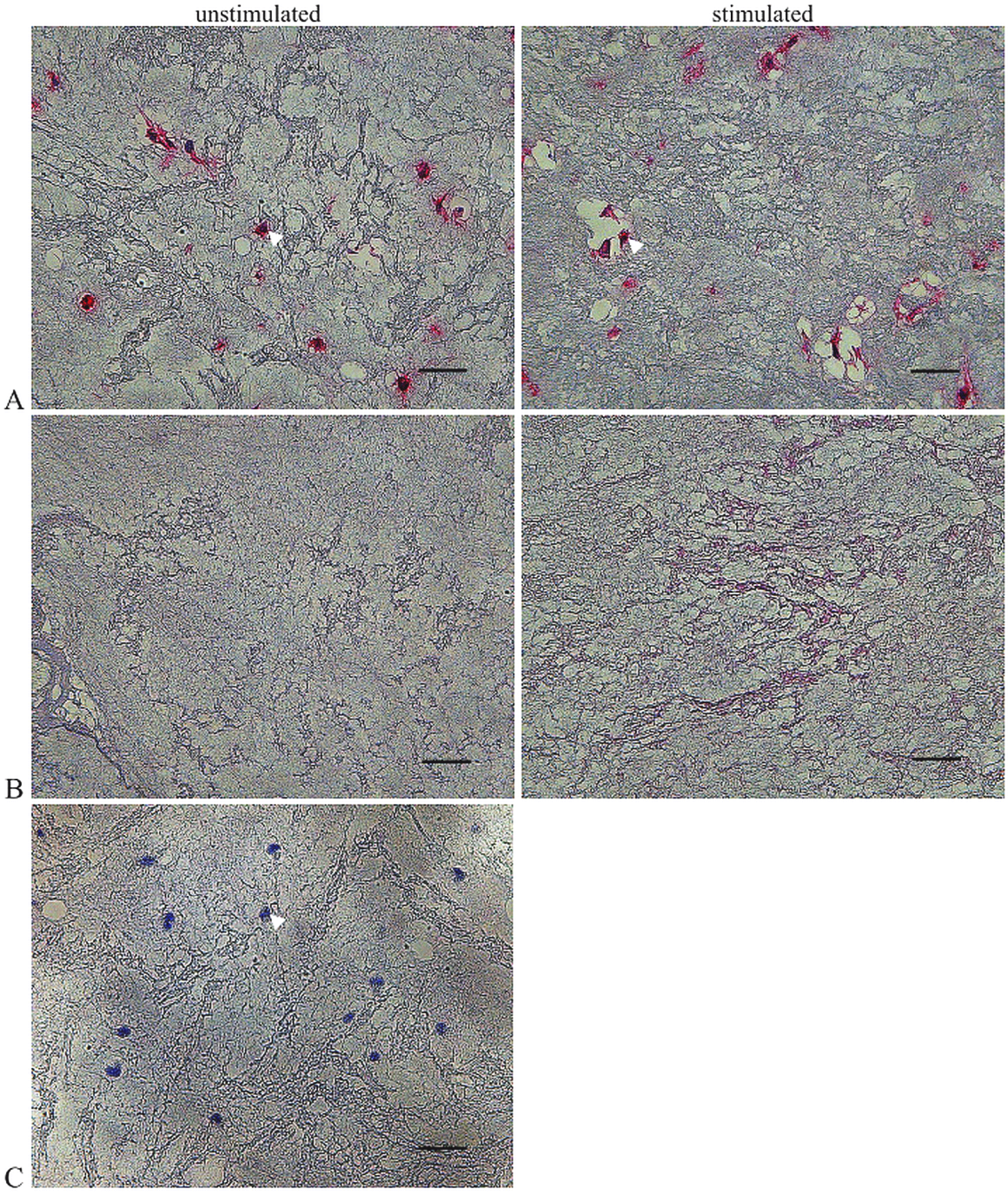

Fig. 3.7: Immunohistochemical staining for MSC-surface marker CD105 (red).

Representative sections of fibrin constructs. White arrow indicates a cell nucleus and the scale bar represents 50µm. A) CD105 positive MSCs, B) cell free controls and C) negative control (containing MSCs) stained with the secondary antibody only.

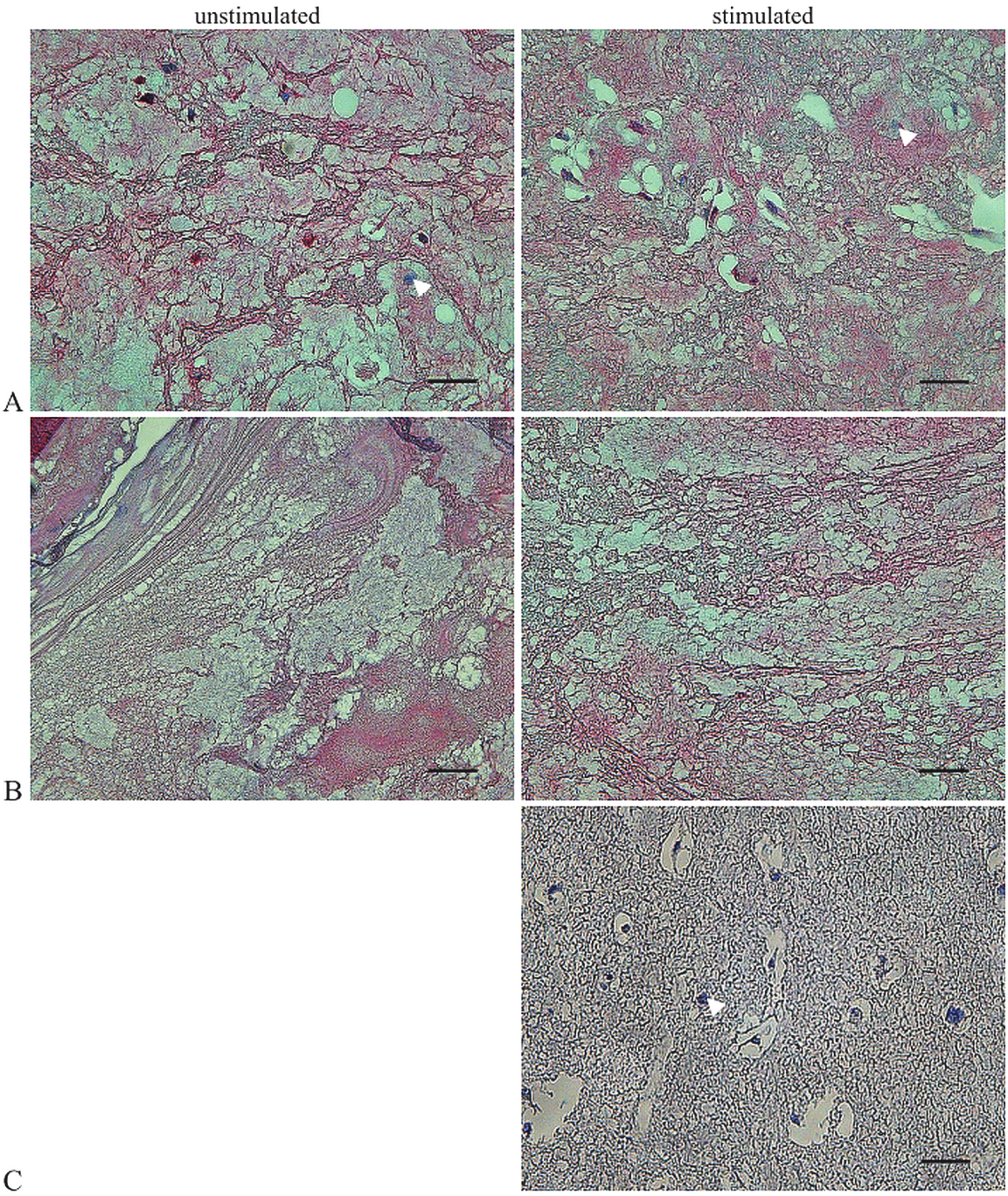

Fig. 3.8: Immunohistochemical staining for VEGF-A (red).

Representative sections of fibrin constructs showing A) MSCs, B) cell free controls and C) negative control (containing MSCs) stained with the secondary antibody only. White arrow indicates a cell nucleus and the scale bar represents 50µm. A) and B) show a strong VEGF-A positive staining of the matrix whereas the negative control C) remained unstained. Hardly any cells could be found that were stained more intense than the matrix.

3.2.1.7 Analysis of MSCs' gene expression: stimulated vs. unstimulated

A cluster analysis of the gene array data revealed a very close relationship between stimulated and unstimulated MSCs (see also chapter 3.2.3.7 and Fig. 3.17). The gene array detected 7622 expressed genes in unstimulated MSCs and 8004 genes in stimulated samples. In total, 136 genes were differentially regulated (fold change: >1.5 = up-regulated, <0.67 = down-regulated) by mechanical stimulation: 90 genes were significantly up-regulated and 46 significantly down-regulated (see also Fig. 3.18).

MSCs did show mRNA expression of MMP2 and TIMP2 but not of TGFB1, VEGFA and IL2. bFGF was only detected in mRNA of stimulated MSCs. However, the gene expression of none of those genes was significantly up-regulated by mechanical stimulation as seen for the protein expression of TGF-β1, VEGF-A and MMP-2.

NRP1 und NRP2, receptors for VEGF165, an isoform of VEGFA, were detected in all MSC samples. MMP9 was only detected in stimulated MSC samples but not significantly regulated.

A table of all differentially regulated genes with their fold-change (ratio) may be found in the appendix (Tab. A3). Generally most differentially up-regulated genes appear to be involved in some kind of metabolism or mRNA transcription regulation whereas the differentially down-regulated genes often appear to be involved in cell-adhesion mediated signalling.

Below in Table 3.3 and 3.4 the only significantly ($p<0.01$) up-regulated biological process "amino acid metabolism" and pathway "plasminogen activating cascade" and the here differentially regulated genes are shown as determined by using the Panther tool. No significantly down-regulated processes were found.

Tab. 3.3: In MSCs mechanically up-regulated biological process amino acid metabolism.

The table shows the genes included in the significantly ($p<0.01$) up-regulated biological process in mechanically stimulated MSCs compared to unstimulated ones by fold change.

Gene Symbol	Entrez Gene ID	Gene Name	Fold Change
SLC7A11	23657	solute carrier family 7, (cationic amino acid transporter, y+ system) member 11	3.24
KYNU	8942	kynureninase	2.60
SLC7A5	8140	solute carrier family 7, (cationic amino acid transporter, y+ system), member 5	2.07
ODC1	4953	ornithine decarboxylase 1	1.54
PGD	5226	phosphogluconate dehydrogenase	1.53

Tab. 3.4: In MSCs mechanically up-regulated pathway plasminogen activating cascade.

The table shows the genes included in the significantly ($p<0.01$) up-regulated pathway in mechanically stimulated MSCs compared to unstimulated ones sorted by fold change.

Gene Symbol	Entrez Gene ID	Gene Name	Fold Change
PLAT	5327	plasminogen activator, tissue	1.97
SERPINE1	5054	plasminogen activator inhibitor type 1	1.90
PLAUR	5329	plasminogen activator, urokinase receptor	1.56

The pathway found to be up-regulated validates the immunohistochemical finding that stimulated MSC show an enhanced fibrin degradation.

3.2.2 Results for T lymphocytes and Co-cultures with MSCs

3.2.2.1 T lymphocytes' isolation quality

The purity of $CD8^+$ T lymphocytes was >90% and that of $CD4^+$ T lymphocytes >97%. The latter appeared purer as their isolation was performed with the negative fraction gained in the isolation of $CD8^+$ T lymphocytes. The missing fraction mainly included double positive cells, likely being progenitor cells, and a small fraction was positive for the opposite marker, CD4 and CD8 respectively.

3.2.2.2 Bioreactor experiment –determination of T lymphocytes' viability after mechanical stimulation

Measurements of cell viability – using a cell counter – revealed that >85% of T lymphocytes were viable after mechanical stimulation compared to >90% before the start of the experiment. After retrieval from fibrin the flow cytometric data indicated a viability of >95%. Again, this viability might be higher due to the fact that one washing step had to be performed before the measurement.

3.2.2.3 2D tube formation induced by CMs of T lymphocytes and co-cultures

CMs of T lymphocytes hardly induce any tube formation and were not affected by mechanical stimulation. The level of tube formation was comparable to CMs of the negative control (Fig. 3.9). However, CMs of stimulated co-cultures induced a significant ($p<0.04$) increase in tube formation. The cumulative tube length was lower with CMs of stimulated co-cultures than with the ones of stimulated MSC but without significance. But the CMs of unstimulated co-cultures induced significantly ($p<0.01$) less tube formation compared to the ones of unstimulated MSCs. After all, in contrast to T lymphocytes the co-cultures have an angiogenic potential (Fig. 3.9).

Negative controls showed no tube formation and CMs of co-culture showed about 56% of the cumulative tube length determined for positive controls. Cell numbers were evenly distributed among wells (deviation <10%), as tested by CellTiter 96® AQueous Non-Radioactive Cell Proliferation Assay.

It was further tested if the combination of CMs of MSCs and T lymphocytes would result in the same induction as a combination of CMs of co-cultures and negative controls. This was investigated for four bioreactor experiments. The induction remained the same (data not shown).

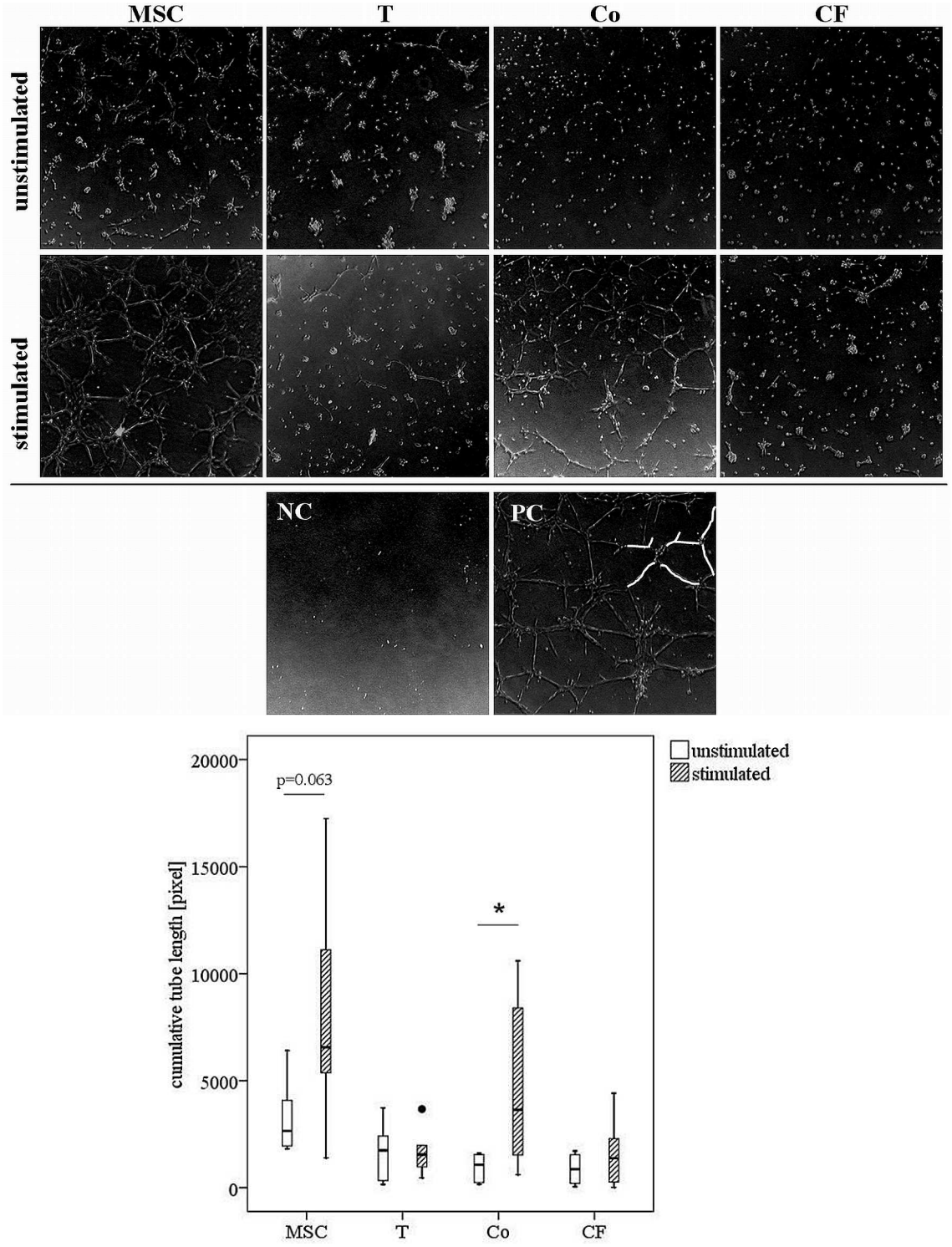

Fig. 3.9: 2D tube formation.

(top) Representative images taken at 30x magnification showing in vitro tube formation induced by CMs of MSCs (MSC), T lymphocytes (T), co-cultures (Co), cell free controls (CF), as well as negative control (NC) without HMEC-1 and positive control (PC) with HMEC-1 in reference medium.

(bottom) Cumulative tube length, way of measurement indicated by white lines in PC (see top), induced in HMEC-1 seeded on Matrigel. CMs of MSC (p=0.063) and co-cultures (p<0.04) showed an increased induction upon stimulation demonstrating their angiogenic potential tending to be lower in co-cultures.*

3.2.2.4 ELISAs

TGF-β1 was only slightly expressed by T lymphocytes alone, with up to 20 pg/ml more than in negative controls, though without statistical significance. But in the co-culture (median [1st quartile – 3rd quartile] stimulated/unstimulated: 766 [745 – 799] pg/ml / 766 pg/ml [753 – 861] pg/ml) it was expressed on a similar level as by mechanically unstimulated MSCs. However, the expression was not mechanically affected if T lymphocytes were present (Fig. 3.10).

VEGF was significantly mechanically down-regulated in the co-cultures ($p<0.04$) but not detected in CMs of T lymphocytes or the negative control (Fig. 3.11).

MMP-2 was significantly mechanically up-regulated from 21 [18 – 25] ng/ml to 24 [22 – 28] ng/ml in CMs of the co-culture ($p<0.04$) on a comparable level as in MSCs, whereas the expression level of its antagonist TIMP-2 was not affected by mechanical stimulation. Both proteins ranged around detection limit (<0.5 ng/ml) in negative controls and CMs of T lymphocytes (Fig. 3.12 + 3.13).

bFGF was expressed by the co-cultures (median: 0.7 pg/ml) but was not affected by mechanical stimulation. T lymphocytes showed an expression level close to the detection limit and the cell free controls (data not shown).

Therefore, the co-cultures secreted pro-angiogenic proteins partially enhanced by mechanical stimulation in contrast to T lymphocytes which hardly secreted any of the studied proteins. Yet, the level of co-cultures' secretion was in some cases different from MSCs alone.

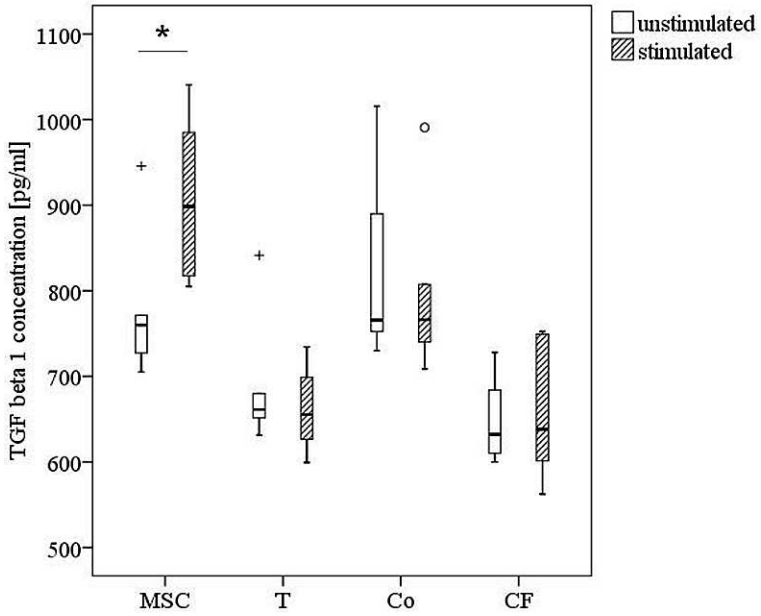

Fig. 3.10: TGF-β1 concentration.

*Determined in CMs (N=6) of MSCs (MSC), T Lymphocytes (T), co-cultures (Co), and negative controls (CF). * indicates the significant increase between unstimulated and stimulated (p<0.04).*

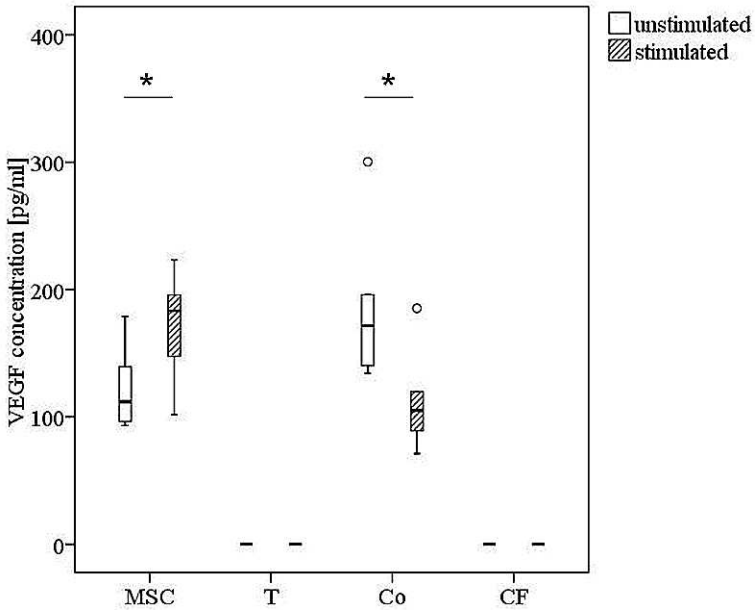

Fig. 3.11: VEGF-A concentration.

*Determined in CMs (N=6) of MSCs (MSC), T Lymphocytes (T), co-cultures (Co), and negative controls (CF). * indicates the significant difference between unstimulated and stimulated (p<0.04).*

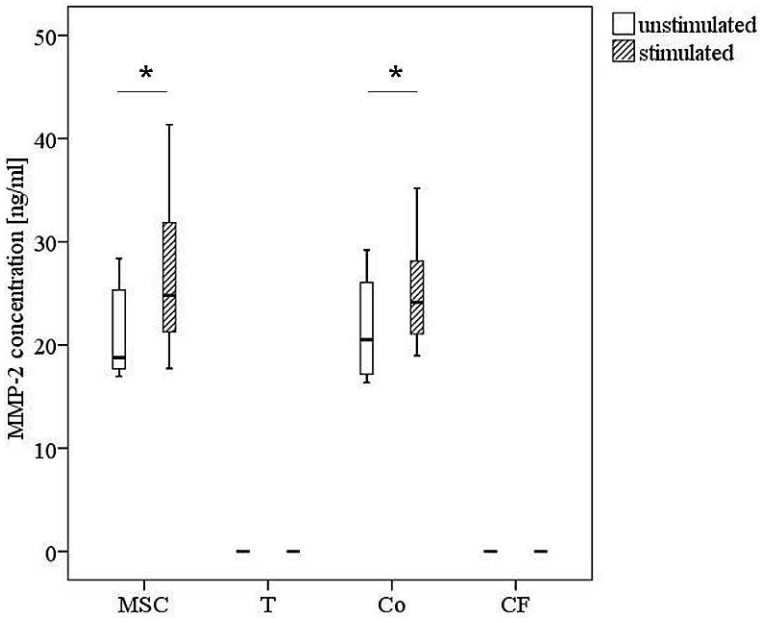

Fig. 3.12: MMP-2 concentration.

*Determined in CMs (N=6) of MSCs (MSC), T Lymphocytes (T), co-cultures (Co), and negative controls (CF). * indicates the significant increase between unstimulated and stimulated ($p<0.04$).*

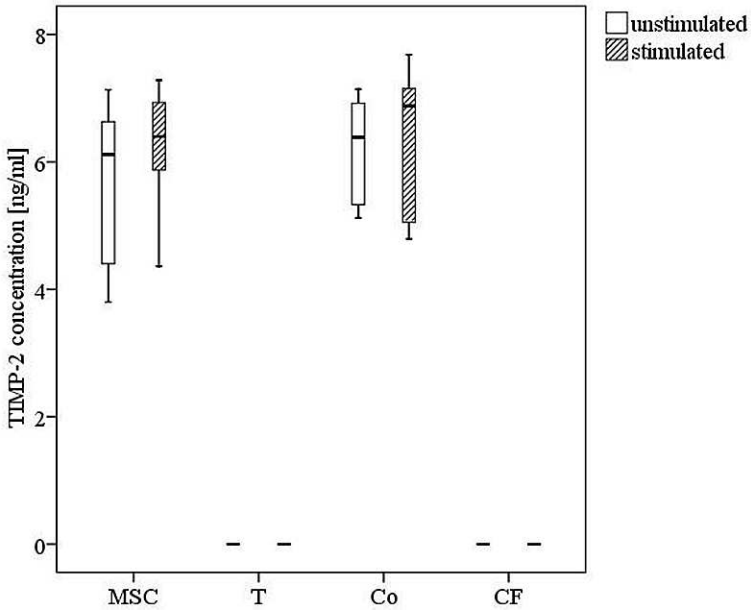

Fig. 3.13: TIMP-2 concentration.

Determined in CMs (N=6) of MSCs (MSC), T Lymphocytes (T), co-cultures (Co), and negative controls (CF).

3.2.2.5 Lactate and Glucose level in CMs of T lymphocytes and co-cultures

The lactate and glucose level was comparable in CMs of T lymphocytes and cell free controls without the detection of differences between CMs of stimulated and unstimulated constructs. Co-cultures produced about twice as much lactate without a significant mechano-sensitivity (Fig. 3.14). Still, the lactate production by unstimulated co-cultures (median [1st quartile – 3rd

quartile]: 7.95 [7.65 – 8.18] mg/dl) tended ($p<0.065$) to be higher than by unstimulated MSCs (8.6 [6.95 – 9.58].

The glucose consumption of the co-cultures was significantly ($p<0.04$) down-regulated if mechanically stimulated (glucose concentration: stimulated 172 [169 – 174] mg/dl vs. unstimulated 175 [172 – 175] mg/dl). The median glucose level determined in the negative control was similar to the one present in original medium (~180mg/dl) and remained unchanged by mechanical stimulation but showed a high variation of >8 mg/dl. In addition, it was similar to the one in CMs of T lymphocytes

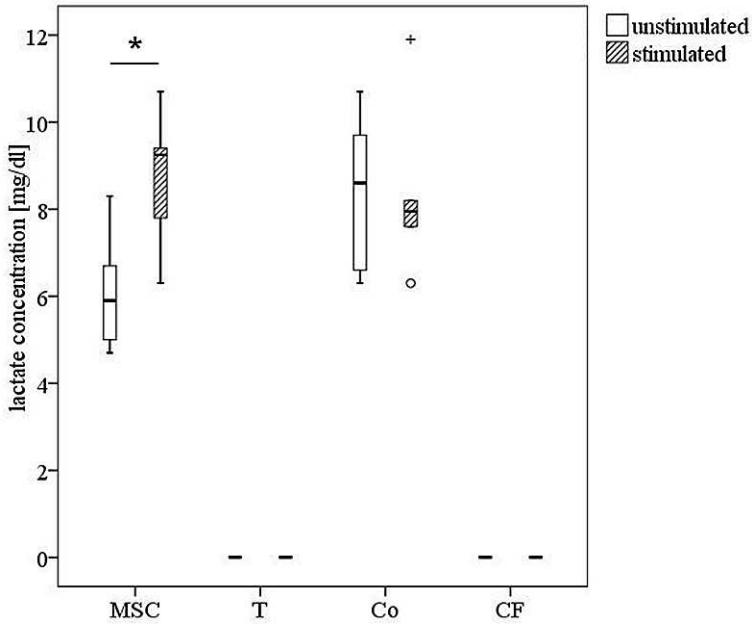

Fig. 3.14: Lactate concentration.

*Determined in CMs (N=6) of MSCs (MSC), T Lymphocytes (T), co-cultures (Co), and negative controls (CF). * indicates the significant increase between unstimulated and stimulated ($p<0.04$), pointing to a switch to anaerobic cell respiration.*

3.2.2.6 Immunohistology

The counter stain with haematoxylin revealed a qualitatively fairly even cell distribution over the cell constructs, which was even more obvious at lower magnifications. The staining for CD105 (Fig. 3.15) proved expression of the MSC specific cell surface marker and further, MSCs and T lymphocytes could easily be distinguished in co-culture samples. Furthermore, the size and colour of their nuclei differed as well: T lymphocytes' nuclei were smaller and darker/denser.

Staining for VEGF-A did not show a distinct red around or within cells. Even though VEGF-A was found to be expressed in the co-cultures as determined by ELISA, the VEGF-A content in the fibrin matrix itself was too high to distinguish between a stained cell and the stained

matrix (Fig. 3.16); also compare the immunohistological results for MSCs (Fig. 3.8). In some cases of stimulated co-cultures, slight fibrin degradation was observed, too, but in none of the samples containing T lymphocytes.

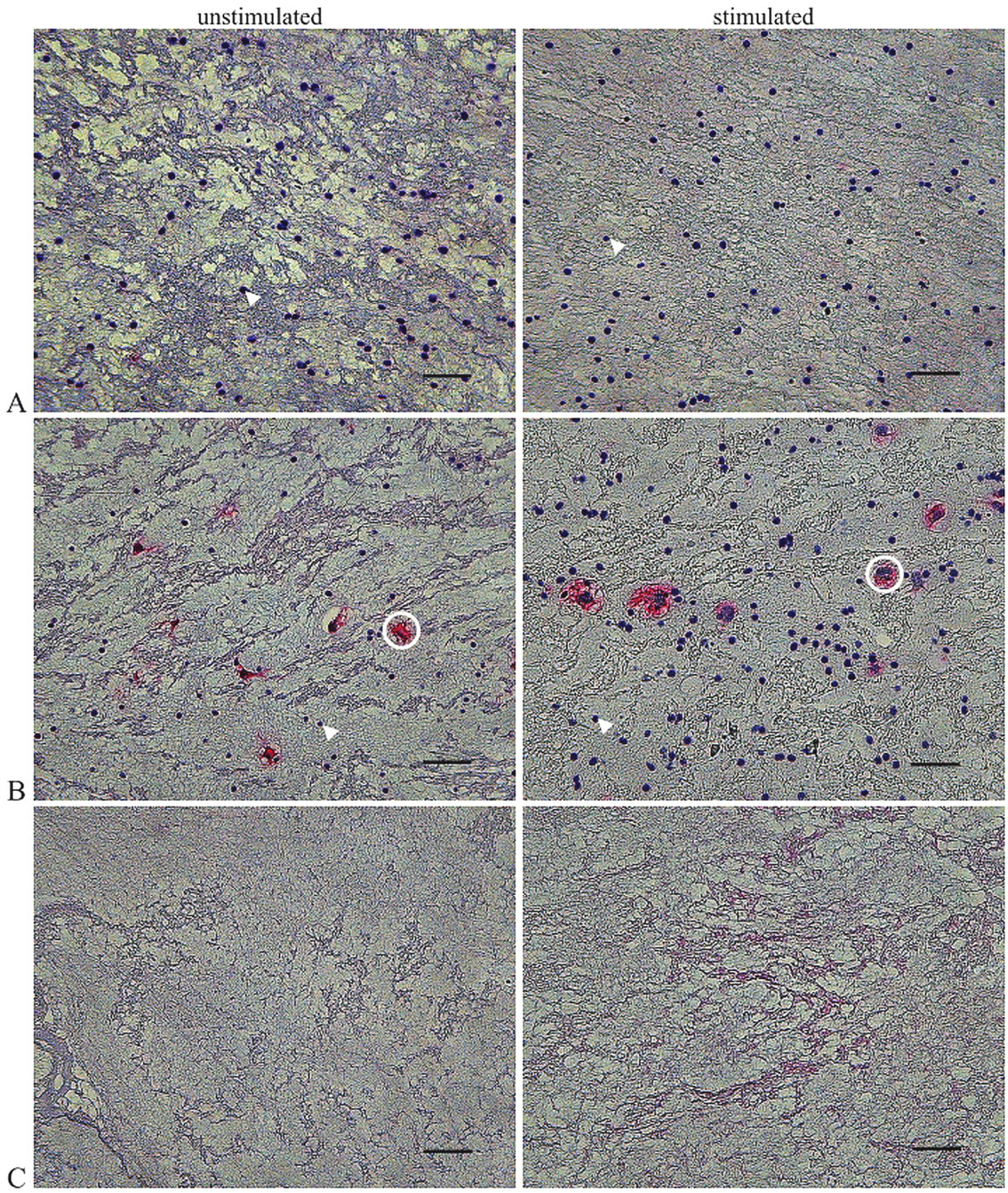

Fig. 3.15: Immunohistochemical staining for MSC-surface marker CD105 (red).

Representative sections of fibrin constructs showing A) CD105 negative T lymphocytes, B) co-culture of T lymphocytes with CD105 positive MSCs, and C) cell free control. The scale bar represents 50µm, the white arrow indicates a T lymphocyte's nucleus and the white circle indicates a MSC. For a negative control section see Fig 3.7C.

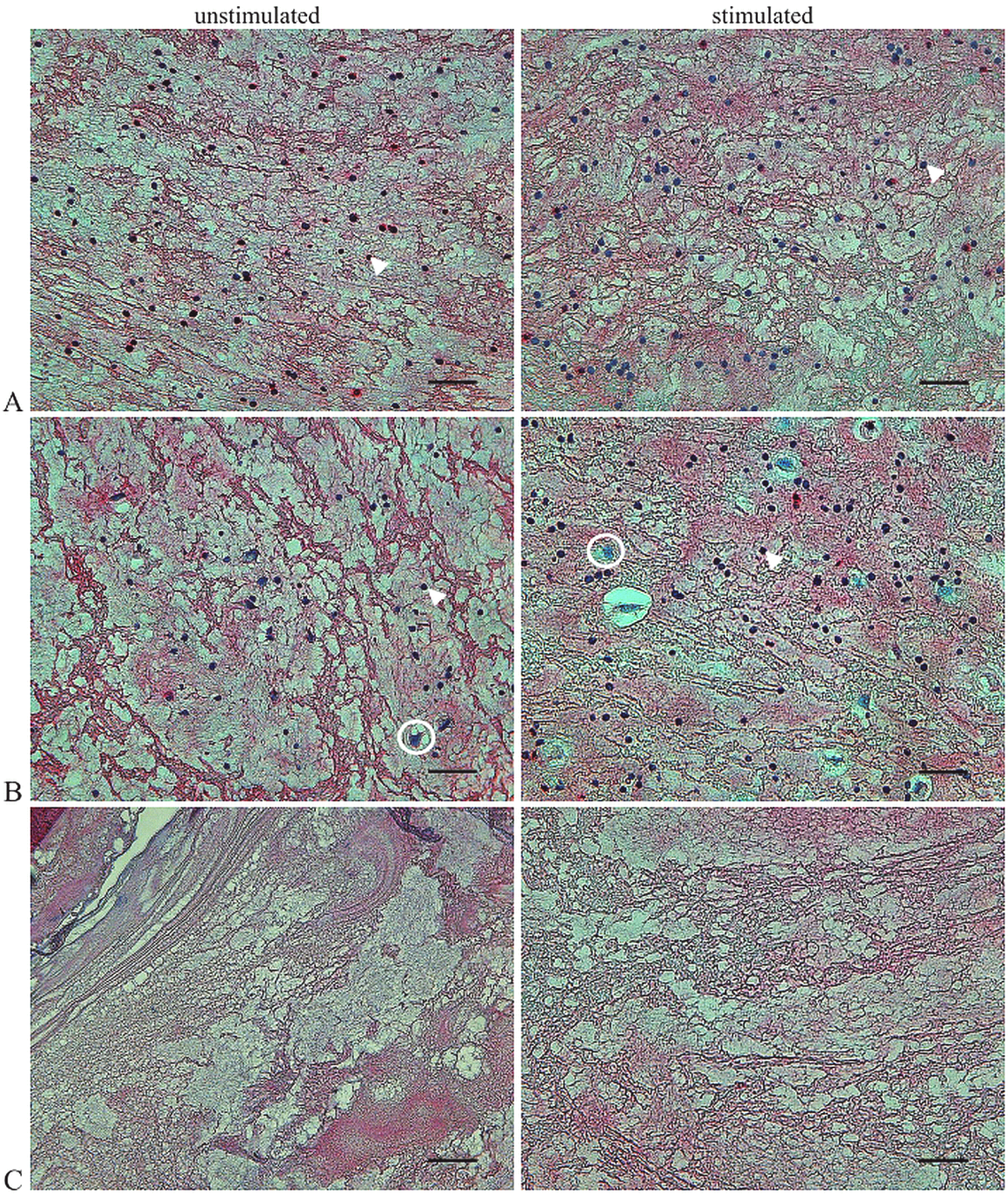

Fig. 3.16: Immunohistochemical staining for VEGF-A (red).

Representative sections of fibrin constructs showing A) T lymphocytes, B) co-culture and C) cell free control. The scale bar represents 50µm, the white arrow indicates a T lymphocyte's nucleus and the white circle indicates a MSC. For a negative control section see Fig 3.8C. In all cases the fibrin matrix was positively stained for VEGF-A, but no obvious staining of VEGF-A positive cells occurred.

3.2.2.7 Analysis of T lymphocytes' and co-cultures' gene expression: stimulated vs. unstimulated

A cluster analysis of the six different groups studied (stimulated and unstimulated MSCs [$1x10^6$ cells], T lymphocytes [$2x10^7$ cells], and co-cultures [$2.1x10^7$ cells], respectively) with the gene array revealed a fairly close relationship ($p \approx 0.06$) between the expression patterns of co-cultures and MSCs. The expression pattern of T lymphocytes was only distantly related (Fig. 3.17).

T lymphocytes showed 63 differentially regulated genes (fold change: >1.5 = up-regulated, <0.67 = down-regulated) of which only 4 were significantly down-regulated (Fig. 3.18). This is a very small number compared to the total number of detected genes: 7360 in unstimulated T lymphocyte samples and 7385 in stimulated ones. Among the up-regulated ones about 30% are involved in mRNA splicing, transcription, or processing. The proteins studied by ELISA that were found to be regulated in MSCs were neither detected on protein nor on mRNA level in T lymphocytes. However, the latter appear to be mechano-responsive as may be concluded from the effect on their general mRNA expression.

In the co-culture 8222 genes were detected in the unstimulated samples and 8014 in the stimulated ones, of which 100 genes were differentially regulated. Of the latter only 4 genes were up-regulated (Fig. 3.18). Co-cultures did show mRNA expression of MMP2, MMP9, and TIMP2, but of none of the other proteins studied. However, the gene expression of none of those genes was significantly up-regulated by mechanical stimulation as seen for the protein expression of TGF-β1, VEGF-A and MMP-2. After all, NRP1, a receptor for VEGF165, an isoform of VEGF-A, was detected in all co-culture samples. A detailed table of all regulated genes in T lymphocytes and co-cultures is in the appendix (Tab. A4 and A5).

Furthermore, MSCs and co-cultures had 13 genes in common that were significantly down regulated (Fig. 4.13). Those included ADM, ALCAM, C10ORF10, CEBPD, EPDR1, FMO3, FZD1, GLDN, LEPR, LEPREL1, RASL11A, SNCAIP, and VCAM1. In 12 out of the 13 cases, the down regulation in co-cultures was slightly more pronounced. ADM and LEPR were about two times stronger down-regulated in co-cultures than in MSCs.

However, three biological processes and two molecular functions (MF) were significantly down-regulated in the stimulated co-cultures. Those were the biological processes signal transduction ($p<0.01$), cell communication ($p<0.01$), immunity and defence ($p<0.05$) as well as the molecular functions ($p<0.05$) cytokine receptor and signalling molecule. For a list of genes here involved see Table 3.5 and 3.6.

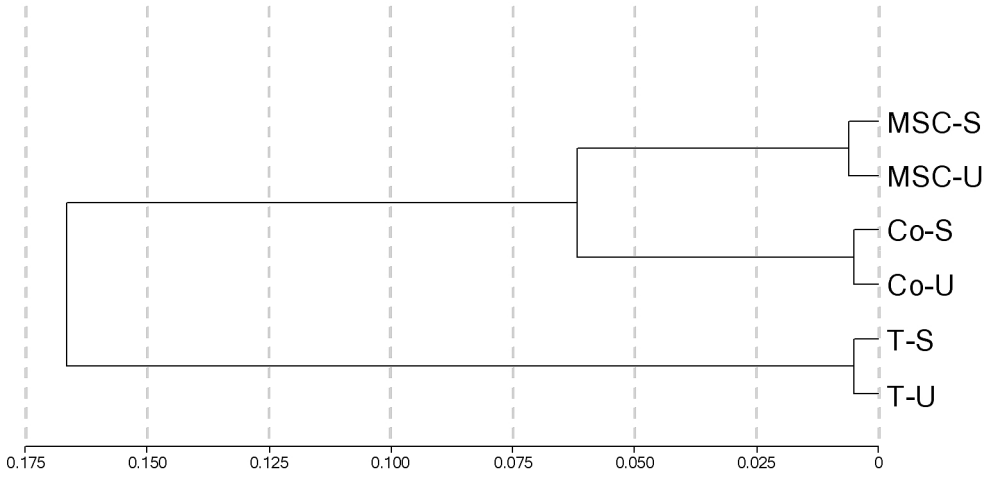

Fig. 3.17: Cluster analysis of the three sample groups (MSCs, T lymphocytes, and co-culture).

Scale gives p-value for correlation of expression pattern. p<0.05 indicates a close relationship between expression patterns. S stands for stimulated and U for unstimulated samples. T lymphocytes' (T) expression profile is only distantly related to MSCs and the co-culture (Co). Within each cell type group there is a very small difference between stimulated and unstimulated samples indicating specifically regulated genes.

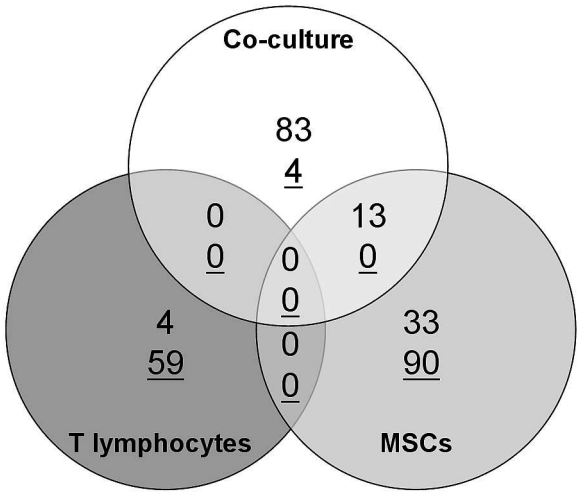

Fig. 3.18: Number of by mechanical stimulation significantly (p<0.05) differentially down- / up-regulated genes.

Tab. 3.5: Mechanically down-regulated biological processes in co-cultures.

Differentially expressed genes, in stimulated co-cultures compared to unstimulated ones, sorted by fold change, which were found to be part of the significantly down-regulated biological processes signal transduction (ST, p<0.01), cell communication (CC, p<0.01), and immunity and defence (IM, p<0.05).

'X' indicates gene is involved in this process.

Gene Symbol	Entrez Gene ID	Gene Name	Fold Change	ST	CC	IM
STC1	6781	stanniocalcin 1	0.11	X	X	
LEPR	3953	leptin receptor	0.16	X		
NCAM2	4685	neural cell adhesion molecule 2	0.30	X	X	
CTHRC1	115908	collagen triple helix repeat containing 1	0.33			X
CXCL10	3627	chemokine (C-X-C motif) ligand 10	0.36	X	X	X
RAB38	23682	RAB38, member RAS oncogene family	0.36	X		
CCL8	6355	chemokine (C-C motif) ligand 8	0.40	X	X	X
FOS	2353	v-fos FBJ murine osteosarcoma viral oncogene homolog	0.40			X
ALCAM	214	activated leukocyte cell adhesion molecule	0.44	X	X	
TF	7018	transferrin	0.45	X	X	X
PTGS2	5743	prostaglandin-endoperoxide synthase 2	0.48			X
GLRB	2743	glycine receptor, beta	0.50	X	X	
VCAM1	7412	vascular cell adhesion molecule 1	0.50	X	X	
CD69	969	CD69 molecule	0.51			X
RASL11A	387496	RAS-like, family 11, member A	0.52	X		
SCG5	6447	secretogranin V	0.52	X	X	
SGCE	8910	sarcoglycan, epsilon	0.52	X		
ANGPT1	284	angiopoietin 1	0.53	X	X	
LEPREL1	55214	leprecan-like 1	0.53	X	X	
MMD	23531	monocyte to macrophage differentiation-associated	0.53	X	X	X
OSMR	9180	oncostatin M receptor	0.53	X		
RGS4	5999	regulator of G-protein signalling 4	0.53	X		
CENTB2	23527	centaurin, beta 2	0.54	X		
LY96	23643	lymphocyte antigen 96	0.54			X
CHEK1	1111	CHK1 checkpoint homolog	0.55	X		X
RHOBTB3	22836	Rho-related BTB domain containing 3	0.55	X		
EFNB2	1948	ephrin-B2	0.56	X	X	
ERRFI1	54206	ERBB receptor feedback inhibitor 1	0.56	X		
HRASLS3	11145	HRAS-like suppressor 3	0.56	X		
ELA2	1991	elastase 2, neutrophil	0.57			X
ACVR2A	92	activin A receptor, type IIA	0.58	X		
SLC1A3	6507	solute carrier family 1 (glial high affinity glutamate transporter), member 3	0.58	X	X	
GADD45A	1647	growth arrest and DNA-damage-inducible, alpha	0.60			X
EFEMP1	2202	EGF-containing fibulin-like extracellular matrix protein 1	0.61	X	X	
WASL	8976	Wiskott-Aldrich syndrome-like	0.64			X
CDH11	1009	OB-cadherin	0.65	X	X	
CYR61	3491	cysteine-rich, angiogenic inducer, 61	0.66	X	X	
PCDH18	54510	protocadherin 18	0.66	X	X	

The biological processes had several down-regulated genes in common. The function of the most interesting ones and their meaning for this study will be discussed in the following chapter.

Tab. 3.6: Mechanically down-regulated molecular functions in co-cultures.

Differentially expressed genes, in stimulated co-cultures compared to unstimulated ones, sorted by fold change, which were found to be part of the significantly ($p<0.05$) down-regulated molecular functions signalling molecule and cytokine receptor. 'X' indicates gene is involved in this molecular function. There were no genes expressed in common.

Gene Symbol	Entrez Gene ID	Gene Name	Fold Change	Signalling Molecule	Cytokine Receptor
STC1	6781	stanniocalcin 1	0.11	X	
LEPR	3953	leptin receptor	0.16		X
ADM	133	adrenomedullin	0.19	X	
CXCL10	3627	chemokine (C-X-C motif) ligand 10	0.36	X	
CCL8	6355	chemokine (C-C motif) ligand 8	0.40	X	
TF	7018	transferrin	0.45		X
SCG5	6447	secretogranin V (7B2 protein)	0.52	X	
ANGPT1	284	angiopoietin 1	0.53	X	
OSMR	9180	oncostatin M receptor	0.53		X
TMED5	50999	transmembrane emp24 protein transport domain containing 5	0.53	X	
EFNB2	1948	ephrin-B2	0.56	X	
ACVR2A	92	activin A receptor, type IIA	0.58		X
EFEMP1	2202	EGF-containing fibulin-like extracellular matrix protein 1	0.61	X	
CYR61	3491	cysteine-rich, angiogenic inducer, 61	0.66	X	

After all, the differential gene expression of MSCs is modulated in the presence of T lymphocytes showing only a small overlap between MSCs and the co-culture and none with T lymphocytes alone.

4 Discussion and Conclusion

Here the results presented in chapter 3 are recapitulated and discussed, and their prospective scientific continuation and also their clinical relevance are assessed.

4.1 Intention of project and summary of findings

As described earlier in detail, mechanical stimulation plays an essential role during bone healing, influencing angiogenesis and therefore nutrition of the newly forming bone. But the ongoing molecular processes are only partly understood. *In vitro* studies can be used to address those processes but only under well defined boundary conditions.

This *in vitro* study aimed to examine effects of mechanical stimuli, as occurring during the onset of bone healing. Firstly, it intended to characterise the mechanical environment in regard to strain and fluid shear in a device that is able to apply tensile strains and to test the determined settings on mesenchymal cells by studying their response in 2D. Therefore, a 2D cell stimulation device was characterised to gain detailed information on the actual substrate strain and fluid shear mechanical conditions. It was shown that the device applies reproducible stimuli, within a short time frame, that are known to induce a mechano-response in osteoblastic cells. However, long-term stimulations encounter a change of the strain environment. As a proof of principle, a combination of strain (4%) and fluid shear stress (~0.09 Pa) was applied to osteoblastic cells and its effect on a known mechanotransducer involved in angiogenesis, αVβ3 integrin, and one of its downstream targets (FAK) was investigated. Only the integrin was seen to be affected by the stimulus observed as clustering.

Secondly, the cellular response of mesenchymal stem cells and T lymphocytes, both separately and in co-culture, to cyclic compression in a haematoma-like environment was compared to determine their importance for mechano-regulated angiogenesis in bone healing and possible immunomodulatory effects. Therefore, a 3D setting employing fibrin matrices was used to study the enhancement of the angiogenic potential of MSCs and T lymphocytes and their co-cultures by cyclic compression. This is the first ever study investigating the mechano-responsiveness of T lymphocytes and their co-cultures to cyclic compression. The presented results for MSCs proved their previously described mechanically induced angiogenic potential with the additional finding that the angiogenic plasminogen activating cascade is also triggered by the stimulation. In comparison, T lymphocytes alone showed no angiogenic potential in the time frame studied but a mechanically driven response at the mRNA level. The co-cultures of the two cell types used showed an angiogenic potential upon mechanical stimulation but less pronounced than with

MSCs alone, perhaps due to an ongoing immune response since allogenic cells were used, although the immune response appeared to be reduced after mechanical stimulation.

Hence, the aims of the investigation were all achieved and the hypothesis that the mechanically triggered angiogenic response is driven by mesenchymal cells and impaired by T lymphocytes has been supported.

4.2 Discussion and conclusion for 2D bioreactor study

The 2D bioractor study was designed to deliver a full-field experimental mechanical characterisation of the strain to which the cells are exposed within the FX-4000T completed by a fluid structure interaction simulation. Additionally, the cellular response of mesenchymal cells to the characterised mechanical environment was to be assessed.

Digital image correlation (DIC) was employed to determine the strain field of $\boldsymbol{\varepsilon_{mem}}$ in BioFlex plates, and its relation to $\boldsymbol{\varepsilon_{rep}}$ and extended use. Previous usage of DIC in biomedical applications [46, 49, 50] and the knowledge of DIC having little measurement (2% of measured strains) [114], systematic (<0.02% strain) [90], and random measurement errors (here: 0.1% - 0.17% strain) suggest DIC as an appropriate method for determining strains in this application.

An analysis of the principal strains on the whole membrane of BioFlex wells across the loading post was performed using DIC, since the radial and circumferential strain are equal to the principal strains in a 2D equibiaxial strain state. It showed that strains were homogeneous (mean of SD approx. 2% of mean $\boldsymbol{\varepsilon_{mem}}$) within a central circular area (R = 9mm) of the BioFlex substrate in agreement with the results of Vande Geest et al. [115]. Their computer model predicted on average, for all strains studied, uniform radial strain within a radius, R = 9.73 ± 0.10mm and uniform circumferential strain within a radius, R = 11.26 ± 0.09mm. Our results show that pooling data from cells across the whole well area could give a misleading impression of mechanically induced effects as only cells adhering in the central area would be subjected to homogenous strain. Hence, correlating mechanically induced effects with magnitude and homogeneity of strain would not be suitable.

The significant offset (1.47% - 3.17% strain) between $\boldsymbol{\varepsilon_{mem}}$ and $\boldsymbol{\varepsilon_{rep}}$, which also significantly increased with an increasing number of cycles, pointed to an inadequate calibration of the FX-4000T though all machine settings and pressures agreed with the manufacturer's settings. Possibly the offset varies between individual FX-4000T systems and, thus, should be characterised for each system used. However, the significant increase of the offset with an increasing number of cycles is cause for concern. As plastic deformation of the membrane material might cause the increase, a comparison of images at minimum applied vacuum was performed. It showed indeed a significant ($p < 0.03$) increase in strain. Additionally, a tensile test on six specimens cut from used BioFlex wells determined, on average, a smaller Young's modulus than for specimens cut from a fresh plate. Both point to a permanent change in the material.

The strains transferred to BMSC cultured in these plates were calculated from changes in vector lengths determined by using an R routine written for the purpose [95].

Uniaxial substrate strain may reach an average transfer to cells of up to 79% in fibroblastic cells whereas biaxial strain was only transferred to 37% in tenocytes [49, 50]. The strain measurement on BMSCs in the present study showed that, on average, about half of the biaxial membrane strain is transferred to the cells. The use of a different cell type, with a different origin and function *in vivo*, and another cell stimulation device may explain the diverging results. The incomplete strain transfer to the cells and the high variation between cells was suggested to be related to the cytoskeletal organisation and the number of adhesion sites [49, 50]. The present study further assumes that disruption of the cytoskeleton takes place due to physical interactions between cytoskeletal molecules [116]. Additionally, isolated cells have more focal adhesions and are more spread than confluent cells [117]; therefore, they are flatter and stiffer, explaining the reduced strain transfer. Further, as partial detachment was observed where no strain transfer may be experienced by the cell, the areas of isolated BMSCs that remain attached experience the full strain. This results in a reduced average strain and high variation between cells. The partial detachment may further explain the reduced cell size after stretching. Additionally, the strain measurements on the cell carpets confirmed the membrane strains measured as well as the offset of $\boldsymbol{\varepsilon_{mem}}$ and $\boldsymbol{\varepsilon_{rep}}$, both determined under dry conditions in the mechanical characterisation.

The maximum random measurement errors estimated for the determination of cell strains were high. One reason is the varying focus position between the acquisitions of images at the same strain. This resulted from the slight vertical movement of the membrane and the cells during stretching. Further, manual adjustment of the focus to compensate for that movement may have affected the choice of the exact location of the measured features. The maximum error of measurement was smallest for the long distance measured cell carpets (1% strain). The high measurement error for cell bodies (2.4% strain) may arise from the difficulty in finding, in every image taken of a cell, the exact prominent location chosen in the reference image. However, these measurements do provide strong insight into the reduced strains actually transferred to single cells within a short-term stimulation.

The fluid structure interaction simulations of the FX-4000T developed by Thompson and colleagues showed that the membrane surface fluid shear stress was inhomogeneously distributed and that the shear stress magnitude, varying linearly over the range of 0.09 – 5.2 Pa, was frequency and culture medium viscosity dependent. This range lies above

previous findings for a similar cell stimulating device with a predicted maximum membrane shear stresses of 0.055 Pa occurring in 6 mm depth of fluid at an operating frequency of 1 Hz [54]. However, that device was substantially different from the present FX-4000T lacking a loading post, resulting in a different spatial and temporal distribution of shear stresses.

Previous studies reported that the shear stress magnitude range predicted for the FX-4000T by Thompson and colleagues is important for bone cells [66, 118]. Furthermore, a linear dependence of the shear stress magnitude on frequency was predicted, which leads to a quadratic dependence of shear stress rate on frequency [96]. Bone cells' sensitivity to fluid shear stress rate has been reported [119-121]. However, a dependency on substrate strain as described elsewhere [85, 86, 122] is not contradicted. Indeed, as known from personal communication (Dr. C.E. Ott, Institute for Medical Genetics, Charité – Universitätsmedizin, Berlin, Germany), changes in stimulation frequency in the FX-4000T were observed to result in strong differences in osteoblastic responses on mRNA level.

As described above, the membrane strain amplitude changes with the number of cycles [51] and as reported elsewhere with frequency and waveform [123], which is due to the viscoelastic nature of the membrane.

On grounds of the computational cost, the assumption of axisymmetry was made for the simulation. The fluorescent microsphere data showed evidence for patterns of non-axisymmetric flow. However, the radial component of the velocity used for the evaluation of the model was always largest [96].

The response of mesenchymal cells to the 2D strain and fluid shear environment was additionally assessed to test the usability of the device under defined boundary conditions: 1200 cycles with consistent (deviation <10%) 4% $\boldsymbol{\varepsilon_{mem}}$ at 1 Hz and an approximate resulting fluid shear stress of 0.09 Pa. The stimulus used was the smallest possible that could be reproducibly applied by the system. As described in section 3.2.3.1, this strain was found to be well tolerated by osteoblast-like cells. Furthermore, strains of up to 5% were predicted to be favourable for intramembranous bone formation [44], resulting in increased proliferation and activity of osteoblasts [43]. Low intermittent shear stress of 0.063 Pa over several hours was also shown to result in an increased proliferation and affected osteoblast metabolism [124]. However, in the present study, only a stimulation of 20 minutes was performed. This is possibly too short to evoke a response so that the observed cellular response is assumed to

mainly result from the strain applied, although an initial stress kick-in is supposed to be present in the used stimulation, as described by Bacabac and colleagues [120].

Surprisingly, this short term mechanical stimulus did not induce phosphorylation of FAK in osteoblasts, as has been described for ultrasound [78]. However, immunocytochemistry of the stimulated osteoblasts revealed affected cell morphology: osteoblasts were less spread and the well organised actin cytoskeleton visible in the unstimulated cells had been disrupted. Cell size was again observed to be reduced after mechanical stimulation, confirming the result reported in the cell deformation study described earlier [51]. Further, the cytoskeleton appeared to be disrupted/unorganised, as suggested in the above mentioned cell deformation study, which might also be related to the biaxial nature of the strain and the magnitude of the stimulus applied. The cell is known to reinforce its structure – stress fibre formation, integrin recruitment to focal adhesions – upon mechanical stimulation resulting in increased cell stiffness and higher traction forces [125]. The same authors suggest the existence of an opposing effect that relieves the cellular stress especially under repetitive tension. They demonstrated that repetitive homogeneous biaxial strain of 10% resulted in fluidisation, seen by a decrease in cytoskeletal stiffness and increase in macro-molecular mobility, whereas, if non-homogeneous strain was applied, reinforcement of the cell and increasing traction forces were observed [125]. In the present study, a homogeneous biaxial strain of 4% was repetitively applied which would accordingly result in fluidisation. This might explain the unorganised cytoskeleton and the missing FAK activation. Katsumi et al. concluded that increased tension in focal adhesions can induce integrin clustering and phosphorylation of FAK [126], resulting in reinforcement. But in the present study, the cytoskeleton appears disrupted, perhaps impairing FAK activation. Integrin signalling usually induces cytoskeletal reorganisation (reviewed by [60]). However, the cellular morphology might also point to a reduced viability. Unfortunately, this was not tested after mechanical stimulation. If such strain was applied uniaxially the cells well tolerated it [43].

Further, as expected the application of the short term mechanical stimulus induced a change in αVβ3 integrin distribution in osteoblastic cells. This was described for a 20min ultrasound stimulation and an application of fluid flow with 1.2 Pa for 15min [77, 78]. More pronounced clusters of this cell adhesion protein, so-called plaques, were observed after longer stimulation at 0.05Hz with an average strain of 7% for two days [76]. This integrin clustering is thought to be involved in angiogenesis and bony matrix production [74, 76].

In the present 2D bioreactor study, it is not possible to determine if the integrin clustering resulted from fluid flow or substrate strain as these variables cannot be uncoupled in the

Flexercell [96]. The same is true for the study of Wozniak and colleagues (2000), and although they used an older version of the Flexercell with lower levels of fluid shear stresses, it is reported that fluid shear stresses have a greater influence than substrate strain on mechanotransduction processes [91, 92]. Indeed, Weyts et al. (2002) saw integrin clustering in osteoblasts due solely to the application of fluid shear stress.

The presented results show that biaxial strain as applied in the Flexercell appears to evoke and then disrupt cell reinforcement responses that are thought to be a good indicator for mechanotransduction. This suggests it is less suitable as a model for normal physiological mechanotransduction but may be applicable in understanding the more extreme environments obtained in bone regeneration. Despite of this, a study at the Institute for Medical Genetics demonstrated that the biaxial setting of the FX-4000T was indeed able to evoke immediate early response genes involved in the MAPK pathway that plays a role in osteoblast differentiation [64]. The latter is a vital step during bone regeneration (see section 1.5).

4.2.1 Conclusion

In conclusion, as demonstrated by the characterisation of the surface $\boldsymbol{\varepsilon_{mem}}$ of BioFlex membranes the FX-4000T applies homogeneous and reproducible strains in the central area of the loading post. Regarding the strain transferred to cells, on average, only half of the applied strain was transferred due to cytoskeletal disruptions and cellular detachment. These results should be considered in the interpretation of any data obtained using this device, especially from high cycle number experiments as $\boldsymbol{\varepsilon_{mem}}$ increased significantly with an increasing number of cycles and was found to be related to changes in the material properties during extended use.

Finally, the present study fulfilled the aim to gain a validated characterisation of the mechanical stimuli applied by Flexcell's FX-4000T. It applies not only strains but also fluid shear stresses which are relevant for osteoblastic responses. Still, some limitations of the present 2D study of mechano-responsiveness of mesenchymal cells are to be considered. The magnitude of the stimuli applied is affected by a gradual change of the material properties of the culture substrate in long term applications that are supposed to be taken into account when using this device. In addition, it is assumed that, though only concluded from a small number of experiments, the biaxial setting chosen may not be optimal for cellular reinforcement studies. Perspectively, a follow-up on the affected cellular morphology and lack of FAK activation is vital to validate those results.

In future, experiments the FX-4000T may be used to have a closer look at the combinatorial effect of fluid flow and strain. This may be assessed using, for instance, different culture medium viscosities and frequencies as already included in the simulation of Thompson et al. (2010). Although the viscosity showed only minor effects on spatial and temporal distribution of the fluid shear stresses, their magnitude was affected. Those experiments are suggested to be performed with cells that are more stretch resistant, keeping the cytoskeleton intact.

After all, 2D experiments, though often used, do not give the full picture. The settings are far away from the three-dimensional situation *in vivo*. Therefore, the results are difficult to translate into the clinic. Conclusions on the effect of mechanical stimulation *in vivo* may be more realistically assessed in 3D *in vitro* experiments as described in the following.

4.3 Discussion and conclusion for 3D bioreactor study

Under clinically relevant conditions present during fracture healing – regarding the cell types, ECM, and the degree of mechanical stimulation – the influence of compression of 3D cell matrix constructs on the cellular response was investigated. This elucidated the importance of MSCs in mechanically promoted angiogenesis which was affected in the presence of T lymphocytes.

4.3.1 Response of MSCs to mechanical stimulation

On the one hand, the effect of mechanical stimulation of MSCs on their angiogenic potential was studied as a proof of principle for the bioreactor system, on the other hand, to elucidate that potential further as well as other mechanically induced effects.

The functional tube formation assay, used to assess the angiogenic potential, demonstrated elevated tube formation by CM from stimulated MSC constructs. Additionally, MMP-2 and TGF-β1 levels in CMs from stimulated MSC constructs were significantly elevated as determined by ELISA. Those results coincide with earlier published data about a pro-angiogenic function of 3D cultured MSCs on ECs [9, 65, 127]. However, neither the level of TIMP-2 nor bFGF was affected on protein level, but VEGF-A was significantly regulated which opposes the data presented in the study of Kasper et al. [9]. Yet, a study by Groothuis et al. (2010) showed that mechanical stimulation of fracture haematomata of young patients (<45 years), embedded in fibrin, resulted in an increase of VEGF-A compared to unstimulated controls, while older patients were unable to regulate VEGF-A under *in vitro* mechanical stimulation [128]. The difference to Kasper's study might result from a different donor cohort (larger age range: 33-84 years), different culture medium (T lymphocyte culture medium instead of MSC culture medium) used for the bioreactor and omitting Trasylol, containing the protease inhibitor aprotinin, from the bioreactor medium. Some aprotinin is already included in the Tissucol fibrin preparation, sufficient to avoid or at least slow down fibrin degradation by embedded cells. Previously, aprotinin was used to maintain the fibrin constructs' mechanical stability, but in a real haematoma, fibrin would be degraded over time, too. Further, as in the present study, the number of donors was limited. Additionally, the method used to up-concentrate the medium for the bFGF ELISA induced a high variation. However, the results demonstrated that the system used is, also with slightly changed conditions, well usable for studying the angiogenic cellular response induced by cyclic compression over three days.

The significantly up-regulated “plasminogen activating cascade” pathway, including its members, the tissue plasminogen activator (PLAT or tPA), the receptor for urokinase plasminogen activator (PLAUR), and the inhibitor of plasminogen activators PAI-1 (SERPINE1) is further supporting the fact that mechanical stimulation enhances the paracrine action of MSCs on ECs inducing tube formation. However, this was only demonstrated on mRNA level by gene expression array analysis. After all, other studies applying compression, cyclic strain or laminar shear stress also demonstrated an induction or inhibition of the plasminogen activation system (PAS), respectively [129-131] where compression results coincide with the present ones. PAS promotes cell adhesion and migration as well as angiogenesis, vital for wound healing but also known for cancer [14, 15]. It consists of a family of serine proteases involved in fibrinolysis. These enzymes degrade the ECM, here fibrin, see also Fig. 3.7 and 3.8, either directly or indirectly, via activation of MMPs and release of growth factors, such as TGF-β1, bFGF and VEGF (Fig. 4.1 + 4.2) [15]. Upon mechanical induction of the plasminogen activation system, MMP-9 and -2 showed an increased activation (Fig. 4.1) [132], with compression in a urokinase dependent manner [129].

MSCs do secrete several paracrine-acting MMPs, including MMP-2 and MMP-3 (Fig.4.1 + 4.2) [65]. MMP-2, which was mechanically up-regulated, is important for angiogenesis as it is involved in creating space for vessel ingrowth and releasing VEGF from the ECM, too (Fig. 3.11) [20, 22, 23, 133], where VEGF is stored upon secretion [25]. Released from the ECM, VEGF mediates angiogenesis by regulation of EC specific mitogen recruitment as well as survival and activity of ECs [26]. In the present study, VEGF, which was mechanically elevated, was present in the fibrin matrix from the beginning, as described by Ho et al. [113] which was supported by the immunohistological findings of the present study. Unfortunately, immunohistology did not reveal if the cells produced VEGF and the gene array analysis showed no mRNA expression of VEGF-A but receptors NRP1 and 2 for its isoform VEGF165. However, MSCs are known to secrete VEGF [134, 135]. From the present results it may be concluded that the ELISA mainly measured VEGF increasingly released from fibrin by the plasminogen activation system (PAS) but not by MMP-2. MMP-2 is not able to degrade fibrin contrary to MMP-3 [136]. The latter was not studied here. Surprisingly, in contrast to Kasper’s study, MMP-2’s antagonist TIMP-2 showed an unchanged level. Possibly the increase of the MMP-2 concentration was so small that TIMP-2 might not need to be regulated yet. However, omitting aprotinin is not supposed to be the reason [137]. As Kasper et al. showed, too, MMP-2 was only mechanically regulated on protein level in the

present study, which likely points to involvement of a post-transcriptional regulatory process in response to mechanical stimulation. In addition, perhaps an affected secretory process explains this result. If the transcriptional control is involved, this could be assessed by employing, for instance, cyclohexamide.

The CMs of cell-free controls showed a basal level of TGF-β1, which is contained in the FBS used to supplement the culture medium. Higher levels of TGF-β1 were determined in CM of MSCs, further enhanced after mechanical stimulation. MSCs therefore seem to secrete TGF-β1, as described earlier (Fig. 4.1 + 4.2) [134, 138]. It is known to enhance proliferation of cells of mesenchymal origin and to induce ECM production, angiogenesis and VEGF [26] acting in an autocrine (e.g. osteogenic differentiation) and paracrine (e.g. angiogenesis) manner (Fig. 4.1) [18, 138-140]. The up-regulation of TGF-β1 could point to an "activation" of the MSCs that they start to proliferate and produce matrix. It was shown earlier that TGF-β1 and proliferation were significantly enhanced after cyclic stimulation [79]. Further, it here coincides with the up-regulation of VEGF (Fig. 4.1) supporting the fact that it mediates VEGF expression. Moreover, proteases, as, for instance, MMP-2, are known to bind to αVβ3 integrin [18, 141] and both MMP-2 and MMP-9 activate latent TGF-β1 (Fig. 4.1 + 4.2) [18, 142]. In contrast, Kasper et al. observed that TGF-β1 is not dependent on MMP-2 *in vitro* [9]. Additionally, mechanics can induce activation of TGF-β1 due to a conformational change mediated by integrins and stress fibres bound to latent TGF-β1 [143, 144]. This is supported by the fact that TGF-β1 signalling is controlled by the regulation of αVβ3 integrin by PAI-1 (SERPINE1) [18], a member of PAS. By PAI-1 reduced MSC adhesion, MSC survival is negatively regulated [145]. The transcription of PAI-1 is, for instance, mediated by TGF-β1 and hypoxia [14, 15, 145]. The MAPK/AP-1 pathway contributes to this transcription. This pathway is activated upon changes in the actin cytoskeleton, which again affect TGF-β1 [146]. TGF-β1 further down-regulates uPA [16] whereas VEGF and bFGF are known to induce both, the activators and the inhibitor, as well as the urokinase activator receptor [19, 147].

Surprisingly, the gene expression array detected no TGF-β1 expression in contrast to the ELISA. However, most likely, the TGF-β1 increase resulted from an increased release from the fibrin by PAS.

For the first time it was shown that mRNA of PAS members was up-regulated by mechanical stimulation in MSCs (Fig. 4.1) contributing to the angiogenic potential of MSCs. In-house studies could likely not reveal this as beforehand the protease inhibitor aprotinin (Trasylol) was used. Aprotinin is known to inhibit PAS [15].

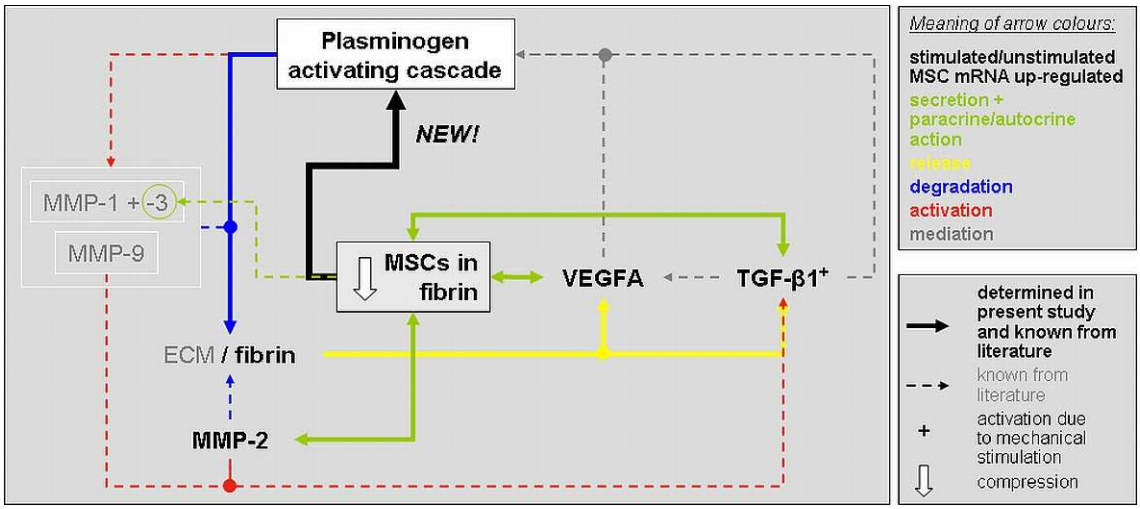

Fig. 4.1: Schematic summary of results for mechanically stimulated MSCs.

The pathway and factors interacting that are part of the angiogenic potential of stimulated MSC are shown.

Not only was the angiogenic potential of MSC studied but also the affect of mechanical stimulation on the glucose and lactate metabolism. The lactate production of MSCs was found to be significantly elevated due to mechanical stimulation. Lactate is generated under anaerobic conditions by reduction of pyruvate, a side product of glycolysis. Therefore, the metabolism of the cells might have switched to anaerobic cell respiration. However, the glucose level remained unchanged. In addition, the glucose level in CM of cell free controls varied highly, which is assumed to mirror the measurement error of the method. Therefore, any differences in the present small sample number are supposed to be interpreted with caution.

The presence of hypoxia within the fibrin matrix is likely as the protein level of VEGF, mRNA expression of PAI-1, and the induction of tube formation were, at least under mechanical stimulation, enhanced in the present study [145, 148]. Still, bFGF levels are supposed to be elevated, too [148] and MMP-2 would be down-regulated [149]. Nevertheless, hypoxia resembles a more realistic environment, as it is thought to be present during the onset of healing due to the disruption of the vasculature upon fracture. With progressed vessel ingrowth, subsequent oxygen tension increases [30]. It is possible that the oxygen content within the constructs was decreased but not as low as in hypoxia. However, on mRNA level the hypoxia related factors HIF1-α and its inhibitor were expressed, though not differentially regulated by mechanical stimulation. To elucidate the oxygen supply and consumption within the fibrin constructs, also under mechanical stimulation, another study is currently performed within another PhD project.

Other effects not directly involved in angiogenesis were observed that are of interest regarding the mechano-response of MSCs in general. Some of the significantly up-regulated genes (ARHGEF2, SLC7A11 and SLC7A5, ITGA5) and down-regulated genes (CTNNAL1 and RAC2) appeared to be of special interest for this study. ARHGEF2 (also GEF-H1) protein is important for cell migration and if phosphorylated it activates Rho-GTPases. Cytoskeletal reorganisation as well as focal adhesion dynamics via Rho activation is depending on it [150-152]. ITGA5 coding for integrin α5 is involved in osteogenic differentiation involving, among others, ERK1/2-MAPKs [153] and is present in focal adhesions [154]. Furthermore, upon the adhesion and spreading of cells integrin α5 clustering and cytoskeletal rearrangements were observed [155]. As described in chapter 1.5, ERK1/2 is involved in cytoskeletal rearrangements, as, for instance, during cell migration and attachment. The significantly down-regulated RAC2 is involved in chemotaxis of neutrophils and superoxide generation. For chemotaxis the actin cytoskeleton requires reorganisation [156]. RAC2 also mediates activation of host defence by affecting the lymphocyte production [157]. CTNNAL1, which belongs to the vinculin/aplha-catenin family, was also down-regulated by mechanical stimulation, and it appears to interact with ARHGEF1 as shown by a yeast two-hybrid study [158]. It seems that CTNNAL is involved in wound repair and FAK phosphorylation promoted by fibronectin [159]. The down-regulation of the named genes could be a result of the up-regulation of ARHGEF2. Unfortunately, it has not been published anywhere how or if they interact. However, it may be concluded that a reorganisation of the cytoskeleton takes place, due to the mechanical stimulus to reinforce the cell. And further, the reorganisation, as described above, could lead to an activation of TGF, contributing to angiogenesis also involving the plasminogen activation system.

The genes SLC7A 11 and 5 (xCT and 4F2, respectively) code for an amino-acid transporter importing cystine [160]. Cysteine, which was converted, for instance, by an antigen presenting cell (APC) from imported cystine and was then exported, is needed for T lymphocyte activation [161]. As only the import is up-regulated in the present study rather than the export, the MSCs might reduce the availability of cystine. Therefore, less cystine for conversion to cysteine would be available and T lymphocytes would be deprived of one activator. Together with the down-regulation of RAC2, those results could be a hint for an immunomodulatory effect of mechanical stimulation.

However, all the above-named genes were neither examined on protein level nor were any cytoskeleton rearrangements studied. Therefore, the results give only hints at their involvement and function in the mechano-response and need further examination. After all,

the immunomodulatory effect was further tackled in the following section including the co-culture of MSCs with T lymphocytes.

In conclusion, mechanical stimulation of MSCs in an *in vivo*-like environment fosters a pro-angiogenic response, perhaps involving cytoskeletal rearrangements and fibrin/haematoma degradation. Hence, mechanical stimuli that are known to improve bone healing do act supportive in angiogenesis. This study offers additional proof, on the molecular level, of the *in vivo* findings described in literature. However, the details on the interaction of the cytoskeleton and angiogenesis deserve further attention.

4.3.2 Response of T lymphocytes and co-cultures to mechanical stimulation

In all aspects studied regarding protein expression and tube formation, T lymphocytes alone showed no mechano-response. Generally, there was hardly any secretion determined for the investigated proteins. In all cases the protein concentrations were comparable to the cell-free control, either resulting from the culture medium and accordingly the included FBS or ranging close to the detection limit. Taken together with the lack of glucose consumption, lactate production, and IL-2 secretion, the T lymphocytes are thought to be resting. A study with thymocytes, premature T lymphocyte, showed that resting cells produced only 3% of the lactate amount produced by activated/proliferating thymocytes. Also, the oxygen consumption, even in absence of glucose, remained unchanged [162]. This is further supported by the fact that they were, in the present study, isolated from peripheral blood and by the lack of known activators, such as antigen presenting cells (APCs) in the present culture. However, allogenic MSC carrying low levels of MHC-I could act as activators for $CD8^+$ T lymphocytes in co-culture, especially if occurring in large numbers, which is not the case in the present study.

Further, mitogenic chemicals, such as concavalin A, activate the T lymphocytes. And a conversion from oxidative to glycolytic metabolism was observed upon stimulation of lymphocytes with interleukins [163].

Nevertheless, the T lymphocytes do have surface receptors that may be important in the transduction of mechanical signals. Lymphocytes, which have been circulating in the blood stream, adhere to ECM components at sites of inflammation and lymphoid tissues. The regulation of their adhesion, including the affinity of integrins for the ECM ligands and subsequent alteration of cell spreading, is mediated by Rac. Upon the cells' adhesion and spreading, integrin α4 and 5 clustering and cytoskeletal rearrangements were observed [155]. This coincides with the findings described in chapter 3 for osteoblastic cells. Additionally, T

lymphocytes express the P2X7 nucleotide receptor (P2X7R) [164], which was mechanically up-regulated by 1.59 fold on mRNA level in the present study. P2X7R is an ATP-gated ion channel, which is also present on osteoblasts and osteocytes needed for bone formation. Fluid shear stress was observed to result in a release of ATP in wild type osteoblastic cells through P2X7R and PGE2 expression increase. Additionally, knock-out of this receptor in mice resulted in a lesser degree of bone formation after mechanical limb loading [165]. Further, P2X7R is required for the effective activation of T lymphocytes via ATP release and a positive feedback loop [164]. Hence, it is likely that T lymphocytes' activation is maintained or even induced by mechanical stimulation.

In general, the mechanical stimulation resulted on mRNA level in the expression of genes used for transcriptional and splicing processes pointing to a kick-off for a mechano-response on protein level. Further studies are needed to elucidate the mechano-response of T lymphocytes on the protein level. So far, T lymphocytes, at least resting ones, are most likely not involved in mechanically improved angiogenesis but MSCs.

Co-cultures showed a more pronounced mechano-response close to that of MSCs. The up-regulation of MMP-2, but not its antagonist TIMP-2 or bFGF, after stimulation of co-cultures, coincided with the finding for MSCs alone. Further, the expression levels of the named proteins as well as the increased induction of tube formation after mechanical stimulation were not significantly different, though the median cumulative tube length was obviously lower in co-cultures. It might therefore be possible that those mechanically induced effects are mainly resulting from the MSCs, which underline their importance for the promotion of angiogenesis. Mechanical stimulation of human fracture haematomata containing mainly immune cells increased their angiogenic potential [166]. However, the CMs of unstimulated co-cultures induced significantly ($p<0.01$) less tube formation compared to the ones of unstimulated MSCs. After all, in the presence of T lymphocytes the angiogenic potential of CMs of unstimulated co-cultures is comparable to the one in controls or by T lymphocytes alone. It is therefore prohibited by the T lymphocytes.

Furthermore, TGF-β1 was expressed by the co-culture (Fig. 4.2) on a comparable level as by mechanically unstimulated MSCs, but it was not affected by mechanical stimulation. As no fibrinolysis-related genes could be detected on mRNA level and only little fibrin degradation in histological sections (but only one sample per condition examined), it is possible that no additional TGF-β1 is released from the matrix upon mechanical stimulation, as observed for MSCs alone. Further, the mRNA level of TGF-β is supposed to increase when activated T

lymphocytes have cell-cell contact with MSCs inhibiting T lymphocyte proliferation (Fig. 4.2) [138, 167] Yet, cell-cell contact is mostly prohibited by the fibrin. It was hardly observed in histological samples, but very small, invisible protrusions may be present

VEGF was significantly mechanically down-regulated in the co-cultures with a similar level, as found in CMs of unstimulated MSCs. It is also known to inhibit the proliferation of T lymphocytes (Fig. 4.2) [167] and to be enhanced in co-cultures [168] suppressing the inflammatory reaction. Further, it is known that VEGF is present in human fracture haematomata [32]. T lymphocytes do, like MSCs, secrete bFGF and VEGF (Fig. 4.2), both promoting angiogenesis, and the mRNA level of VEGF was further enhanced under hypoxia [169]. Therefore, it is not surprising that $CD4^+$ T lymphocytes were earlier found to be involved in angiogenesis depending on the CD4 receptor. Injection of lymphocytes into mice showed lower vessel formation if the cells were pre-treated with a specific antibody against the CD4 receptor [170]. However, in the present study T lymphocytes alone did not show bFGF or VEGF expression. In spite of this, VEGF was significantly higher in unstimulated co-cultures than in stimulated ones, which could point to an interaction of T lymphocytes and MSCs or even activation of the former. Possibly further supporting is the observed trend to a higher lactate production and glucose consumption in unstimulated co-cultures compared to unstimulated MSCs. Still, the glucose level in CM of cell free controls varied highly. This is assumed to represent the measurement error of the method. Therefore, any significant differences in glucose levels between samples are possibly not valid. The determined amount of lactate is not the sum of lactate produced by T lymphocytes and MSCs as one might suggest. After all, this higher lactate production in co-cultures could also be a result of the higher cell number reducing the available amount of oxygen within the fibrin construct. Besides, the metabolism of the MSCs might increase in the presence of T lymphocytes. However, it cannot be safely concluded on the activation status of the T lymphocytes from the experimental data gained as it is difficult to distinguish which cell type caused the effect. Cell sorting after the bioreactor experiment would have been necessary to elucidate this.

Moreover, in stimulated co-cultures compared to unstimulated ones, the gene expression array revealed mechanical down-regulation of the signalling molecules cystein-rich protein 61 (CYR61) and angiopoietin 1 (ANGPT1). Both were detected together with VEGF in the transcriptome and secretome of MSCs as well as in tissue treated with MSCs [134, 135, 171, 172]. Also, those factors were shown to induce an angiogenic response *in vitro* or even neovascularisation and improve wound healing *in vivo* [134, 171, 172]. It was surprising that

this down-regulation was not present in MSCs and that the tube formation induced by CMs of stimulated co-cultures was not significantly different from the one of stimulated MSCs, because CMs of one MSC donor induced no increase upon stimulation, though it appeared to be lower.

Additionally, MSCs are known to express the chemokines interferon-inducible protein 10 (IP-10 or CXCL10) and, only weakly, monocyte chemoattractant protein-2 (MCP-2 or CCL8) (Fig. 4.2) [134]. Both are chemoattractants for immune cells but only CCL8 is known to attract $CD4^+CD8^+$ T lymphocytes [173]. They were the only signalling molecules involved in all significantly down-regulated biological processes found in the present study, pointing to reduced need for immune/inflammatory cells under mechanical stimulation.

The 13 genes significantly down-regulated by mechanical stimulation in both MSCs and co-cultures included among others ADM, ALCAM, LEPR, and VCAM1 (Fig. 4.2). Adrenomedullin (ADM) is a target gene product of HIF1A, both needed for survival of activated T lymphocytes under hypoxia [174]. It codes for an angiogenic protein enhanced under hypoxia [175, 176]. However, the hypoxia inducible factor 1α (HIF1A) was detected but not regulated in stimulated T lymphocytes and co-cultures as well as unstimulated co-cultures. Further, adrenomedullin is known to reduce osteoclastic activity and to perform an immunomodulatory function by inducing regulatory T lymphocytes, regulating T lymphocyte action, and affecting cytokine expression: decreasing inflammatory cytokines but increasing anti-inflammatory cytokines such as IL-10 and TGF-β1 [177]. Additionally, it is described as a paracrine-acting antifibrotic factor secreted by MSCs [178]. ADMs' down-regulation could point to a reduction of angiogenesis and the lack of a need for an immunomodulator in the presence of a mechanical stimulus. Further, its down- regulation might be another explanation for the unchanged level of TGF- β1 after mechanical stimulation together with the lack of PAS induction in co-cultures.

The activated leukocyte cell adhesion molecule (ALCAM or CD166) is, as a complex with CD6, vital for long-term binding of T lymphocytes to APCs and T lymphocyte proliferation [179]. Together with vascular cell adhesion molecule 1 (VCAM1 or CD106), it is expressed by a MSC subpopulation. The function of that subpopulation is still under investigation [180]. VCAM1 might be vital for antigen presentation because MSCs showed an increased affinity for activated T lymphocytes via VCAM1 [181]. ALCAM and VCAM1 down-regulation may be a hint at a reduced T lymphocyte activation capacity under mechanical stimulation.

ACVR2A and cyclooxygenase-2 (COX-2 or PTGS2) are both involved in osteogenic differentiation vital for subsequent bone formation [182-184]. However, the role of ACVR2A,

a type II BMP receptor, is controversially described in literature. On the one hand, ACVR2A was determined as an essential receptor for BMP6 and 7 signalling [182] and, on the other hand, as inhibitor of osteogenic differentiation [183].

Also, COX-2 and FOS, an AP-1 member, are both involved in the biological process immunity and defence together with LY96, and CD69 (Fig. 4.2). Cyclooxygenase-2, which is a down-stream target of FOS, is the target of nonsteroidal anti-inflammatory drugs since it synthesises prostaglandins, mediates inflammation, pain, and fever [185]. COX-2 is, for instance, expressed by monocytes [186] and mesenchymal cells [66, 69, 78]. It can be up-regulated in monocytes by T lymphocytes [186] and, due to mechanical stimulation, as well as FOS [66, 69, 78]. Surprisingly, COX-2 is down- regulated possibly again pointing to a reduced immune response. However, there seem to be additional effects on MSC differentiation but those need to be addressed further in another study.

CD69 is a marker for T lymphocyte activation which remains unchanged in the presence of MSC co-cultured 1:10 with T lymphocytes. However, the proliferation was inhibited [187]. Switching the ratio to 10:1, expression of CD69 was reduced [138]. After co-culture with MSCs T lymphocytes revealed a regulatory phenotype [188]. Together with the down-regulation of ADM, it may be suggested that regulatory T lymphocytes are not essential under mechanical stimulation.

The leptin receptor CD295 (LEPR) functions as a cytokine receptor. It is expressed on resting $CD4^+CD8^+$ T lymphocytes, up-regulated upon activation and was described to be involved in T lymphocyte mediated immunity [189]. Further, $CD4^+$ T lymphocytes of LEPR deficient mice showed a reduced proliferation [189]. This receptor was also found on MSCs but on those of increasing age or even dying ones [190]. Additionally, CD295 is vital for glucose homeostasis [189, 191]. In addition, the down-regulated Lymphocyte antigen 96 (Ly96 or MD-2) forms a complex with toll-like receptor 4 (TLR4) that is needed for recognition of a bacterial glycolipid (LPS) which induces $CD8^+$ T lymphocyte activation [192, 193]. This might again show that T lymphocyte activation is reduced under mechanical stimulation.

In summary, the gene expression profile of the mechanically stimulated co-culture points to a reduction of an apparently ongoing immune response which was present due to the co-culture of allogenic, immunomodulatory MSCs with T lymphocytes. The activation of T lymphocytes was reduced and, therefore, no additional regulatory T lymphocytes might be needed. Due to the immune response the angiogenic response was affected on mRNA and

protein level perhaps playing a secondary role. However, the appearance of an immune response, as in the present system, and the effect of mechanical stimulation on it require further elucidation, especially as the T lymphocytes alone were thought to be in a resting state and no further validating experiments have been performed so far.

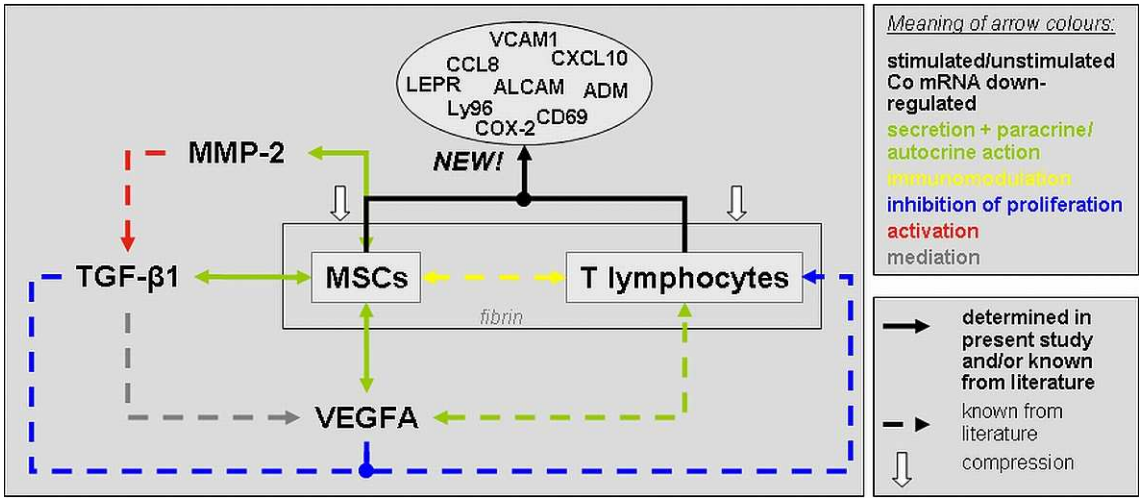

Fig. 4.2: Schematic summary of results for mechanically stimulated co-cultures.

The regulated genes and proteins and their interactions are shown, all affecting the angiogenic potential on mRNA and protein level.

4.3.3 Conclusion

The study described in this subchapter aimed to compare the mechano-response of MSCs, T lymphocytes and their co-culture to cyclic compression in a haematoma like environment in order to determine their importance for mechano-regulated angiogenesis in tissue regeneration. It was found that MSCs are essential for mechano-regulated angiogenesis. Only media conditioned in their presence (MSCs, co-culture) induced angiogenesis, which was further enhanced by mechanical stimulation. T lymphocytes alone did not induce angiogenesis, but they are mechano-sensitive. This is the first study that examined if mechanical stimulation influences angiogenesis mediated by immune cells.

Largely, the proteins enhanced in conditioned media (CM) of MSCs upon mechanical stimulation are suggested to be released by the plasminogen activation system (PAS). Further, PAS is likely part of the angiogenic potential of MSCs. Furthermore, the Rho-GTPase RAC2 down-regulated on mRNA level and the up-regulated cystine transporter (SCL7A11 and 5) could be a hint at an immunomodulatory effect of mechanical stimulation. Co-culture of MSCs with T lymphocytes diminished the amount of some pro-angiogenic proteins (TGF-β1, VEGF) and mRNAs (CYR61, ANGPT1) if a mechanical stimulus was applied. Two reasons are suggested. First, neither PAS was found to be regulated nor was strong matrix degradation visualised in histological sections needed for the release of additional pro-angiogenic factors to the ones secreted by the MSCs. Second, the co-culture of allogenic cells seemed to induce a slight immune reaction (enhanced VEGF, enhanced biological process immunity and defence), which is diminished upon mechanical stimulation.

This 3D bioreactor study was able to further elucidate the molecular processes possibly ongoing in the fracture haematoma due to the interaction between mesenchymal and immune cells. Improved healing due to mechanical stimulation may be driven by the angiogenic potential of MSCs and an immunomodulating effect of the stimulus. However, further studies will have to be performed to get a better insight into the effects of mechanics on immunomodulation. This study only gives a first hint.

4.4 Limitations of study and perspective continuation

Two complementary experimental models were used. The 2D stimulation device enabled an accurate characterisation of the mechanical environment that could be directly related to measured biological effects while the 3D device provided an environment resembling the fracture haematoma in terms of extracellular matrix, cellular composition and mechanical boundary conditions, thus getting closer to the clinical situation for ease of knowledge transfer.

Though this study offers promising results helping to elucidate how bone healing may be improved by mechanical stimulation of mesenchymal cells promoting angiogenesis and therefore the progression of healing, there are some limitations that slightly narrow the explanatory power.

The mechanical characterisation of the 2D stimulation device revealed a change of the mechanical environment correlating with the duration of stimulation. However, for short-term-stimulation the device offers a consistent environment. It was not tested if the observed change in mechanical environment had a measurable effect on the molecular response. This could be done, for instance, by a comparative gene expression analysis of immediate early response genes, like FOS and COX2, with fresh and extensively stimulated plates. For instance, mesenchymal cells could be seeded at the same density onto a fresh BioFlex plate and onto one that has previously been stimulated for at least 5000 cycles. Both plate conditions are exposed to a short-term stimulation and mRNA expression levels are assessed to determine if the strain deviation (~0.5%strain) matters. At least three different sets of experiments should be performed.

In addition, this study points to further experiments to decouple the effects of substrate strain and fluid shear stresses on cultured cells. These would use varying concentrations of carboxymethyl cellulose (CMC) to increase culture media viscosity and, consequently, shear stresses. This would offer the opportunity to answer the controversial question of which form of stimulation is most critical for bone healing.

Regarding the molecular response to the 2D stimulation, a higher number of experiments is to be performed to support the interpretation and, especially, a validation of the lack of FAK activation is of interest. Here a SDS page with subsequent Western blot for detection of inactive and activated FAK could be employed. In addition, as the integrin studied is thought to be involved in angiogenesis [74, 75], a functional analysis of the media conditioned by the Flexercell stimulation with a tube formation assay could be added. But the stimulation of

MSCs cultured on Matrigel did not result in an angiogenic response induced by their conditioned media [194], as described for MSCs stimulated in fibrin constructs [9]. *In vitro* experiments using osteoblasts observed expression of pro-angiogenic VEGF-A [195, 196], and their conditioned media induced tube formation [196]. Possibly, present VEGF could in future experiments be detected in the conditioned medium of mechanically stimulated osteoblasts using, for instance, ELISA.

Although the 2D stimulation device appeared not to be usable for the examination of reinforcement responses to a short-term stimulation, the author would recommend performing a follow-up of this because the present study only analysed a small number of experiments. In conclusion, the 2D study presents a characterisation of the strain and fluid shear environment, which allows better correlation of the mechanical environment and cellular responses, opening new possibilities to directly correlate short-term strain and fluid shear application to a cellular response, which was difficult earlier.

The mechanical environment in the 3D bioreactor used is not that well characterised but is thought to closely resemble the *in vivo* situation during fracture healing. The mechano-responsiveness study omitted the proteinase inhibitor aprotinin, previously used by Kasper et al. (2007), from the culture medium as it is not present *in vivo* resulting in a closer resemblance of the *in vivo* situation. However, the proof of principle showed that most responses of MSCs are conserved, compared to the previous studies of Kasper and colleagues, though the fibrin constructs appeared to be more compact after stimulation than with additional proteinase inhibitor in the medium. Nevertheless, the fibrin constructs themselves contain some aprotinin prohibiting major degradation of the constructs by the included cells to enable strain transfer. It is thought that the strain distribution within fibrin constructs is heterogeneous, which does not allow any conclusion on the strain reaching single cells as could be estimated in the 2D study. Since the bioreactor is a closed system it will be difficult to tackle this issue by methods such as 3D digital image correlation.

Another issue that might be problematic for the cells is the possibly occurring hypoxia within the fibrin constructs. However, this would again just make the situation more *in vivo*-like, as due to the disruption of the vasculature upon bone fracture, the haematoma is in an hypoxic environment (in closed fractures). A currently ongoing study at the Julius Wolff Institute, performed by Florian Witt, employs optical oxygen sensors to determine the oxygen content and consumption of different cell types embedded in fibrin constructs. This is supposed to give further clues on the oxygen supply. Recent results with MSCs embedded in fibrin point to a hypoxic environment which supports the presented findings. Hypoxia can be overcome

by usage of additional perfusion during the experiment though introducing additional shear stresses.

An analysis of differentially expressed genes between, for instance, stimulated MSCs and stimulated T lymphocytes would have been interesting, but such an analysis was not possible due to the different cell numbers used.

The resting $CD8^+$ T lymphocytes used were thought to possibly be activated by the presence of (MHC-I expressing) allogenic MSCs in the co-culture. Activation seems to happen as concluded from the gene expression array data. Unfortunately, this was not further confirmed on protein level. This is supposed to be done in forthcoming experiments. The allogenic setting chosen resembles partly the situation that would be present in an off-the-shelf cell therapeutic approach where pre-expanded allogenic MSCs are applied to the fracture site. However, to avoid additionally immune reactions the use of autologous cells is preferable.

The use of mitogenic activated T lymphocytes would have probably given a better insight into the mechano-responsiveness of this cell type when mechanically stimulated alone, and the regulatory function of MSCs in the presence of T lymphocytes possibly acting during the course of bone healing. Especially, during the inflammation phase the T lymphocytes are likely activated. Future studies will have to be performed to further elucidate this. Those studies can include the comparison of the expression profile of resting and mitogen activated T lymphocytes before and after mechanical stimulation and also in combination with MSCs. Furthermore, as mechanical stimulation was observed to reduce an ongoing immune response in the co-cultures on mRNA level, this should be further examined on protein level. In addition, 2D co-cultures of either unstimulated or stimulated MSCs with T lymphocytes could be used to elucidate the mechanically affected immunomodulatory effect of MSCs. Again, the protein level needs to be assessed additionally to the mRNA level.

The results gained with the T lymphocyte population used can, of course, not elucidate the action of all the different immune cells present during the onset of fracture healing, but they make up about a fourth of all the cells present in sheep haematomata [31]. Therefore, the mixed CD4/CD8 population appeared to be a good starting point to study the effects of mechanical stimulation of T lymphocytes and their angiogenic potential. The CD8 population, which could be activated via MSCs' MHC-I, is known to slow down the wound healing process whereas the CD4 population appears not to have an influence [107], but both populations are thought to be involved in angiogenesis [169, 170]. In addition, the ratio of those two populations present in the fracture haematoma is known [32] and was well applicable *in vitro*.

The bioreactor experiments to assess the gene expression of MSCs and the co-cultures were performed with cryo-preserved MSCs. This is also to be considered regarding the deviations between the results on protein and mRNA level. However, the study of Kasper et al. (2007) neither detected differential regulation of the mechanically regulated proteins on mRNA level.

In general, the bioreactor, with well acceptable deviations regarding the assays' results for the small sample numbers examined, proved to be well usable for the study of pro-angiogenic responses.

The follow-up of cellular responses to 2D and 3D stimulation is supposed to emphasise the presented results and give further insight into the molecular processes that were addressed here. Still, other bioreactors, stimulation regimens, species or matrices can be used to test if the results presented are conserved.

4.5 Overall conclusion and clinical relevance

In conclusion, mesenchymal cells are mechano-responsive to stimuli as occurring during the onset of bone healing, especially regarding the expression of pro-angiogenic proteins. This is concluded from clustering of the αVβ3 integrin, which is known to be involved in angiogenesis, observed in the 2D *in vitro* experiment and the increased secretion of pro-angiogenic proteins in a 3D haematoma-like environment acting in a paracrine manner on endothelial tube formation. Furthermore, T lymphocytes alone showed no angiogenic potential inducible by mechanical stimulation in the time frame analysed. However, the co-culture results imply that mechanically stimulated MSCs act not only pro-angiogenically but also seem to act suppressively regarding an ongoing immune response. This is a new aspect that explains the positive effect of mechanical stimulation during the onset of bone healing but needs follow-up.

During the onset of bone healing mechanical stimuli are therefore likely to result in a response of mesenchymal cells (MSCs and osteoblast-like cells) improving angiogenesis and tissue formation and suppressing/reducing the immune response and, therefore, supporting a positive progress in bone healing. Hence, closure of non-unions or improved course of healing in delayed healers might be achieved if mechanical stimuli, for instance, by physiotherapy are applied in the right amount and at the right time. The perfect point in time and window, as well as the optimal size of the mechanical stimulus will have to be determined in *in vivo* studies. However, such *in vitro* studies as the present one will give hints at the direction that needs to be taken.

Furthermore, mesenchymal cells may be administered in a cell therapeutic and/or tissue engineering approach to foster bone healing by promoting angiogenesis in poor healing environments. Cells that are locally applied in suspension likely do not stay in place and high cell numbers are needed to improve the healing outcome, as known from muscle crush trauma treatment in rats [197]. Tissue engineering approaches help to keep cells in place and can additionally offer fracture stabilisation and gap closure in larger bone defects. Mechanical stimulation of human fracture haematomata increases their pro-angiogenic potential [166]. In fractures that require surgical treatment, the haematoma is usually removed to enable alignment of the bone fragments, remove bone splinters, and reduce the risk of infection. But it is known that especially late removal of fracture haematomata has a negative effect on the healing outcome [198]. The removal takes away mesenchymal and immune cells: On the one hand, $CD8^+$ T lymphocytes are removed, which is supposed to have a positive effect on wound healing [107], but, on the other hand, APCs are removed that are needed for MHC-II

antigen presentation to $CD4^+$ T lymphocytes, which impairs wound healing [108] and pro-angiogenic MSCs. And thus, the angiogenic potential of the haematoma cannot act. If a haematoma needs to be removed from a clinical point of view, mesenchymal (stem) cells embedded in fibrin could be used to replace the haematoma and bleeding into the cleaned fracture gap should be allowed. The MSCs hold the T lymphocyte-driven immune response at bay by inhibiting their proliferation but not their effector function [187] and, in addition, by inducing a regulatory T lymphocyte phenotype [188]. They further act in a paracrine manner by recruiting and directing endothelial and immune cells [134] to the fracture site whereby the healing progress is supported. The fibrin will be degraded and replaced by newly formed vessels and subsequently newly formed tissue. Additionally, load bearing after implantation would, concluded from the presented results, further support the immunomodulating effect, fibrin degradation and angiogenesis induced by MSCs. However, the composition of the fibrin is also to be considered in a tissue engineering approach because higher diluted fibrinogen improves the proliferation rates of the MSCs and yields more open, homogeneous microstructures likely easing the proliferation [113]. Thereby the fibrin degradation, chemotactic and immunomodulating action may be additionally enhanced. Furthermore, a more homogenous structure increases the chance of a homogeneous mechanical stimulation of the embedded cells.

Still, cell therapeutic approaches do have some negative implications that need to be kept in mind. The multipotency and immunomodulating action of MSCs, as well as their angiogenic potential, could support tumour growth [99, 100]. In addition, their longevity compared to further differentiated cells might foster mutations that lead to cancer development. However, in the treatment of graft versus host disease, autoimmune diseases and support of haematopoietic recovery following haematopoietic stem cell transplantation, MSCs are thought to be of high value for the clinic [100]. Therefore, if a patient, experiencing impaired tissue regeneration, is not predisposed for cancer development, which, of course, needs to be assessed, he may be treated with MSCs. Future research is, however, necessary to be able for sure to determine a predisposition for cancer and assess the applicability of fibrin embedded MSCs in bone regeneration.

In conclusion, fibrin-embedded mesenchymal cells may in future be used to improve/accelerate healing in patients experiencing delayed healing or non-union further supported by mechanical stimulation enhancing angiogenesis and likely reducing the immune responses.

List of Abbreviations

Abbreviation	Full Name
ABC or AB complex	avidin-biotin complex
ACVR2A	activin receptor type IIA
ADM	adrenomedullin
aFGF	acidic fibroblast growth factor
ALCAM	activated leukocyte cell adhesion molecule
alpha-MEM	minimum essential medium
ANGPT	angiopoietin
AP	alkaline phosphatase
AP-1	transcription factor activating protein-1
APC	antigen presenting cell
APC	allophycocyanin
ARHGEF	Rho guanine nucleotide exchange factor
ATP	adenosine-5'-triphosphate
bFGF	basic fibroblast growth factor
BMP	bone morphogenetic protein
BMSC	bone marrow-derived stromal cell
BP	biological process
BSA	bovine serum albumin
Ca	calcium
CCL	monocyte chemoattractant protein
CD	cluster of differentiation
cDNA	complementary DNA
CEBPD	CCAAT/enhancer-binding protein delta
CF	cell free control
CFD	computational fluid dynamics
CM	conditioned medium
CMC	carboxymethyl cellulose
Co	co-culture
CO_2	carbon dioxide
COX2	cyclooxygenase-2
cRNA	RNA derived from cDNA
CTNNAL	catenin alpha-like protein

Abbreviation	Full Name
CXCL	chemokines interferon-inducible protein
CYR	cystein-rich protein
DAPI	(4´-6-diamidino-2-phenylindole, dihydrochloride)
DIC	digital image correlation
DMEM	Dulbeccos' Modefied Eagle Medium
DNA	deoxyribonucleic acid
EC	endothelial cell
EDTA	ethylenediaminetetraacetic acid
ELISA	enzyme-linked immunosorbent assay
EPDR	ependymin related protein
ERK	extracellular signal-regulated kinase
FACS	fluorecence activated cell sorting
FAK	focal adhesion kinase
FBS	fetal bovine serum
FEM	finite element model
FITC	fluorescein isothiocyanate
FMO	flavin containing monooxygenase
FOS	FBJ murine osteosarcoma viral oncogene homolog
FZD	frizzled
GF	growth factor
GLDN	gliomedin
GO	gene ontology
GTPase	guanosine triphosphate hydrolase
HEPES	4-(2-hydroxyethyl)-1-piperazineethanesulfonic acid
HIF	hypoxia inducible factor
HLA	human leukocyte antigen
HMEC	human microvascular endothelial cell
HMEC -1	human microvascular endothelial cell line-1
hPBMC	human peripheral blood mononuclear cell
IGF	insulin-like growth factor
IL	interleukin
INF	interferon
ITGA	integrin alpha

Abbreviation	Full Name
JNK	c-Jun NH_2-terminal kinase
JUN	see AP
K	potassium
KIU	Kallikrein-Inhibitor-Unit
LEPR	leptin receptor
LEPREL	leprecan-like
LPS	lipopolysaccharide
LY	lymphocyte antigen
MACS	magnetic cell sorting
MAPK	mitogen-activated protein kinase
MCDB	reduced serum-supplemented medium for the culture of HMEC
M-CSF	macrophage colony stimulating growth factor
MF	molecular function
MHC	major histocompatibility complex
MMP	matrix metalloprotease
mRNA	messenger RNA
MSC	mesenchymal stem cell
Na	sodium
NaCl	sodium chloride
NO_2	nitrogen dioxide
NRP	neuroprolin
PAI	plasminogen activator inhibitor
PAS	plasminogen activation system
PBS	phosphate buffered saline
PC	personal computer
PDGF	platelet-derived growth factor
PE	phycoerythrin
PFA	paraformaldehyde
RAC	RAS-related C3 botulinum toxin substrate
RAG	recombination activating gene
RANKL	receptor activator of nuclear factor kappa B ligand
RASL11A	RAS-like, family 11, member A
RCAS	replication-competent ASLV long terminal repeat with a splice acceptor

Abbreviation	Full Name
RNA	ribonucleic acid
RPMI	(medium developed at) Roswell Park Memorial Institute
rRNA	ribosomal ribonucleic acid
RT	room temperature
RTK	receptor tyrosine kinase
SAC	stretch activated ion channel
SD	standard deviation
SLC7	solute carrier family 7
SNCAIP	synuclein alpha interacting protein
T	T lymphocyte
TGF	transforming growth factor
TIMP	tissue inhibitor of matrix metalloprotease
TLR	toll-like receptor
TNF	tumor necrosis factor
tPA	tissue-type plasminogen activator
Tris Base	Tris(hydroxymethyl)aminomethane
Tris HCL	Tris(hydroxymethyl)aminomethane hydrochloride
U	unit
uPA	urokinase plasminogen activator
uPAR	urokinase plasminogen activator receptor
VCAM	vascular cell adhesion molecule
VEGF	vascular endothelial growth factor
VEGF-A	vascular endothelial growth factor A
ε_{cell}	cellular strain
ε_{mem}	membrane strains
ε_{prog}	programmed strain
ε_{rep}	reported strain

List of Figures

List of Tables

List of References

1. Phieffer, L.S. and Goulet, J.A., *Delayed unions of the tibia.* J Bone Joint Surg Am, 2006. **88**(1): p. 206-16.

2. Kolar, P., Schmidt-Bleek, K., Schell, H., Gaber, T., Toben, D., Schmidmaier, G., Perka, C., Buttgereit, F., and Duda, G.N., *The Early Fracture Hematoma and Its Potential Role in Fracture Healing.* Tissue Eng Part B Rev, 2010. **16**(4): p. 427-34.

3. Kanakaris, N.K. and Giannoudis, P.V., *The health economics of the treatment of long-bone non-unions.* Injury, 2007. **38 Suppl 2**: p. S77-84.

4. Kenwright, J. and Goodship, A.E., *Controlled mechanical stimulation in the treatment of tibial fractures.* Clin Orthop Relat Res, 1989(241): p. 36-47.

5. Pauly, S., Luttosch, F., Morawski, M., Haas, N.P., Schmidmaier, G., and Wildemann, B., *Simvastatin locally applied from a biodegradable coating of osteosynthetic implants improves fracture healing comparable to BMP-2 application.* Bone, 2009. **45**(3): p. 505-11.

6. Schmidmaier, G., Lucke, M., Schwabe, P., Raschke, M., Haas, N.P., and Wildemann, B., *Collective review: bioactive implants coated with poly(D,L-lactide) and growth factors IGF-I, TGF-beta1, or BMP-2 for stimulation of fracture healing.* J Long Term Eff Med Implants, 2006. **16**(1): p. 61-9.

7. Schmidmaier, G., Schwabe, P., Wildemann, B., and Haas, N.P., *Use of bone morphogenetic proteins for treatment of non-unions and future perspectives.* Injury, 2007. **38 Suppl 4**: p. S35-41.

8. Peters, A., Toben, D., Lienau, J., Schell, H., Bail, H.J., Matziolis, G., Duda, G.N., and Kaspar, K., *Locally applied osteogenic predifferentiated progenitor cells are more effective than undifferentiated mesenchymal stem cells in the treatment of delayed bone healing.* Tissue Eng Part A, 2009. **15**(10): p. 2947-54.

9. Kasper, G., Dankert, N., Tuischer, J., Hoeft, M., Gaber, T., Glaeser, J.D., Zander, D., Tschirschmann, M., Thompson, M., Matziolis, G., and Duda, G.N., *Mesenchymal stem cells regulate angiogenesis according to their mechanical environment.* Stem Cells, 2007. **25**(4): p. 903-10.

10. Toben, D., Schroeder, I., El Khassawna, T., Mehta, M., Hoffmann, J., Frisch, J., Schell, H., Lienau, J., Serra, A., Radbruch, A., and Duda, G., *Fracture healing is accelerated in the absence of the adaptive immune system.* J Bone Miner Res, 2010. **Epub ahead of print**.

11. Glowacki, J., *Angiogenesis in fracture repair.* Clin Orthop Relat Res, 1998(355 Suppl): p. S82-9.

12. Ponce, M.L., *Tube formation: an in vitro matrigel angiogenesis assay.* Methods Mol Biol, 2009. **467**: p. 183-8.

13. Carmeliet, P., *Mechanisms of angiogenesis and arteriogenesis.* Nat Med, 2000. **6**(4): p. 389-95.

14. McMahon, B. and Kwaan, H.C., *The plasminogen activator system and cancer*. Pathophysiol Haemost Thromb, 2008. **36**(3-4): p. 184-94.

15. Rakic, J.M., Maillard, C., Jost, M., Bajou, K., Masson, V., Devy, L., Lambert, V., Foidart, J.M., and Noel, A., *Role of plasminogen activator-plasmin system in tumor angiogenesis.* Cell Mol Life Sci, 2003. **60**(3): p. 463-73.

16. Rifkin, D.B., Mazzieri, R., Munger, J.S., Noguera, I., and Sung, J., *Proteolytic control of growth factor availability.* Apmis, 1999. **107**(1): p. 80-5.

17. Collen, D. and Lijnen, H.R., *Basic and clinical aspects of fibrinolysis and thrombolysis.* Blood, 1991. **78**(12): p. 3114-24.

18. Pedroja, B.S., Kang, L.E., Imas, A.O., Carmeliet, P., and Bernstein, A.M., *Plasminogen activator inhibitor-1 regulates integrin alphavbeta3 expression and autocrine transforming growth factor beta signaling.* J Biol Chem, 2009. **284**(31): p. 20708-17.

19. Pepper, M.S., Ferrara, N., Orci, L., and Montesano, R., *Vascular endothelial growth factor (VEGF) induces plasminogen activators and plasminogen activator inhibitor-1 in microvascular endothelial cells.* Biochem Biophys Res Commun, 1991. **181**(2): p. 902-6.

20. Page-McCaw, A., Ewald, A.J., and Werb, Z., *Matrix metalloproteinases and the regulation of tissue remodelling.* Nat Rev Mol Cell Biol, 2007. **8**(3): p. 221-33.

21. Nagase, H. and Woessner (Jr.), J.F., *Matrix metalloproteinases.* J Biol Chem., 1999. **274**(31): p. 21491-21494.

22. Sternlicht, M.D. and Werb, Z., *How matrix metalloproteinases regulate cell behavior.* Annu Rev Cell Dev Biol, 2001. **17**: p. 463-516.

23. Kato, T., Kure, T., Chang, J.-H., Gabison, E.E., Itoh, T., Itohara, S., and Azar, D.T., *Diminished corneal angiogenesis in gelatinase A-deficient mice.* FEBS Letters, 2001. **508**: p. 187-190.

24. Wang, Z., Juttermann, R., and Soloway, P.D., *TIMP-2 is required for efficient activation of proMMP-2 in vivo.* J Biol Chem, 2000. **275**(34): p. 26411-5.

25. Park, J.E., Keller, G.A., and Ferrara, N., *The vascular endothelial growth factor (VEGF) isoforms: differential deposition into the subepithelial extracellular matrix and bioactivity of extracellular matrix-bound VEGF.* Mol Biol Cell, 1993. **4**(12): p. 1317-26.

26. Carano, R.A. and Filvaroff, E.H., *Angiogenesis and bone repair.* Drug Discov Today, 2003. **8**(21): p. 980-9.

27. Beamer, B., Hettrich, C., and Lane, J., *Vascular Endothelial Growth Factor: An Essential Component of Angiogenesis and Fracture Healing.* Hss J, 2009.

28. Webb, J.C.J. and Tricker, J., *A review of fracture healing.* Current Orthopaedics, 2000. **14**(6): p. 457-463.

29. Tsiridis, E., Upadhyay, N., and Giannoudis, P., *Molecular aspects of fracture healing: which are the important molecules?* Injury, 2007. **38 Suppl 1**: p. S11-25.

30. Schindeler, A., McDonald, M.M., Bokko, P., and Little, D.G., *Bone remodeling during fracture repair: The cellular picture.* Semin Cell Dev Biol, 2008. **19**(5): p. 459-66.

31. Schmidt-Bleek, K., Schell, H., Kolar, P., Pfaff, M., Perka, C., Buttgereit, F., Duda, G., and Lienau, J., *Cellular composition of the initial fracture hematoma compared to a muscle hematoma: a study in sheep.* J Orthop Res, 2009. **27**(9): p. 1147-51.

32. Kolar, P., Gaber, T., Maschmeyer, P., Hahne, M., Wagegg, M., Schmidt-Bleek, K., Sentürk, U., Matziolis, D., Matziolis, G., Kasper, G., Unterhauser, F., Burmester, G., Schmidmaier, G., Perka, C., Duda, G., and Buttgereit, F., *Immunologic contribution to the onset of bone healing in the early human fracture hematoma.* Osteologie, 2009. **4**: p. A3.

33. Bielby, R., Jones, E., and McGonagle, D., *The role of mesenchymal stem cells in maintenance and repair of bone.* Injury, 2007. **38 Suppl 1**: p. S26-32.

34. Oe, K., Miwa, M., Sakai, Y., Lee, S.Y., Kuroda, R., and Kurosaka, M., *An in vitro study demonstrating that haematomas found at the site of human fractures contain progenitor cells with multilineage capacity.* J Bone Joint Surg Br, 2007. **89**(1): p. 133-8.

35. Colnot, C., *Skeletal cell fate decisions within periosteum and bone marrow during bone regeneration.* J Bone Miner Res, 2009. **24**(2): p. 274-82.

36. Gardner, T.N., Evans, M., Hardy, J., and Kenwright, J., *Dynamic interfragmentary motion in fractures during routine patient activity.* Clin Orthop Relat Res, 1997(336): p. 216-25.

37. Hente, R., Fuchtmeier, B., Schlegel, U., Ernstberger, A., and Perren, S.M., *The influence of cyclic compression and distraction on the healing of experimental tibial fractures.* J Orthop Res, 2004. **22**(4): p. 709-15.

38. Claes, L., Eckert-Hubner, K., and Augat, P., *The effect of mechanical stability on local vascularization and tissue differentiation in callus healing.* J Orthop Res, 2002. **20**(5): p. 1099-105.

39. Klein, S.M., Pierce, T., Rubin, Y., Nielsen, K.C., and Steele, S.M., *Successful resuscitation after ropivacaine-induced ventricular fibrillation.* Anesth Analg, 2003. **97**(3): p. 901-3.

40. Lienau, J., Schell, H., Duda, G.N., Seebeck, P., Muchow, S., and Bail, H.J., *Initial vascularization and tissue differentiation are influenced by fixation stability.* J Orthop Res, 2005. **23**(3): p. 639-45.

41. Lienau, J., Schmidt-Bleek, K., Peters, A., Haschke, F., Duda, G.N., Perka, C., Bail, H.J., Schutze, N., Jakob, F., and Schell, H., *Differential regulation of blood vessel formation between standard and delayed bone healing.* J Orthop Res, 2009. **27**(9): p. 1133-40.

42. Pauwels, F., *[A new theory on the influence of mechanical stimuli on the differentiation of supporting tissue. The tenth contribution to the functional anatomy and causal morphology of the supporting structure.]*. Z Anat Entwicklungsgesch, 1960. **121**: p. 478-515.

43. Neidlinger-Wilke, C., Wilke, H.J., and Claes, L., *Cyclic stretching of human osteoblasts affects proliferation and metabolism: a new experimental method and its application.* J Orthop Res, 1994. **12**(1): p. 70-8.

44. Claes, L.E. and Heigele, C.A., *Magnitudes of local stress and strain along bony surfaces predict the course and type of fracture healing.* J Biomech, 1999. **32**(3): p. 255-66.

45. Epari, D.R., Taylor, W.R., Heller, M.O., and Duda, G.N., *Mechanical conditions in the initial phase of bone healing.* Clin Biomech (Bristol, Avon), 2006. **21**(6): p. 646-55.

46. Thompson, M.S., Schell, H., Lienau, J., and Duda, G.N., *Digital image correlation: a technique for determining local mechanical conditions within early bone callus.* Med Eng Phys, 2007. **29**(7): p. 820-3.

47. Brown, T.D., *Techniques for mechanical stimulation of cells in vitro: a review.* J Biomech, 2000. **33**(1): p. 3-14.

48. Lee, A.A., Delhaas, T., Waldman, L.K., MacKenna, D.A., Villarreal, F.J., and McCulloch, A.D., *An equibiaxial strain system for cultured cells.* Am J Physiol, 1996. **271**(4 Pt 1): p. C1400-8.

49. Gilchrist, C.L., Witvoet-Braam, S.W., Guilak, F., and Setton, L.A., *Measurement of intracellular strain on deformable substrates with texture correlation.* J Biomech, 2007. **40**(4): p. 786-94.

50. Wall, M.E., Weinhold, P.S., Siu, T., Brown, T.D., and Banes, A.J., *Comparison of cellular strain with applied substrate strain in vitro.* J Biomech, 2007. **40**(1): p. 173-81.

51. Bieler, F.H., Ott, C.E., Thompson, M.S., Seidel, R., Ahrens, S., Epari, D.R., Wilkening, U., Schaser, K.D., Mundlos, S., and Duda, G.N., *Biaxial cell stimulation: A mechanical validation.* J Biomech, 2009. **42**(11): p. 1692-6.

52. Banes, A.J., Gilbert, J., Taylor, D., and Monbureau, O., *A new vacuum-operated stress-providing instrument that applies static or variable duration cyclic tension or compression to cells in vitro.* J Cell Sci, 1985. **75**: p. 35-42.

53. Gilbert, J.A., Weinhold, P.S., Banes, A.J., Link, G.W., and Jones, G.L., *Strain profiles for circular cell culture plates containing flexible surfaces employed to mechanically deform cells in vitro.* J Biomech, 1994. **27**(9): p. 1169-77.

54. Brown, T.D., Bottlang, M., Pedersen, D.R., and Banes, A.J., *Development and Experimental Validation of a Fluid/Structure-Interaction Finite Element Model of a Vacuum-Driven Cell Culture Mechanostimulus System.* Comput Methods Biomech Biomed Engin, 2000. **3**(1): p. 65-78.

55. Schulz, R.M. and Bader, A., *Cartilage tissue engineering and bioreactor systems for the cultivation and stimulation of chondrocytes.* Eur Biophys J, 2007. **36**(4-5): p. 539-68.

56. Bilodeau, K. and Mantovani, D., *Bioreactors for tissue engineering: focus on mechanical constraints. A comparative review.* Tissue Eng, 2006. **12**(8): p. 2367-83.

57. Matziolis, G., Tuischer, J., Kasper, G., Thompson, M., Bartmeyer, B., Krocker, D., Perka, C., and Duda, G., *Simulation of cell differentiation in fracture healing: mechanically loaded composite scaffolds in a novel bioreactor system.* Tissue Eng, 2006. **12**(1): p. 201-8.

58. Fredberg, J.J. and Kamm, R.D., *Stress transmission in the lung: pathways from organ to molecule.* Annu Rev Physiol, 2006. **68**: p. 507-41.

59. Ingber, D.E., *Tensegrity-based mechanosensing from macro to micro.* Prog Biophys Mol Biol, 2008. **97**(2-3): p. 163-79.

60. Wang, J.H. and Thampatty, B.P., *An introductory review of cell mechanobiology.* Biomech Model Mechanobiol, 2006. **5**(1): p. 1-16.

61. Rubin, J., Rubin, C., and Jacobs, C.R., *Molecular pathways mediating mechanical signaling in bone.* Gene, 2006. **367**: p. 1-16.

62. Banes, A.J., Lee, G., Graff, R., Otey, C., Archambault, J., Tsuzaki, M., Elfervig, M., and Qi, J., *Mechanical forces and signaling in connective tissue cells: cellular mechanisms of detection, transduction, and responses to mechanical deformation.* Curr Opin Orthop, 2001. **12**: p. 389-396.

63. Alberts, B., Johnson, A., Lewis, J., Raff, M., Roberts, K., and Walter, P., *Molekularbiologie der Zelle*. 4th ed. 2003: Jaenicke, L. . 1863.

64. Ott, C.E., Bauer, S., Manke, T., Ahrens, S., Rodelsperger, C., Grunhagen, J., Kornak, U., Duda, G., Mundlos, S., and Robinson, P.N., *Promiscuous and depolarization-induced immediate-early response genes are induced by mechanical strain of osteoblasts.* J Bone Miner Res, 2009. **24**(7): p. 1247-62.

65. Kasper, G., Glaeser, J.D., Geissler, S., Ode, A., Tuischer, J., Matziolis, G., Perka, C., and Duda, G.N., *Matrix metalloprotease activity is an essential link between mechanical stimulus and mesenchymal stem cell behavior.* Stem Cells, 2007. **25**(8): p. 1985-94.

66. Pavalko, F.M., Chen, N.X., Turner, C.H., Burr, D.B., Atkinson, S., Hsieh, Y.F., Qiu, J., and Duncan, R.L., *Fluid shear-induced mechanical signaling in MC3T3-E1 osteoblasts requires cytoskeleton-integrin interactions.* Am J Physiol, 1998. **275**(6 Pt 1): p. C1591-601.

67. Meazzini, M.C., Toma, C.D., Schaffer, J.L., Gray, M.L., and Gerstenfeld, L.C., *Osteoblast cytoskeletal modulation in response to mechanical strain in vitro.* J Orthop Res, 1998. **16**(2): p. 170-80.

68. Hamilton, D.W., Maul, T.M., and Vorp, D.A., *Characterization of the response of bone marrow-derived progenitor cells to cyclic strain: implications for vascular tissue-engineering applications.* Tissue Eng, 2004. **10**(3-4): p. 361-9.

69. Granet, C., Vico, A.G., Alexandre, C., and Lafage-Proust, M.H., *MAP and src kinases control the induction of AP-1 members in response to changes in mechanical environment in osteoblastic cells.* Cell Signal, 2002. **14**(8): p. 679-88.

70. Hess, J., Angel, P., and Schorpp-Kistner, M., *AP-1 subunits: quarrel and harmony among siblings.* J Cell Sci, 2004. **117**(Pt 25): p. 5965-73.

71. Simmons, C.A., Matlis, S., Thornton, A.J., Chen, S., Wang, C.Y., and Mooney, D.J., *Cyclic strain enhances matrix mineralization by adult human mesenchymal stem cells via the extracellular signal-regulated kinase (ERK1/2) signaling pathway.* J Biomech, 2003. **36**(8): p. 1087-96.

72. Miyauchi, A., Gotoh, M., Kamioka, H., Notoya, K., Sekiya, H., Takagi, Y., Yoshimoto, Y., Ishikawa, H., Chihara, K., Takano-Yamamoto, T., Fujita, T., and Mikuni-Takagaki, Y., *AlphaVbeta3 integrin ligands enhance volume-sensitive calcium influx in mechanically stretched osteocytes.* J Bone Miner Metab, 2006. **24**(6): p. 498-504.

73. Schwartz, E.A., Bizios, R., Medow, M.S., and Gerritsen, M.E., *Exposure of human vascular endothelial cells to sustained hydrostatic pressure stimulates proliferation. Involvement of the alphaV integrins.* Circ Res, 1999. **84**(3): p. 315-22.

74. Brooks, P.C., Clark, R.A., and Cheresh, D.A., *Requirement of vascular integrin alpha v beta 3 for angiogenesis.* Science, 1994. **264**(5158): p. 569-71.

75. Kanda, S., Kuzuya, M., Ramos, M.A., Koike, T., Yoshino, K., Ikeda, S., and Iguchi, A., *Matrix metalloproteinase and alphavbeta3 integrin-dependent vascular smooth muscle cell invasion through a type I collagen lattice.* Arterioscler Thromb Vasc Biol, 2000. **20**(4): p. 998-1005.

76. Wozniak, M., Fausto, A., Carron, C.P., Meyer, D.M., and Hruska, K.A., *Mechanically strained cells of the osteoblast lineage organize their extracellular matrix through unique sites of alphavbeta3-integrin expression.* J Bone Miner Res, 2000. **15**(9): p. 1731-45.

77. Weyts, F.A., Li, Y.S., van Leeuwen, J., Weinans, H., and Chien, S., *ERK activation and alpha v beta 3 integrin signaling through Shc recruitment in response to mechanical stimulation in human osteoblasts.* J Cell Biochem, 2002. **87**(1): p. 85-92.

78. Tang, C.H., Yang, R.S., Huang, T.H., Lu, D.Y., Chuang, W.J., Huang, T.F., and Fu, W.M., *Ultrasound stimulates cyclooxygenase-2 expression and increases bone formation through integrin, focal adhesion kinase, phosphatidylinositol 3-kinase, and Akt pathway in osteoblasts.* Mol Pharmacol, 2006. **69**(6): p. 2047-57.

79. Neidlinger-Wilke, C., Stalla, I., Claes, L., Brand, R., Hoellen, I., Rubenacker, S., Arand, M., and Kinzl, L., *Human osteoblasts from younger normal and osteoporotic donors show differences in proliferation and TGF beta-release in response to cyclic strain.* J Biomech, 1995. **28**(12): p. 1411-8.

80. Schulz, R.M., Wustneck, N., van Donkelaar, C.C., Shelton, J.C., and Bader, A., *Development and validation of a novel bioreactor system for load- and perfusion-controlled tissue engineering of chondrocyte-constructs.* Biotechnol Bioeng, 2008. **101**(4): p. 714-28.

81. Einhorn, T.A., *The cell and molecular biology of fracture healing.* Clin Orthop Relat Res, 1998(355 Suppl): p. S7-21.

82. McKibbin, B., *The biology of fracture healing in long bones.* J Bone Joint Surg Br, 1978. **60-B**(2): p. 150-62.

83. Bhatt, K.A., Chang, E.I., Warren, S.M., Lin, S.E., Bastidas, N., Ghali, S., Thibboneir, A., Capla, J.M., McCarthy, J.G., and Gurtner, G.C., *Uniaxial mechanical strain: an in vitro correlate to distraction osteogenesis.* J Surg Res, 2007. **143**(2): p. 329-36.

84. Chen, X., Macica, C.M., Ng, K.W., and Broadus, A.E., *Stretch-induced PTH-related protein gene expression in osteoblasts.* J Bone Miner Res, 2005. **20**(8): p. 1454-61.

85. Liu, X., Zhang, X., and Luo, Z.P., *Strain-related collagen gene expression in human osteoblast-like cells.* Cell Tissue Res, 2005. **322**(2): p. 331-4.

86. Tang, L., Lin, Z., and Li, Y.M., *Effects of different magnitudes of mechanical strain on Osteoblasts in vitro.* Biochem Biophys Res Commun, 2006. **344**(1): p. 122-8.

87. Grabner, B., Varga, F., Fratzl-Zelman, N., Luegmayr, E., Glantschnig, H., Rumpler, M., Tatschl, A., Fratzl, P., and Klaushofer, K., *A new stretching apparatus for applying anisotropic mechanical strain to bone cells in-vitro* Review of Scientific Instruments, 2000. **71**(9): p. 3522-3529.

88. Bottlang, M., Simnacher, M., Schmitt, H., Brand, R.A., and Claes, L., *A cell strain system for small homogeneous strain applications.* Biomed Tech (Berl), 1997. **42**(11): p. 305-9.

89. Matheson, L.A., Fairbank, N.J., Maksym, G.N., Paul Santerre, J., and Labow, R.S., *Characterization of the Flexcell Uniflex cyclic strain culture system with U937 macrophage-like cells.* Biomaterials, 2006. **27**(2): p. 226-33.

90. Sutton, M.A., McNeill, S.R., Helm, J.D., and Chao, Y.J., *Advances in Two-Dimensional and Three-Dimensional Computer Vision*, in *Topics in Applied Physics (Photomechanics)*, Rastogi, P.K., Editor. 2000, Springer: Berlin / Heidelberg. p. 323-372.

91. Owan, I., Burr, D.B., Turner, C.H., Qiu, J., Tu, Y., Onyia, J.E., and Duncan, R.L., *Mechanotransduction in bone: osteoblasts are more responsive to fluid forces than mechanical strain.* Am J Physiol, 1997. **273**(3 Pt 1): p. C810-5.

92. Smalt, R., Mitchell, F.T., Howard, R.L., and Chambers, T.J., *Induction of NO and prostaglandin E2 in osteoblasts by wall-shear stress but not mechanical strain.* Am J Physiol, 1997. **273**(4 Pt 1): p. E751-8.

93. McGarry, J.G., Klein-Nulend, J., Mullender, M.G., and Prendergast, P.J., *A comparison of strain and fluid shear stress in stimulating bone cell responses--a computational and experimental study.* Faseb J, 2005. **19**(3): p. 482-4.

94. Hughes, S.H., *The RCAS vector system.* Folia Biol (Praha), 2004. **50**(3-4): p. 107-19.

95. R Development Core Team, *R: A language and environment for statistical computing*. 2007, Vienna, Austria: R Foundation for Statistical Computing.

96. Thompson, M.S., Abercrombie, S.R., Ott, C.E., Bieler, F.H., Duda, G.N., and Ventikos, Y., *Quantification and significance of fluid shear stress field in biaxial cell stretching device.* Biomech Model Mechanobiol, 2010. **Epub ahead of print**.

97. Sbalzarini, I.F. and Koumoutsakos, P., *Feature point tracking and trajectory analysis for video imaging in cell biology.* J Struct Biol, 2005. **151**(2): p. 182-95.

98. Lienau, J., Schmidt-Bleek, K., Peters, A., Weber, H., Bail, H.J., Duda, G.N., Perka, C., and Schell, H., *Insight into the Molecular Pathophysiology of Delayed Bone Healing in a Sheep Model.* Tissue Eng Part A, 2010. **16**(1): p. 191-9.

99. Kode, J.A., Mukherjee, S., Joglekar, M.V., and Hardikar, A.A., *Mesenchymal stem cells: immunobiology and role in immunomodulation and tissue regeneration.* Cytotherapy, 2009. **11**(4): p. 377-91.

100. Sotiropoulou, P.A. and Papamichail, M., *Immune properties of mesenchymal stem cells.* Methods Mol Biol, 2007. **407**: p. 225-43.

101. Maccario, R., Podesta, M., Moretta, A., Cometa, A., Comoli, P., Montagna, D., Daudt, L., Ibatici, A., Piaggio, G., Pozzi, S., Frassoni, F., and Locatelli, F., *Interaction of human mesenchymal stem cells with cells involved in alloantigen-specific immune response favors the differentiation of CD4+ T-cell subsets expressing a regulatory/suppressive phenotype.* Haematologica, 2005. **90**(4): p. 516-25.

102. Krampera, M., Glennie, S., Dyson, J., Scott, D., Laylor, R., Simpson, E., and Dazzi, F., *Bone marrow mesenchymal stem cells inhibit the response of naive and memory antigen-specific T cells to their cognate peptide.* Blood, 2003. **101**(9): p. 3722-9.

103. Suva, D., Passweg, J., Arnaudeau, S., Hoffmeyer, P., and Kindler, V., *In vitro activated human T lymphocytes very efficiently attach to allogenic multipotent mesenchymal stromal cells and transmigrate under them.* J Cell Physiol, 2008. **214**(3): p. 588-94.

104. Siegel, G., Schafer, R., and Dazzi, F., *The immunosuppressive properties of mesenchymal stem cells.* Transplantation, 2009. **87**(9 Suppl): p. S45-9.

105. Abbas, A.K., Lichtman, A.H., and Pillai, S., *Cellular and Molecular Immunology*. 6th ed, ed. Schmitt, W. and Gruliow, R. 2007, Philadelphia: Saunders, an imprint of Elsevier Inc.

106. Schaffer, M. and Barbul, A., *Lymphocyte function in wound healing and following injury.* Br J Surg, 1998. **85**(4): p. 444-60.

107. Barbul, A., Breslin, R.J., Woodyard, J.P., Wasserkrug, H.L., and Efron, G., *The effect of in vivo T helper and T suppressor lymphocyte depletion on wound healing.* Ann Surg, 1989. **209**(4): p. 479-83.

108. Schaffer, M., Bongartz, M., Hoffmann, W., and Viebahn, R., *MHC-class-II-deficiency impairs wound healing.* J Surg Res, 2007. **138**(1): p. 100-5.

109. Peterson, J.M., Barbul, A., Breslin, R.J., Wasserkrug, H.L., and Efron, G., *Significance of T-lymphocytes in wound healing.* Surgery, 1987. **102**(2): p. 300-5.

110. Dominici, M., Le Blanc, K., Mueller, I., Slaper-Cortenbach, I., Marini, F., Krause, D., Deans, R., Keating, A., Prockop, D., and Horwitz, E., *Minimal criteria for defining multipotent mesenchymal stromal cells. The International Society for Cellular Therapy position statement.* Cytotherapy, 2006. **8**(4): p. 315-7.

111. Thomas, P.D., Campbell, M.J., Kejariwal, A., Mi, H., Karlak, B., Daverman, R., Diemer, K., Muruganujan, A., and Narechania, A., *PANTHER: a library of protein families and subfamilies indexed by function.* Genome Res, 2003. **13**(9): p. 2129-41.

112. Thomas, P.D., Kejariwal, A., Guo, N., Mi, H., Campbell, M.J., Muruganujan, A., and Lazareva-Ulitsky, B., *Applications for protein sequence-function evolution data: mRNA/protein expression analysis and coding SNP scoring tools.* Nucleic Acids Res, 2006. **34**(Web Server issue): p. W645-50.

113. Ho, W., Tawil, B., Dunn, J.C., and Wu, B.M., *The behavior of human mesenchymal stem cells in 3D fibrin clots: dependence on fibrinogen concentration and clot structure.* Tissue Eng, 2006. **12**(6): p. 1587-95.

114. Zhang, D. and Arola, D.D., *Applications of digital image correlation to biological tissues.* J Biomed Opt, 2004. **9**(4): p. 691-9.

115. Vande Geest, J.P., Di Martino, E.S., and Vorp, D.A., *An analysis of the complete strain field within Flexercell membranes.* J Biomech, 2004. **37**(12): p. 1923-8.

116. Trepat, X., Deng, L., An, S.S., Navajas, D., Tschumperlin, D.J., Gerthoffer, W.T., Butler, J.P., and Fredberg, J.J., *Universal physical responses to stretch in the living cell.* Nature, 2007. **447**(7144): p. 592-5.

117. Nelson, C.M., Pirone, D.M., Tan, J.L., and Chen, C.S., *Vascular endothelial-cadherin regulates cytoskeletal tension, cell spreading, and focal adhesions by stimulating RhoA.* Mol Biol Cell, 2004. **15**(6): p. 2943-53.

118. Bakker, A.D., Soejima, K., Klein-Nulend, J., and Burger, E.H., *The production of nitric oxide and prostaglandin E(2) by primary bone cells is shear stress dependent.* J Biomech, 2001. **34**(5): p. 671-7.

119. Bacabac, R.G., Smit, T.H., Mullender, M.G., Dijcks, S.J., Van Loon, J.J., and Klein-Nulend, J., *Nitric oxide production by bone cells is fluid shear stress rate dependent.* Biochem Biophys Res Commun, 2004. **315**(4): p. 823-9.

120. Bacabac, R.G., Smit, T.H., Mullender, M.G., Van Loon, J.J., and Klein-Nulend, J., *Initial stress-kick is required for fluid shear stress-induced rate dependent activation of bone cells.* Ann Biomed Eng, 2005. **33**(1): p. 104-10.

121. Jacobs, C.R., Yellowley, C.E., Davis, B.R., Zhou, Z., Cimbala, J.M., and Donahue, H.J., *Differential effect of steady versus oscillating flow on bone cells.* J Biomech, 1998. **31**(11): p. 969-76.

122. Zhu, J., Zhang, X., Wang, C., Peng, X., and Zhang, X., *Different Magnitudes of Tensile Strain Induce Human Osteoblasts Differentiation Associated with the Activation of ERK1/2 Phosphorylation.* Int J Mol Sci, 2008. **9**(12): p. 2322-32.

123. Colombo, A., Cahill, P.A., and Lally, C., *An analysis of the strain field in biaxial Flexcell membranes for different waveforms and frequencies.* Proc Inst Mech Eng H, 2008. **222**(8): p. 1235-45.

124. Liegibel, U.M., Sommer, U., Bundschuh, B., Schweizer, B., Hilscher, U., Lieder, A., Nawroth, P., and Kasperk, C., *Fluid shear of low magnitude increases growth and expression of TGFbeta1 and adhesion molecules in human bone cells in vitro.* Exp Clin Endocrinol Diabetes, 2004. **112**(7): p. 356-63.

125. Krishnan, R., Park, C.Y., Lin, Y.C., Mead, J., Jaspers, R.T., Trepat, X., Lenormand, G., Tambe, D., Smolensky, A.V., Knoll, A.H., Butler, J.P., and Fredberg, J.J., *Reinforcement versus fluidization in cytoskeletal mechanoresponsiveness.* PLoS One, 2009. **4**(5): p. e5486.

126. Katsumi, A., Orr, A.W., Tzima, E., and Schwartz, M.A., *Integrins in mechanotransduction.* J Biol Chem, 2004. **279**(13): p. 12001-4.

127. Potapova, I.A., Gaudette, G.R., Brink, P.R., Robinson, R.B., Rosen, M.R., Cohen, I.S., and Doronin, S.V., *Mesenchymal stem cells support migration, extracellular matrix invasion, proliferation, and survival of endothelial cells in vitro.* Stem Cells, 2007. **25**(7): p. 1761-8.

128. Groothuis, A., Duda, G.N., Wilson, C.J., Hunter, M.R., Bail, H.J., van Scherpenzeel, K.M., and Kasper, G., *Mechanical stimulation of the pro-angiogenic capacity of human fracture haematoma: involvement of age-specific VEGF mechano-regulation.* Bone, 2010. **47**(2): p. 438-44.

129. Chu, E.K., Cheng, J., Foley, J.S., Mecham, B.H., Owen, C.A., Haley, K.J., Mariani, T.J., Kohane, I.S., Tschumperlin, D.J., and Drazen, J.M., *Induction of the plasminogen activator system by mechanical stimulation of human bronchial epithelial cells.* Am J Respir Cell Mol Biol, 2006. **35**(6): p. 628-38.

130. Ulfhammer, E., Carlstrom, M., Bergh, N., Larsson, P., Karlsson, L., and Jern, S., *Suppression of endothelial t-PA expression by prolonged high laminar shear stress.* Biochem Biophys Res Commun, 2009. **379**(2): p. 532-6.

131. Ulfhammer, E., Ridderstrale, W., Andersson, M., Karlsson, L., Hrafnkelsdottir, T., and Jern, S., *Prolonged cyclic strain impairs the fibrinolytic system in cultured vascular endothelial cells.* J Hypertens, 2005. **23**(8): p. 1551-7.

132. Prajapati, R.T., Eastwood, M., and Brown, R.A., *Duration and orientation of mechanical loads determine fibroblast cyto-mechanical activation: monitored by protease release.* Wound Repair Regen, 2000. **8**(3): p. 238-46.

133. Dean, R.A. and Overall, C.M., *Proteomics discovery of metalloproteinase substrates in the cellular context by iTRAQ labeling reveals a diverse MMP-2 substrate degradome.* Mol Cell Proteomics, 2007. **6**(4): p. 611-23.

134. Chen, L., Tredget, E.E., Wu, P.Y., and Wu, Y., *Paracrine factors of mesenchymal stem cells recruit macrophages and endothelial lineage cells and enhance wound healing.* PLoS One, 2008. **3**(4): p. e1886.

135. Phinney, D.G., *Biochemical heterogeneity of mesenchymal stem cell populations: clues to their therapeutic efficacy.* Cell Cycle, 2007. **6**(23): p. 2884-9.

136. Bini, A., Itoh, Y., Kudryk, B.J., and Nagase, H., *Degradation of cross-linked fibrin by matrix metalloproteinase 3 (stromelysin 1): hydrolysis of the gamma Gly 404-Ala 405 peptide bond.* Biochemistry, 1996. **35**(40): p. 13056-63.

137. Kuyvenhoven, J.P., Molenaar, I.Q., Verspaget, H.W., Veldman, M.G., Palareti, G., Legnani, C., Moolenburgh, S.E., Terpstra, O.T., Lamers, C.B., van Hoek, B., and Porte, R.J., *Plasma MMP-2 and MMP-9 and their inhibitors TIMP-1 and TIMP-2 during human orthotopic liver transplantation. The effect of aprotinin and the relation to ischemia/reperfusion injury.* Thromb Haemost, 2004. **91**(3): p. 506-13.

138. Zheng, Z.H., Li, X.Y., Ding, J., Jia, J.F., and Zhu, P., *Allogeneic mesenchymal stem cell and mesenchymal stem cell-differentiated chondrocyte suppress the responses of type II collagen-reactive T cells in rheumatoid arthritis.* Rheumatology (Oxford), 2008. **47**(1): p. 22-30.

139. Bosnakovski, D., Mizuno, M., Kim, G., Takagi, S., Okumur, M., and Fujinag, T., *Gene expression profile of bovine bone marrow mesenchymal stem cell during spontaneous chondrogenic differentiation in pellet culture system.* Jpn J Vet Res, 2006. **53**(3-4): p. 127-39.

140. Mayer, H., Bertram, H., Lindenmaier, W., Korff, T., Weber, H., and Weich, H., *Vascular endothelial growth factor (VEGF-A) expression in human mesenchymal stem cells: autocrine and paracrine role on osteoblastic and endothelial differentiation.* J Cell Biochem, 2005. **95**(4): p. 827-39.

141. Brooks, P.C., Stromblad, S., Sanders, L.C., von Schalscha, T.L., Aimes, R.T., Stetler-Stevenson, W.G., Quigley, J.P., and Cheresh, D.A., *Localization of matrix metalloproteinase MMP-2 to the surface of invasive cells by interaction with integrin alpha v beta 3.* Cell, 1996. **85**(5): p. 683-93.

142. Yu, Q. and Stamenkovic, I., *Cell surface-localized matrix metalloproteinase-9 proteolytically activates TGF-beta and promotes tumor invasion and angiogenesis.* Genes Dev, 2000. **14**(2): p. 163-76.

143. Hinz, B., *Formation and function of the myofibroblast during tissue repair.* J Invest Dermatol, 2007. **127**(3): p. 526-37.

144. Wipff, P.J., Rifkin, D.B., Meister, J.J., and Hinz, B., *Myofibroblast contraction activates latent TGF-beta1 from the extracellular matrix.* J Cell Biol, 2007. **179**(6): p. 1311-23.

145. Copland, I.B., Lord-Dufour, S., Cuerquis, J., Coutu, D.L., Annabi, B., Wang, E., and Galipeau, J., *Improved autograft survival of mesenchymal stromal cells by plasminogen activator inhibitor 1 inhibition.* Stem Cells, 2009. **27**(2): p. 467-77.

146. Yang, C., Patel, K., Harding, P., Sorokin, A., and Glass, W.F., 2nd, *Regulation of TGF-beta1/MAPK-mediated PAI-1 gene expression by the actin cytoskeleton in human mesangial cells.* Exp Cell Res, 2007. **313**(6): p. 1240-50.

147. Mandriota, S.J., Seghezzi, G., Vassalli, J.D., Ferrara, N., Wasi, S., Mazzieri, R., Mignatti, P., and Pepper, M.S., *Vascular endothelial growth factor increases urokinase receptor expression in vascular endothelial cells.* J Biol Chem, 1995. **270**(17): p. 9709-16.

148. Potier, E., Ferreira, E., Andriamanalijaona, R., Pujol, J.P., Oudina, K., Logeart-Avramoglou, D., and Petite, H., *Hypoxia affects mesenchymal stromal cell osteogenic differentiation and angiogenic factor expression.* Bone, 2007. **40**(4): p. 1078-87.

149. Annabi, B., Lee, Y.T., Turcotte, S., Naud, E., Desrosiers, R.R., Champagne, M., Eliopoulos, N., Galipeau, J., and Beliveau, R., *Hypoxia promotes murine bone-marrow-derived stromal cell migration and tube formation.* Stem Cells, 2003. **21**(3): p. 337-47.

150. Callow, M.G., Zozulya, S., Gishizky, M.L., Jallal, B., and Smeal, T., *PAK4 mediates morphological changes through the regulation of GEF-H1.* J Cell Sci, 2005. **118**(Pt 9): p. 1861-72.

151. Nalbant, P., Chang, Y.C., Birkenfeld, J., Chang, Z.F., and Bokoch, G.M., *Guanine nucleotide exchange factor-H1 regulates cell migration via localized activation of RhoA at the leading edge.* Mol Biol Cell, 2009. **20**(18): p. 4070-82.

152. Zenke, F.T., Krendel, M., DerMardirossian, C., King, C.C., Bohl, B.P., and Bokoch, G.M., *p21-activated kinase 1 phosphorylates and regulates 14-3-3 binding to GEF-H1, a microtubule-localized Rho exchange factor.* J Biol Chem, 2004. **279**(18): p. 18392-400.

153. Hamidouche, Z., Fromigue, O., Ringe, J., Haupl, T., Vaudin, P., Pages, J.C., Srouji, S., Livne, E., and Marie, P.J., *Priming integrin alpha5 promotes human mesenchymal stromal cell osteoblast differentiation and osteogenesis.* Proc Natl Acad Sci U S A, 2009. **106**(44): p. 18587-91.

154. Burghardt, R.C., Burghardt, J.R., Taylor, J.D., 2nd, Reeder, A.T., Nguen, B.T., Spencer, T.E., Bayless, K.J., and Johnson, G.A., *Enhanced focal adhesion assembly reflects increased mechanosensation and mechanotransduction at maternal-conceptus interface and uterine wall during ovine pregnancy.* Reproduction, 2009. **137**(3): p. 567-82.

155. D'Souza-Schorey, C., Boettner, B., and Van Aelst, L., *Rac regulates integrin-mediated spreading and increased adhesion of T lymphocytes.* Mol Cell Biol, 1998. **18**(7): p. 3936-46.

156. Filippi, M.D., Harris, C.E., Meller, J., Gu, Y., Zheng, Y., and Williams, D.A., *Localization of Rac2 via the C terminus and aspartic acid 150 specifies superoxide generation, actin polarity and chemotaxis in neutrophils.* Nat Immunol, 2004. **5**(7): p. 744-51.

157. Gomez, J.C., Soltys, J., Okano, K., Dinauer, M.C., and Doerschuk, C.M., *The role of Rac2 in regulating neutrophil production in the bone marrow and circulating neutrophil counts.* Am J Pathol, 2008. **173**(2): p. 507-17.

158. Park, B., Nguyen, N.T., Dutt, P., Merdek, K.D., Bashar, M., Sterpetti, P., Tosolini, A., Testa, J.R., and Toksoz, D., *Association of Lbc Rho guanine nucleotide exchange*

factor with alpha-catenin-related protein, alpha-catulin/CTNNAL1, supports serum response factor activation. J Biol Chem, 2002. **277**(47): p. 45361-70.

159. Xiang, Y., Tan, Y.R., Zhang, J.S., Qin, X.Q., Hu, B.B., Wang, Y., Qu, F., and Liu, H.J., *Wound repair and proliferation of bronchial epithelial cells regulated by CTNNAL1.* J Cell Biochem, 2008. **103**(3): p. 920-30.

160. Srivastava, M.K., Sinha, P., Clements, V.K., Rodriguez, P., and Ostrand-Rosenberg, S., *Myeloid-derived suppressor cells inhibit T-cell activation by depleting cystine and cysteine.* Cancer Res, 2010. **70**(1): p. 68-77.

161. Gmunder, H., Eck, H.P., Benninghoff, B., Roth, S., and Droge, W., *Macrophages regulate intracellular glutathione levels of lymphocytes. Evidence for an immunoregulatory role of cysteine.* Cell Immunol, 1990. **129**(1): p. 32-46.

162. Guppy, M., Greiner, E., and Brand, K., *The role of the Crabtree effect and an endogenous fuel in the energy metabolism of resting and proliferating thymocytes.* Eur J Biochem, 1993. **212**(1): p. 95-9.

163. Bauer, D.E., Harris, M.H., Plas, D.R., Lum, J.J., Hammerman, P.S., Rathmell, J.C., Riley, J.L., and Thompson, C.B., *Cytokine stimulation of aerobic glycolysis in hematopoietic cells exceeds proliferative demand.* Faseb J, 2004. **18**(11): p. 1303-5.

164. Yip, L., Woehrle, T., Corriden, R., Hirsh, M., Chen, Y., Inoue, Y., Ferrari, V., Insel, P.A., and Junger, W.G., *Autocrine regulation of T-cell activation by ATP release and P2X7 receptors.* Faseb J, 2009. **23**(6): p. 1685-93.

165. Li, J., Liu, D., Ke, H.Z., Duncan, R.L., and Turner, C.H., *The P2X7 nucleotide receptor mediates skeletal mechanotransduction.* J Biol Chem, 2005. **280**(52): p. 42952-9.

166. Groothuis, A., Kasper, G., Lehnigk, U., Bail, H., van Scherpenzeel, K., and Duda, G., *Angiogenic potential of the early fracture haematoma is increased by mechanical stimulation.* European Cells and Materials, 2008. **16**(Suppl. 4): p. 48.

167. Nasef, A., Chapel, A., Mazurier, C., Bouchet, S., Lopez, M., Mathieu, N., Sensebe, L., Zhang, Y., Gorin, N.C., Thierry, D., and Fouillard, L., *Identification of IL-10 and TGF-beta transcripts involved in the inhibition of T-lymphocyte proliferation during cell contact with human mesenchymal stem cells.* Gene Expr, 2007. **13**(4-5): p. 217-26.

168. Aggarwal, S. and Pittenger, M.F., *Human mesenchymal stem cells modulate allogeneic immune cell responses.* Blood, 2005. **105**(4): p. 1815-22.

169. Freeman, M.R., Schneck, F.X., Gagnon, M.L., Corless, C., Soker, S., Niknejad, K., Peoples, G.E., and Klagsbrun, M., *Peripheral blood T lymphocytes and lymphocytes infiltrating human cancers express vascular endothelial growth factor: a potential role for T cells in angiogenesis.* Cancer Res, 1995. **55**(18): p. 4140-5.

170. Hadar, E.J., Ershler, W.B., Kreisle, R.A., Ho, S.P., Volk, M.J., and Klopp, R.G., *Lymphocyte-induced angiogenesis factor is produced by L3T4+ murine T lymphocytes, and its production declines with age.* Cancer Immunol Immunother, 1988. **26**(1): p. 31-4.

171. Estrada, R., Li, N., Sarojini, H., An, J., Lee, M.J., and Wang, E., *Secretome from mesenchymal stem cells induces angiogenesis via Cyr61.* J Cell Physiol, 2009. **219**(3): p. 563-71.

172. Wu, Y., Chen, L., Scott, P.G., and Tredget, E.E., *Mesenchymal stem cells enhance wound healing through differentiation and angiogenesis.* Stem Cells, 2007. **25**(10): p. 2648-59.

173. Roth, S.J., Carr, M.W., and Springer, T.A., *C-C chemokines, but not the C-X-C chemokines interleukin-8 and interferon-gamma inducible protein-10, stimulate transendothelial chemotaxis of T lymphocytes.* Eur J Immunol, 1995. **25**(12): p. 3482-8.

174. Nakamura, H., Makino, Y., Okamoto, K., Poellinger, L., Ohnuma, K., Morimoto, C., and Tanaka, H., *TCR engagement increases hypoxia-inducible factor-1 alpha protein synthesis via rapamycin-sensitive pathway under hypoxic conditions in human peripheral T cells.* J Immunol, 2005. **174**(12): p. 7592-9.

175. Olbryt, M., Jarzab, M., Jazowiecka-Rakus, J., Simek, K., Szala, S., and Sochanik, A., *Gene expression profile of B 16(F10) murine melanoma cells exposed to hypoxic conditions in vitro.* Gene Expr, 2006. **13**(3): p. 191-203.

176. Ribatti, D., Guidolin, D., Conconi, M.T., Nico, B., Baiguera, S., Parnigotto, P.P., Vacca, A., and Nussdorfer, G.G., *Vinblastine inhibits the angiogenic response induced by adrenomedullin in vitro and in vivo.* Oncogene, 2003. **22**(41): p. 6458-61.

177. Gonzalez-Rey, E., Chorny, A., O'Valle, F., and Delgado, M., *Adrenomedullin Protects from Experimental Arthritis by Down-Regulating Inflammation and Th1 Response and Inducing Regulatory T Cells.* Am. J. Pathol., 2007. **170**(1): p. 263-271.

178. Li, L., Zhang, S., Zhang, Y., Yu, B., Xu, Y., and Guan, Z., *Paracrine action mediate the antifibrotic effect of transplanted mesenchymal stem cells in a rat model of global heart failure.* Mol Biol Rep, 2009. **36**(4): p. 725-31.

179. Zimmerman, A.W., Joosten, B., Torensma, R., Parnes, J.R., van Leeuwen, F.N., and Figdor, C.G., *Long-term engagement of CD6 and ALCAM is essential for T-cell proliferation induced by dendritic cells.* Blood, 2006. **107**(8): p. 3212-20.

180. Buhring, H.J., Treml, S., Cerabona, F., de Zwart, P., Kanz, L., and Sobiesiak, M., *Phenotypic characterization of distinct human bone marrow-derived MSC subsets.* Ann N Y Acad Sci, 2009. **1176**: p. 124-34.

181. Majumdar, M.K., Keane-Moore, M., Buyaner, D., Hardy, W.B., Moorman, M.A., McIntosh, K.R., and Mosca, J.D., *Characterization and functionality of cell surface molecules on human mesenchymal stem cells.* J Biomed Sci, 2003. **10**(2): p. 228-41.

182. Lavery, K., Swain, P., Falb, D., and Alaoui-Ismaili, M.H., *BMP-2/4 and BMP-6/7 differentially utilize cell surface receptors to induce osteoblastic differentiation of human bone marrow-derived mesenchymal stem cells.* J Biol Chem, 2008. **283**(30): p. 20948-58.

183. Li, Z., Hassan, M.Q., Jafferji, M., Aqeilan, R.I., Garzon, R., Croce, C.M., van Wijnen, A.J., Stein, J.L., Stein, G.S., and Lian, J.B., *Biological functions of miR-29b contribute*

to positive regulation of osteoblast differentiation. J Biol Chem, 2009. **284**(23): p. 15676-84.

184. Nakai, K., Tanaka, S., Sakai, A., Nagashima, M., Tanaka, M., Otomo, H., and Nakamura, T., *Cyclooxygenase-2 selective inhibition suppresses restoration of tibial trabecular bone formation in association with restriction of osteoblast maturation in skeletal reloading after hindlimb elevation of mice.* Bone, 2006. **39**(1): p. 83-92.

185. Nelson, D. and Cox, M., *Lehninger Biochemie*. 3 ed. 2001, Berlin and Heidelberg: Springer Verlag. 852-853.

186. Stamp, Lisa, K., James, Michael, J., Cleland, and Leslie, G., *Paracrine upregulation of monocyte cyclooxygenase-2 by mediators produced by T lymphocytes: Role of interleukin 17 and interferon-γ.* Journal of Rheumatology, 2004. **31**(7): p. 1255-1264

187. Ramasamy, R., Tong, C.K., Seow, H.F., Vidyadaran, S., and Dazzi, F., *The immunosuppressive effects of human bone marrow-derived mesenchymal stem cells target T cell proliferation but not its effector function.* Cell Immunol, 2008. **251**(2): p. 131-6.

188. Batten, P., Sarathchandra, P., Antoniw, J.W., Tay, S.S., Lowdell, M.W., Taylor, P.M., and Yacoub, M.H., *Human mesenchymal stem cells induce T cell anergy and downregulate T cell allo-responses via the TH2 pathway: relevance to tissue engineering human heart valves.* Tissue Eng, 2006. **12**(8): p. 2263-73.

189. Papathanassoglou, E., El-Haschimi, K., Li, X.C., Matarese, G., Strom, T., and Mantzoros, C., *Leptin receptor expression and signaling in lymphocytes: kinetics during lymphocyte activation, role in lymphocyte survival, and response to high fat diet in mice.* J Immunol, 2006. **176**(12): p. 7745-52.

190. Laschober, G.T., Brunauer, R., Jamnig, A., Fehrer, C., Greiderer, B., and Lepperdinger, G., *Leptin receptor/CD295 is upregulated on primary human mesenchymal stem cells of advancing biological age and distinctly marks the subpopulation of dying cells.* Exp Gerontol, 2009. **44**(1-2): p. 57-62.

191. Robertson, S., Ishida-Takahashi, R., Tawara, I., Hu, J., Patterson, C.M., Jones, J.C., Kulkarni, R.N., and Myers, M.G., Jr., *Insufficiency of Jak2-autonomous leptin receptor signals for most physiologic leptin actions.* Diabetes, 2010. **59**(4): p. 782-790.

192. Fitzgerald, K.A. and Golenbock, D.T., *Immunology. The shape of things to come.* Science, 2007. **316**(5831): p. 1574-6.

193. Komai-Koma, M., Gilchrist, D.S., and Xu, D., *Direct recognition of LPS by human but not murine CD8+ T cells via TLR4 complex.* Eur J Immunol, 2009. **39**(6): p. 1564-72.

194. Wilson, C.J., Kasper, G., Schutz, M.A., and Duda, G.N., *Cyclic strain disrupts endothelial network formation on Matrigel.* Microvasc Res, 2009. **78**(3): p. 358-63.

195. Bouletreau, P.J., Warren, S.M., Spector, J.A., Steinbrech, D.S., Mehrara, B.J., and Longaker, M.T., *Factors in the fracture microenvironment induce primary osteoblast angiogenic cytokine production.* Plast Reconstr Surg, 2002. **110**(1): p. 139-48.

196. Deckers, M.M., van Bezooijen, R.L., van der Horst, G., Hoogendam, J., van Der Bent, C., Papapoulos, S.E., and Lowik, C.W., *Bone morphogenetic proteins stimulate angiogenesis through osteoblast-derived vascular endothelial growth factor A.* Endocrinology, 2002. **143**(4): p. 1545-53.

197. Winkler, T., von Roth, P., Matziolis, G., Mehta, M., Perka, C., and Duda, G.N., *Dose-response relationship of mesenchymal stem cell transplantation and functional regeneration after severe skeletal muscle injury in rats.* Tissue Eng Part A, 2009. **15**(3): p. 487-92.

198. Grundnes, O. and Reikeras, O., *The importance of the hematoma for fracture healing in rats.* Acta Orthop Scand, 1993. **64**(3): p. 340-2.

Appendix

Buffers used for (immuno)histology

PBS

1:10 in aqua dest.

Tris-EDTA buffer

10mM Tris Base

1mM EDTA

ad 1L Aqua dest., ph 9.0

0.05% Tween 20

Chromogen buffer

Tris HCl	3.96g
Tris Base	0.54g
NaCl	2.63g

ad 300ml A.dest., ph 8.2

Tab. A1: Number of differentially regulated genes compared to total number of detected genes.

		Number of Genes
MSCs	up-regulated	90
	down-regulated	46
	total of differentially regulated	136
	detected in stimulated	8004
	detected in unstimulated	7622
T lymphocytes	up-regulated	59
	down-regulated	4
	total of differentially regulated	63
	detected in stimulated	7385
	detected in unstimulated	7360
Co-culture	up-regulated	4
	down-regulated	96
	total of differentially regulated	100
	detected in stimulated	8014
	detected in unstimulated	8222

detected genes: $p<0.01$
differentially regulated genes: $p<0.05$
fold-change: 1.5

Tab. A2: Number of detected genes that are commonly expressed.

S stands for stimulated samples, U for unstimulated samples.

	MSC-S	**MSC-U**	**T-S**	**T-U**	**Co-S**	**Co-U**
MSC-S	8004	7397	6302	6245	7281	7744
MSC-U	7397	7622	6054	6054	7017	7214
T-S	6302	6104	7385	6999	6784	6883
T-U	6245	6054	6999	7360	6730	6817
Co-S	7281	7017	6784	6730	8014	7733
Co-U	7744	7214	6883	6817	7733	8222

Tab. A3: Differentially regulated genes in MSCs due to mechanical stimulation.

Determined in gene array experiment with p<0.01 (grey) and p<0.05. Sorted by fold change (FC), FC >1.5 indicates up-regulated genes, FC <0.67 indicates down-regulated genes.

Gene Symbol	Gene Name	Entrez Gene ID	FC	p-value
MAMDC2	MAM domain containing 2	256691	5.15	0.004
HSD11B1	hydroxysteroid (11-beta) dehydrogenase 1, transcript variant 2	3290	4.38	0.043
WISP1	WNT1 inducible signaling pathway protein 1, transcript variant 1	8840	3.36	0.028
G0S2	G0/G1switch 2	50486	3.28	0.017
SLC47A1	solute carrier family 47, member 1	55244	3.28	0.021
SLC7A11	solute carrier family 7, (cationic amino acid transporter, y+ system) member 11	23657	3.24	0.008
GPR68	G protein-coupled receptor 68	8111	3.10	0.027
CHST6	carbohydrate (N-acetylglucosamine 6-O) sulfotransferase 6	4166	3.06	0.049
AKR1B10	aldo-keto reductase family 1, member B10 (aldose reductase)	57016	3.00	0.002
IER3	immediate early response 3	8870	3.00	0.001
KLF4	Kruppel-like factor 4 (gut)	9314	2.92	0.019
TMEM100	transmembrane protein 100, transcript variant 2	55273	2.90	0.049
HES1	hairy and enhancer of split 1, (Drosophila)	3280	2.90	0.016
LGR4	leucine-rich repeat-containing G protein-coupled receptor 4	55366	2.89	0.003
KYNU	kynureninase (L-kynurenine hydrolase), transcript variant 2	8942	2.60	0.008
SHISA2	shisa homolog 2 (Xenopus laevis)	387914	2.55	0.005
CDC42EP2	CDC42 effector protein (Rho GTPase binding) 2	10435	2.55	0.001
C14ORF126	chromosome 14 open reading frame 126	112487	2.48	0.040
CAMK1G	calcium/calmodulin-dependent protein kinase IG	57172	2.45	0.035
PNO1	partner of NOB1 homolog (S. cerevisiae)	56902	2.39	0.015
HBEGF	heparin-binding EGF-like growth factor	1839	2.37	0.005
SYNJ2	synaptojanin 2	8871	2.37	0.035
C2ORF27	chromosome 2 open reading frame 27	29798	2.31	0.041
SNORD56	small nucleolar RNA, C/D box 56, non-coding RNA	26793	2.27	0.021
SRXN1	sulfiredoxin 1 homolog (S. cerevisiae)	140809	2.27	0.000
RBM3	RNA binding motif (RNP1, RRM) protein 3, transcript variant 2	5935	2.24	0.046
LINGO1	leucine rich repeat and Ig domain containing 1	84894	2.23	0.017
NP	nucleoside phosphorylase	4860	2.17	0.002
EGR2	early growth response 2 (Krox-20 homolog, Drosophila)	1959	2.13	0.005
UAP1	UDP-N-acteylglucosamine pyrophosphorylase 1	6675	2.12	0.020
TMEM155	transmembrane protein 155	132332	2.11	0.018
IGF2BP3	insulin-like growth factor 2 mRNA binding protein 3	10643	2.10	0.010
FZD9	frizzled homolog 9 (Drosophila)	8326	2.09	0.013
SLC7A5	solute carrier family 7 (cationic amino acid transporter, y+ system), member 5	8140	2.07	0.001
SCG5	secretogranin V (7B2 protein)	6447	2.02	0.004
TRIB1	tribbles homolog 1 (Drosophila)	10221	2.01	0.037
TLK1	tousled-like kinase 1	9874	1.98	0.008
RAB30	RAB30, member RAS oncogene family	27314	1.98	0.037
PLAT	plasminogen activator, tissue, transcript variant 1	5327	1.97	0.002
MSC	musculin (activated B-cell factor-1)	9242	1.95	0.001
GPR56	G protein-coupled receptor 56, transcript variant 2	9289	1.92	0.022
BHLHB2	basic helix-loop-helix domain containing, class B, 2	8553	1.91	0.041
SERPINE1	serpin peptidase inhibitor, clade E (nexin, plasminogen activator inhibitor type 1), member 1	5054	1.90	0.010
CYCS	cytochrome c, somatic, nuclear gene encoding mitochondrial protein	54205	1.88	0.019
C6ORF85	chromosome 6 open reading frame 85	63027	1.88	0.016

Continued on following page.

Tab. A3: continued 1.

Gene Symbol	Gene Name	Entrez Gene ID	FC	p-value
KLF2	Kruppel-like factor 2 (lung)	10365	1.88	0.003
APCDD1L	adenomatosis polyposis coli down-regulated 1-like	164284	1.87	0.001
AXUD1	AXIN1 up-regulated 1	64651	1.84	0.002
SRPX2	sushi-repeat-containing protein, X-linked 2	27286	1.83	0.004
HIST1H2AC	histone cluster 1, H2ac	8334	1.80	0.005
TIPARP	TCDD-inducible poly(ADP-ribose) polymerase	25976	1.79	0.002
MTHFD2L	methylenetetrahydrofolate dehydrogenase (NADP+ dependent) 2-like	441024	1.78	0.038
C14ORF149	chromosome 14 open reading frame 149	112849	1.75	0.012
WWC3	WWC family member 3	55841	1.75	0.004
FJX1	four jointed box 1 (Drosophila)	24147	1.73	0.015
FOSB	FBJ murine osteosarcoma viral oncogene homolog B	2354	1.73	0.014
ATP13A2	ATPase type 13A2	23400	1.71	0.028
PANX2	pannexin 2	56666	1.71	0.020
SLC3A2	solute carrier family 3 (activators of dibasic and neutral amino acid transport), member 2, transcript variant 1	6520	1.70	0.008
NAV1	neuron navigator 1	89796	1.69	0.021
CCRN4L	CCR4 carbon catabolite repression 4-like (S. cerevisiae)	25819	1.69	0.018
IRAK2	interleukin-1 receptor-associated kinase 2	3656	1.69	0.017
B3GALTL	beta 1,3-galactosyltransferase-like	145173	1.68	0.011
MTMR9	myotubularin related protein 9	66036	1.67	0.008
PHLDB1	pleckstrin homology-like domain, family B, member 1	23187	1.67	0.037
KIAA1217	KIAA1217, transcript variant 2	56243	1.66	0.012
OAF	OAF homolog (Drosophila)	220323	1.65	0.010
GLA	galactosidase, alpha	2717	1.65	0.005
TMEM41A	transmembrane protein 41A	90407	1.64	0.016
GFPT2	glutamine-fructose-6-phosphate transaminase 2	9945	1.64	0.015
CTPS	CTP synthase	1503	1.63	0.009
TNFRSF12A	tumor necrosis factor receptor superfamily, member 12A	51330	1.62	0.014
TNFAIP3	tumor necrosis factor, alpha-induced protein 3	7128	1.62	0.012
E2F7	E2F transcription factor 7	144455	1.60	0.041
FLJ14213	protor-2	79899	1.60	0.030
SPSB1	splA/ryanodine receptor domain and SOCS box containing 1	80176	1.59	0.030
KIAA0247	KIAA0247	9766	1.58	0.016
ANGPTL2	angiopoietin-like 2	23452	1.58	0.012
ITGA5	integrin, alpha 5 (fibronectin receptor, alpha polypeptide)	3678	1.58	0.011
ARHGEF2	rho/rac guanine nucleotide exchange factor (GEF) 2	9181	1.57	0.034
KIAA1754	KIAA1754	85450	1.57	0.012
GCLM	glutamate-cysteine ligase, modifier subunit	2730	1.56	0.018
PLAUR	plasminogen activator, urokinase receptor, transcript variant 1	5329	1.56	0.029
NDUFAB1	NADH dehydrogenase (ubiquinone) 1, alpha/beta subcomplex, 1, 8kDa	4706	1.54	0.016
ODC1	ornithine decarboxylase 1	4953	1.54	0.037
EIF2S2	eukaryotic translation initiation factor 2, subunit 2 beta, 38kDa	8894	1.53	0.041
PGD	phosphogluconate dehydrogenase	5226	1.53	0.015
UCK2	uridine-cytidine kinase 2	7371	1.52	0.022
PIM1	pim-1 oncogene	5292	1.52	0.025
UBE2Q1	ubiquitin-conjugating enzyme E2Q (putative) 1	55585	1.50	0.034

Continued on following page.

Tab. A3: continued 2.

Gene Symbol	Gene Name	Entrez Gene ID	FC	p-value
GLDN	gliomedin	342035	0.19	0.009
ASIP	agouti signaling protein, nonagouti homolog (mouse)	434	0.27	0.001
WISP2	WNT1 inducible signaling pathway protein 2	8839	0.30	0.013
LEPR	leptin receptor, transcript variant 1	3953	0.32	0.020
FZD5	frizzled homolog 5 (Drosophila)	7855	0.32	0.008
COL9A2	collagen, type IX, alpha 2	1298	0.39	0.032
RASL11A	RAS-like, family 11, member A	387496	0.40	0.022
ADM	adrenomedullin	133	0.45	0.000
DAPK2	death-associated protein kinase 2	23604	0.45	0.003
MYOM1	myomesin 1, 185kDa, transcript variant 1	8736	0.47	0.000
MAN1C1	mannosidase, alpha, class 1C, member 1	57134	0.47	0.038
ADAMTS9	ADAM metallopeptidase with thrombospondin type 1 motif, 9	56999	0.47	0.033
C10ORF11	chromosome 10 open reading frame 11	83938	0.49	0.005
ALCAM	activated leukocyte cell adhesion molecule	214	0.51	0.020
APBB1IP	amyloid beta (A4) precursor protein-binding, family B, member 1 interacting protein	54518	0.52	0.003
SNCAIP	synuclein, alpha interacting protein	9627	0.53	0.000
PNCK	pregnancy upregulated non-ubiquitously expressed CaM kinase	139728	0.53	0.002
CEBPA	CCAAT/enhancer binding protein (C/EBP), alpha	1050	0.53	0.003
NEURL2	neuralized homolog 2 (Drosophila)	140825	0.54	0.003
BGLAP	bone gamma-carboxyglutamate (gla) protein (osteocalcin)	632	0.54	0.024
DENND2D	DENN/MADD domain containing 2D	79961	0.54	0.032
DYSF	dysferlin, limb girdle muscular dystrophy 2B (autosomal recessive)	8291	0.55	0.045
LEPREL1	leprecan-like 1	55214	0.57	0.001
C4ORF31	chromosome 4 open reading frame 31	79625	0.58	0.026
HSD17B8	hydroxysteroid (17-beta) dehydrogenase 8	7923	0.59	0.028
YPEL1	yippee-like 1 (Drosophila)	29799	0.60	0.032
FMO3	flavin containing monooxygenase 3, transcript variant 1	2328	0.60	0.041
B3GALT4	UDP-Gal:betaGlcNAc beta 1,3-galactosyltransferase, polypeptide 4	8705	0.61	0.019
CFD	complement factor D (adipsin)	1675	0.61	0.047
VCAM1	vascular cell adhesion molecule 1, transcript variant 1	7412	0.63	0.006
GYS1	glycogen synthase 1 (muscle)	2997	0.63	0.016
C10ORF10	chromosome 10 open reading frame 10	11067	0.63	0.005
REEP6	receptor accessory protein 6	92840	0.63	0.016
RABGAP1	RAB GTPase activating protein 1	23637	0.64	0.013
WDR27	WD repeat domain 27	253769	0.65	0.042
FZD1	frizzled homolog 1 (Drosophila)	8321	0.65	0.030
AMDHD2	amidohydrolase domain containing 2	51005	0.65	0.029
SAT2	spermidine/spermine N1-acetyltransferase family member 2	112483	0.65	0.009
RAC2	ras-related C3 botulinum toxin substrate 2 (rho family, small GTP binding protein Rac2)	5880	0.65	0.010
ALDOC	aldolase C, fructose-bisphosphate	230	0.65	0.010
CYP27A1	cytochrome P450, family 27, subfamily A, polypeptide 1, nuclear gene encoding mitochondrial protein	1593	0.65	0.010
CEBPD	CCAAT/enhancer binding protein (C/EBP), delta	1052	0.66	0.013
EPDR1	ependymin related protein 1 (zebrafish)	54749	0.66	0.014
C12ORF62	chromosome 12 open reading frame 62	84987	0.66	0.049
CTNNAL1	catenin (cadherin-associated protein), alpha-like 1	8727	0.66	0.023
TXNIP	thioredoxin interacting protein	10628	0.66	0.016

Tab. A4: Differentially regulated genes in T lymphocytes due to mechanical stimulation.

Determined in gene array experiment with p<0.01 (grey) and p<0.05. Sorted by fold change (FC), FC >1.5 indicates up-regulated genes, FC <0.67 indicates down-regulated genes.

Gene Symbol	Gene Name	Entrez Gene ID	FC	p-value
SCD	stearoyl-CoA desaturase (delta-9-desaturase)	6319	3.30	0.000
C1ORF56	chromosome 1 open reading frame 56	54964	2.76	0.016
SQLE	squalene epoxidase	6713	2.73	0.003
VPS53	vacuolar protein sorting 53 homolog (S. cerevisiae)	55275	2.66	0.016
HSF1	heat shock transcription factor 1 (HSF1)	3297	2.61	0.016
FAM21C	family with sequence similarity 21, member C	253725	2.26	0.048
PIP4K2B	phosphatidylinositol-5-phosphate 4-kinase, type II, beta	8396	2.25	0.032
PHC3	polyhomeotic homolog 3 (Drosophila)	80012	2.18	0.041
MORC3	MORC family CW-type zinc finger 3	23515	2.13	0.037
GNAQ	guanine nucleotide binding protein (G protein), q polypeptide	2776	2.09	0.041
FASTKD3	FAST kinase domains 3	79072	2.02	0.029
PNMA1	paraneoplastic antigen MA1	9240	1.98	0.009
MRS2	MRS2 magnesium homeostasis factor homolog (S. cerevisiae)	57380	1.98	0.033
HERPUD1	homocysteine-inducible, endoplasmic reticulum stress-inducible, ubiquitin-like domain member 1, transcript variant 3	9709	1.98	0.020
FAM18B	family with sequence similarity 18, member B	51030	1.96	0.041
APP	amyloid beta (A4) precursor protein (APP), transcript variant 1	351	1.96	0.043
LDLR	low density lipoprotein receptor (familial hypercholesterolemia)	3949	1.93	0.002
RICS	Rho GTPase-activating protein	9743	1.93	0.011
DDX21	DEAD (Asp-Glu-Ala-Asp) box polypeptide 21	9188	1.92	0.017
MTHFD1L	methylenetetrahydrofolate dehydrogenase (NADP+ dependent) 1-like	25902	1.91	0.027
IPO5	importin 5	3843	1.91	0.028
HIST1H4B	histone cluster 1, H4b	8366	1.88	0.041
HELB	helicase (DNA) B	92797	1.85	0.034
UTP18	UTP18, small subunit (SSU) processome component, homolog (yeast)	51096	1.83	0.037
LRCH3	leucine-rich repeats and calponin homology (CH) domain containing 3	84859	1.83	0.048
ZNF236	zinc finger protein 236	7776	1.80	0.048
SMA4	SMA4	11039	1.80	0.041
SCOC	short coiled-coil protein	60592	1.79	0.033
YPEL2	yippee-like 2 (Drosophila)	388403	1.79	0.019
C1ORF109	chromosome 1 open reading frame 109	54955	1.77	0.037
WDR26	WD repeat domain 26	80232	1.75	0.034
CHMP2B	chromatin modifying protein 2B	25978	1.74	0.025

Continued on following page.

Tab. A4: continued.

Gene Symbol	Gene Name	Entrez Gene ID	FC	p-value
NUP160	nucleoporin 160kDa	23279	1.73	0.009
DDX60	DEAD (Asp-Glu-Ala-Asp) box polypeptide 60	55601	1.72	0.029
TMEM14A	transmembrane protein 14A	28978	1.72	0.034
RAB5A	RAB5A, member RAS oncogene family	5868	1.71	0.029
STARD3NL	STARD3 N-terminal like	83930	1.71	0.029
HIATL1	hippocampus abundant transcript-like 1	84641	1.70	0.042
PPIL1	peptidylprolyl isomerase (cyclophilin)-like 1	51645	1.69	0.027
ZNF235	zinc finger protein 235	9310	1.69	0.028
SDCBP	syndecan binding protein (syntenin), transcript variant 2	6386	1.68	0.027
TXK	TXK tyrosine kinase	7294	1.67	0.041
ABHD3	abhydrolase domain containing 3	171586	1.67	0.023
PSMG2	proteasome (prosome, macropain) assembly chaperone 2	56984	1.66	0.037
STXBP3	syntaxin binding protein 3	6814	1.65	0.043
STRN3	striatin, calmodulin binding protein 3, transcript variant 2	29966	1.64	0.024
SELI	selenoprotein I	85465	1.63	0.049
METTL3	methyltransferase like 3	56339	1.63	0.021
FUBP3	far upstream element (FUSE) binding protein 3, XM_945904 XM_945906 XM_945907	8939	1.62	0.031
RIOK2	RIO kinase 2 (yeast)	55781	1.62	0.029
TAF2	TAF2 RNA polymerase II, TATA box binding protein (TBP)-associated factor, 150kDa	6873	1.61	0.036
DNAJC24	DnaJ (Hsp40) homolog, subfamily C, member 24	120526	1.59	0.037
NDFIP1	Nedd4 family interacting protein 1	80762	1.59	0.046
P2RX7	purinergic receptor P2X, ligand-gated ion channel, 7	5027	1.59	0.048
UNC84A	unc-84 homolog A (C. elegans)	23353	1.57	0.031
ZCCHC8	zinc finger, CCHC domain containing 8	55596	1.57	0.044
C9ORF46	chromosome 9 open reading frame 46	55848	1.55	0.038
KIAA2026	KIAA2026	158358	1.54	0.045
KIF2A	kinesin heavy chain member 2A	3796	1.52	0.046
MTF2	metal response element binding transcription factor 2	22823	0.30	0.036
TNC	tenascin C (hexabrachion)	3371	0.32	0.044
DSCC1	defective in sister chromatid cohesion 1 homolog (S. cerevisiae)	79075	0.33	0.048
HLA-DMB	major histocompatibility complex, class II, DM beta	3109	0.60	0.047

Tab. A5: Differentially regulated genes in co-culture due to mechanical stimulation.

Determined in gene array experiment with p<0.01 (grey) and p<0.05. Sorted by fold change (FC), FC >1.5 indicates up-regulated genes, FC <0.67 indicates down-regulated genes.

Gene Symbol	Gene Name	Entrez Gene ID	FC	p-value
SCARA5	scavenger receptor class A, member 5 (putative)	286133	7.94	0.009
S1PR3	sphingosine-1-phosphate receptor 3	1903	2.68	0.031
COL5A3	collagen, type V, alpha 3	50509	2.25	0.020
PHGDH	phosphoglycerate dehydrogenase	26227	1.88	0.040
GLDN	gliomedin	342035	0.07	0.000
STC1	stanniocalcin 1	6781	0.11	0.000
LEPR	leptin receptor, transcript variant 1	3953	0.16	0.000
ADM	adrenomedullin	133	0.19	0.000
KIAA1199	KIAA1199	57214	0.29	0.000
NCAM2	neural cell adhesion molecule 2	4685	0.30	0.010
CTHRC1	collagen triple helix repeat containing 1	115908	0.33	0.015
VGLL3	vestigial like 3 (Drosophila)	389136	0.35	0.002
CXCL10	chemokine (C-X-C motif) ligand 10	3627	0.36	0.000
RAB38	RAB38, member RAS oncogene family	23682	0.36	0.015
TP73L	tumor protein p73-like	8626	0.38	0.040
SBSN	suprabasin	374897	0.38	0.028
FOS	v-fos FBJ murine osteosarcoma viral oncogene homolog	2353	0.40	0.019
PROS1	protein S (alpha)	5627	0.40	0.000
CCL8	chemokine (C-C motif) ligand 8	6355	0.40	0.002
FMO3	flavin containing monooxygenase 3, transcript variant 1	2328	0.41	0.000
FZD1	frizzled homolog 1 (Drosophila)	8321	0.42	0.003
RNF141	ring finger protein 141	50862	0.42	0.013
TWISTNB	TWIST neighbor	221830	0.43	0.048
TM4SF1	transmembrane 4 L six family member 1	4071	0.43	0.001
ALCAM	activated leukocyte cell adhesion molecule	214	0.44	0.005
INA	internexin neuronal intermediate filament protein, alpha	9118	0.44	0.008
TF	transferrin	7018	0.45	0.016
ATP8B4	ATPase, class I, type 8B, member 4	79895	0.45	0.008
C10ORF10	chromosome 10 open reading frame 10	11067	0.46	0.028
GPM6B	glycoprotein M6B (GPM6B), transcript variant 1	2824	0.46	0.040
CEBPD	CCAAT/enhancer binding protein (C/EBP), delta	1052	0.46	0.000
ASS1	argininosuccinate synthetase 1, transcript variant 1.	445	0.46	0.015
CCDC99	coiled-coil domain containing 99	54908	0.47	0.047
AOX1	aldehyde oxidase 1	316	0.48	0.006
PTGS2	prostaglandin-endoperoxide synthase 2 (prostaglandin G/H synthase and cyclooxygenase)	5743	0.48	0.029
LXN	latexin	56925	0.48	0.007
PRRG1	proline rich Gla (G-carboxyglutamic acid) 1	5638	0.49	0.007
SNCAIP	synuclein, alpha interacting protein	9627	0.49	0.004
STK3	serine/threonine kinase 3 (STE20 homolog, yeast)	6788	0.50	0.010
VCAM1	vascular cell adhesion molecule 1, transcript variant 1	7412	0.50	0.001
GLRB	glycine receptor, beta	2743	0.50	0.009
LOX	lysyl oxidase	4015	0.50	0.029
SVEP1	sushi, von Willebrand factor type A, EGF and pentraxin domain containing 1	79987	0.50	0.009
MAOA	monoamine oxidase A, nuclear gene encoding mitochondrial protein	4128	0.51	0.042
CD69	CD69 molecule	969	0.51	0.032
TMEM200A	transmembrane protein 200A	114801	0.51	0.013
ZFHX4	zinc finger homeobox 4	79776	0.52	0.033
SCG5	secretogranin V (7B2 protein)	6447	0.52	0.032
RASL11A	RAS-like, family 11, member A	387496	0.52	0.019
TMEM30B	transmembrane protein 30B	161291	0.52	0.022

Continued on following page.

Tab. A5: continued.

Gene Symbol	Gene Name	Entrez Gene ID	FC	p-value
SGCE	sarcoglycan, epsilon, transcript variant 3	8910	0.52	0.016
RFTN2	raftlin family member 2	130132	0.52	0.015
SPRED1	sprouty-related, EVH1 domain containing 1	161742	0.53	0.003
LEPREL1	leprecan-like 1	55214	0.53	0.004
OSMR	oncostatin M receptor	9180	0.53	0.007
ANKRD37	ankyrin repeat domain 37	353322	0.53	0.002
MMD	monocyte to macrophage differentiation-associated	23531	0.53	0.007
ANGPT1	angiopoietin 1	284	0.53	0.011
RGS4	regulator of G-protein signalling 4	5999	0.53	0.005
TMED5	transmembrane emp24 protein transport domain containing 5	50999	0.53	0.019
RSBN1L	round spermatid basic protein 1-like	222194	0.54	0.047
EPSTI1	epithelial stromal interaction 1 (breast), transcript variant 2	94240	0.54	0.003
BNIP3	BCL2/adenovirus E1B 19kDa interacting protein 3, nuclear gene encoding mitochondrial protein	664	0.54	0.005
SHROOM2	shroom family member 2	357	0.54	0.047
LY96	lymphocyte antigen 96	23643	0.54	0.004
CENTB2	centaurin, beta 2	23527	0.54	0.047
CHEK1	CHK1 checkpoint homolog (S. pombe)	1111	0.55	0.024
SLC40A1	solute carrier family 40 (iron-regulated transporter), member 1	30061	0.55	0.008
RHOBTB3	Rho-related BTB domain containing 3	22836	0.55	0.018
GBE1	glucan (1,4-alpha-), branching enzyme 1 (glycogen branching enzyme, Andersen disease, glycogen storage disease type IV)	2632	0.55	0.032
HRASLS3	HRAS-like suppressor 3	11145	0.56	0.005
ERRFI1	ERBB receptor feedback inhibitor 1	54206	0.56	0.027
EFNB2	ephrin-B2	1948	0.56	0.030
RAD23B	RAD23 homolog B (S. cerevisiae)	5887	0.57	0.027
OXR1	oxidation resistance 1	55074	0.57	0.023
ELA2	elastase 2, neutrophil	1991	0.57	0.029
AP1S2	adaptor-related protein complex 1, sigma 2 subunit	8905	0.57	0.037
IQCK	IQ motif containing K	124152	0.58	0.036
EPDR1	ependymin related protein 1 (zebrafish)	54749	0.58	0.007
ACVR2A	activin A receptor, type IIA	92	0.58	0.038
SLC1A3	solute carrier family 1 (glial high affinity glutamate transporter), member 3	6507	0.58	0.026
C11ORF74	chromosome 11 open reading frame 74	119710	0.58	0.019
DCUN1D4	DCN1, defective in cullin neddylation 1, domain containing 4 (S. cerevisiae)	23142	0.59	0.017
ST13	suppression of tumorigenicity 13 (colon carcinoma) (Hsp70 interacting protein)	6767	0.59	0.041
GPNMB	glycoprotein (transmembrane) nmb, transcript variant 1	10457	0.59	0.031
CMC1	COX assembly mitochondrial protein homolog (S. cerevisiae), nuclear gene encoding mitochondrial protein	152100	0.59	0.031
FMO4	flavin containing monooxygenase 4	2329	0.59	0.041
GADD45A	growth arrest and DNA-damage-inducible, alpha	1647	0.60	0.029
TXNDC1	thioredoxin domain containing 1	81542	0.60	0.046
GRAMD3	GRAM domain containing 3	65983	0.61	0.033
NDRG1	N-myc downstream regulated gene 1	10397	0.61	0.018
EFEMP1	EGF-containing fibulin-like extracellular matrix protein 1, transcript variant 2	2202	0.61	0.042
SUSD1	sushi domain containing 1	64420	0.62	0.035
WASL	Wiskott-Aldrich syndrome-like	8976	0.64	0.046
FER1L3	fer-1-like 3, myoferlin (C. elegans), transcript variant 1	26509	0.64	0.039
THOC7	THO complex 7 homolog (Drosophila)	80145	0.65	0.048
STXBP5	syntaxin binding protein 5 (tomosyn)	134957	0.65	0.050
CDH11	cadherin 11, type 2, OB-cadherin (osteoblast)	1009	0.65	0.044
PCDH18	protocadherin 18	54510	0.66	0.048
CYR61	cysteine-rich, angiogenic inducer, 61	3491	0.66	0.049

Curriculum Vitae

Friederike Hanna Bieler, née Bleckwehl

1980 born in Bremen, Germany

Education

1993 – 2000	Gymnasium Syke in Syke, Germany Abitur
2000 – 2004	University of Applied Sciences Oldenburg/Ostfriesland/Wilhelmshaven in Wilhelmshaven (today: Jade Hochschule), Germany Diploma Thesis at RJAH Orthopaedic Hospital, Oswestry, UK Degree: Diplom-Ingenieurin (FH) in Biomedical Engineering
2004 – 2006	Albstadt-Sigmaringen University in Sigmaringen, Germany Master Thesis at TU Eindhoven, The Netherlands Degree: Master of Science in Biomedical Engineering

Work experience

2006 – 2010	Julius Wolff Institute Charité – Universitätsmedizin Berlin, Germany Research Associate in Mechanobiology
Since June 2010	Biotronik SE & Co. KG, Berlin, Germany Junior Manager Regulatory Affairs

Publications

Accepted Abstracts

Mechanical characterisation of the BioFlex® membrane
Kongress der Deutschen Gesellschaft für Biomechanik, DGfB 2007, Köln, D
F.H. Bleckwehl; C.E. Ott; D.R. Epari; M.S. Thompson; G.N. Duda

Equibiaxial deformation of RCAS-GFP transfected primary chicken bone marrow cells
1st Workshop on Correlative Microscopy for 3-D Cell Imaging, CORMIC 2007, Motzen, D
F.H. Bleckwehl; C.E. Ott; S. Ahrens; D.R. Epari; M.S. Thompson; G.N. Duda

Biaxial cell stimulation: mechanical validation and biological response
16th Congress of the European Society of Biomechanics, ESB2008, Luzern, CH
F.H. Bleckwehl, C.E. Ott, M.S. Thompson, S. Ahrens, R. Seidel, S. Mundlos, G.N. Duda

Are T lymphocytes mechanosensitive?
17th Congress of the European Society of Biomechanics, ESB2010, Edinburgh, UK
F.H. Bieler, A. Groothuis, M.S. Thompson, G. Kasper, G.N. Duda

Manuscripts

Biaxial cell stimulation: A mechanical validation
Journal of Biomechanics 42 (2009) 1692-1696

F.H. Bieler[1], C.E. Ott[2], M.S. Thompson[3], R. Seidel[1], S. Ahrens[2], D.R. Epari[1], U. Wilkening[4], K.D. Schaser[1], S. Mundlos[2,4], G.N.Duda[1]

In vitro models for bone mechanobiology: application in bone regeneration and tissue engineering
Proceedings of the Institution of Mechanical Engineers, Part H, Journal of Engineering in Medicine, 224 (2010) 1533-1541

M.S. Thompson[1], D.R. Epari[2], F. Bieler[3], G.N. Duda[3]

Quantification and significance of fluid shear stress field in biaxial cell stretching device
Biomechanics and Modelling in Mechanobiology, DOI: 10.1007/s10237-010-0255-1, Epub ahead of print

M.S. Thompson[1,2], S.R. Abercrombie[1], C.E. Ott[4], F.H. Bieler[3], G.N. Duda[3], Y. Ventikos[1]